Gerald Wriessnegger, BSc

Sensors in high efficiency Drive Systems - Construction of a Drive test bench

MASTERARBEIT

zur Erlangung des akademischen Grades

Diplom-Ingenieur

Masterstudium Elektrotechnik

eingereicht an der

Technischen Universität Graz

Betreuer

Krischan, Klaus, Ass.Prof. Dipl.-Ing. Dr.techn.

Institut für Elektrische Antriebstechnik und Maschinen

Graz, Mai 2014

EIDESSTATTLICHE ERKLÄRUNG

AFFIDAVIT

Ich erkläre an Eides statt, dass ich die vorliegende Arbeit selbstständig verfasst, andere als die angegebenen Quellen/Hilfsmittel nicht benutzt, und die den benutzten Quellen wörtlich und inhaltlich entnommenen Stellen als solche kenntlich gemacht habe. Das in TUGRAZonline hochgeladene Textdokument ist mit der vorliegenden Masterarbeit identisch.

I declare that I have authored this thesis independently, that I have not used other than the declared sources/resources, and that I have explicitly indicated all material which has been quoted either literally or by content from the sources used. The text document uploaded to TUGRAZonline is identical to the present master‘s thesis.

Datum / Date

Unterschrift / Signature

Abstract

The scope of this thesis is the developement and construction of a brushless direct current motor drive demonstrator for Infineons advanced sensor solutions. Beside the demonstration effect, the testbench should help to develop system expertise in the area of motor control, especially with respect to feature set and performance requirements of the individual sensors. The testbench consists of two coupled brushless direct current motors, one for driving and one for braking. To cover many different applications, several commutation methods are included, as well as different sensing techniques for rotor position sensing and different phase current measurement techniques. As further application the testbench is used to evaluate new sensing techniques, which requires a flexible partitioning of the hardware and software.

Zusammenfassung

Zweck der Arbeit ist die Entwicklung und Konstruktion eines bürstenlosen Gleichstrommotorprüfstandes für Sensortechnologien der Firma Infineon. Neben dem Demonstrationseffekt soll der Prüfstand helfen, sich Wissen im Bereich der Motorensteuerung aufzubauen, insbesondere in Bezug zu Anforderungen und Merkmale der einzelnen Sensoren. Der Prüfstand besteht aus zwei gekoppelten bürstenlosen Gleichstrommotoren, einem als Antrieb und einem als Bremse. Um unterschiedliche Anwendungsfälle abzudecken, sind verschiedenste Kommutierungsvarianten wie auch Sensor Methoden für die Bestimmung der Rotor Position und Messung der Phasenströme implementiert. Eine weitere Anwendungsmöglichkeit des Prüfstandes ist die Evaluierung neuer Sensortechniken, welche eine flexible Aufteilung der Hardware und Software erfordern.

Acknowledgements

This thesis has been written with the help and support of people, to which I would like to express my gratitude and appreciation.

First of all I would like to thank my girlfriend Monica for the unconditional support through this long process. You always motivated and encouraged me and have never lost your faith in me. Without you I would not be able to come this far.

Furthermore I would like to thank my family for the opportunity to study and in particular my mother Renate for the encouragement throughout my life.

Last but not least I would like to express my deepest gratitude to my advisor Leo Aichriedler, who is my mentor and friend since several years now. It is a pleasure to work with him and I appreciate his outstanding knowledge and advises.

Contents

List of Figures **v**

List of Tables **viii**

Glossary **ix**

1 Introduction **1**

1.1 Motivation 1

1.1.1 Electrification of vehicles 1

1.1.2 Electric motor types 3

1.1.2.1 Brushed DC Motor 4

1.1.2.2 PM Motors 5

1.1.2.3 Switched Reluctance Motors 5

1.1.2.4 Comparison of motor types 7

1.1.3 Application of sensors 8

1.1.3.1 Rotor Position sensors 8

1.1.3.2 Current sensors 9

2 Brushless DC Motors **11**

2.1 Mechanical Construction 11

2.1.1 Difference BLAC - BLDC 11

2.2 Theory of operation 12

2.3 Operating Modes 13

2.3.1 Block commutation 13

2.3.2 Sinusoidal commutation 14

2.3.3 Field Oriented Control - FOC 16

3 Sensing - angle **20**
3.1 Resolver . . . 21
3.2 Incremental Optical Encoder . . . 21
3.3 Magnetic Angle Sensing . . . 23
3.3.1 Hall effect . . . 23
3.3.2 Magneto-Resistive Effect . . . 25
3.3.2.1 AMR . . . 25
3.3.2.2 GMR . . . 25
3.3.2.3 TMR . . . 29
3.3.3 End of shaft angle sensing . . . 29
3.3.4 Out of shaft angle sensing . . . 30

4 Sensing - current **31**
4.1 Methods . . . 31
4.1.1 Precision Resistor . . . 31
4.1.2 Electromagnetic Current Transducer . . . 32
4.1.3 Coreless Hall Effect Sensor . . . 32

5 Implementation **34**
5.1 Scope . . . 34
5.2 Requirements . . . 34
5.2.1 General Conept . . . 35
5.3 Motor Selection . . . 35
5.4 Mechanical Implementation . . . 36
5.4.1 Requirements . . . 36
5.4.2 Concept . . . 36
5.4.3 Actual Implementation . . . 36
5.4.3.1 EOS Encoder . . . 38
5.4.3.2 Final Setup . . . 38
5.5 Hardware . . . 41
5.5.1 Requirements . . . 41
5.5.2 Concept . . . 41
5.5.2.1 Supply Concept . . . 42
5.5.3 Actual Implementation . . . 44

5.5.3.1 Microcontroller . . . 44
5.5.3.2 PreDriver . . . 44
5.5.3.3 Supply . . . 45
5.5.3.4 Bus voltage level translation . . . 45
5.5.3.5 B6 power inverter sub-board . . . 47
5.5.3.6 Speed Sense Sub-board . . . 50
5.5.3.7 Angle Sense Sub-board . . . 50
5.5.3.8 Layout of B6 power inverter sub-board . . . 52
5.6 Software . . . 55
5.6.1 Requirements . . . 55
5.6.1.1 Firmware . . . 55
5.6.1.2 PC GUI Configuration Control . . . 56
5.6.2 Concept . . . 57
5.6.2.1 Firmware Structure . . . 57
5.6.2.2 USB Commands . . . 58
5.6.3 Actual Implementation . . . 59
5.6.3.1 USB Communication . . . 59
5.6.3.2 Commutation sequence . . . 60
5.6.3.3 Block Commutation . . . 61
5.6.3.4 Sinusoidal Commutation . . . 61
5.6.3.5 Field oriented control (FOC) . . . 61
5.6.3.6 GUI interface . . . 63
5.6.3.7 Data recorders . . . 65

6 Results **68**
6.1 Measurements . . . 68
6.1.1 Accuracy of Angle Measurements . . . 68
6.1.1.1 Angle error of TLE5012 . . . 68
6.1.1.2 Angle error of Hall switch estimation . . . 69
6.1.2 Output stage . . . 71
6.1.2.1 Current Distortion . . . 73
6.1.2.2 Phase currents in sinusoidal commutation . . . 74
6.1.3 FOC drive measurements . . . 76

6.1.3.1 Speed controller jitter 76
6.1.3.2 Speed Step 77
6.1.3.3 Speed Controller Load 78
6.1.3.4 Torque Controller Step 79
6.1.4 FOC load measurements 80
6.1.4.1 FOC load motor 80

7 Conclusion and Outlook **82**
7.1 Conclusion 82
7.2 Outlook 84

References **85**

List of Figures

1.1 Emission Limits 2
1.2 Motor Applications 3
1.3 Motor Types 4
1.4 DC Motor 5
1.5 BLDC Motor 6
1.6 Switched Reluctance Motor 7
1.7 Sensor Applications 9
1.8 Rotor Position Sensors 10
1.9 Current Sensors 10

2.1 BLDC 12
2.2 Back-EMF 13
2.3 Block commutation 15
2.4 Sinusoidal commutation 15
2.5 FOC commutation 16
2.6 Clarke Transform 17
2.7 Park Transform 17
2.8 RCS 18
2.9 SVM 19

3.1 Resolver 21
3.2 Incremental Encoder 22
3.3 Incremental Encoder 23
3.4 Hall effect 24
3.5 Hall effect 24

3.6 AMR . . . 25
3.7 GMR . . . 27
3.8 GMR . . . 27
3.9 GMR . . . 28
3.10 TMR . . . 29
3.11 End of shaft . . . 30
3.12 Out of shaft . . . 30

4.1 Shunt current measurement . . . 32
4.2 Electromagnetic current transducer . . . 33
4.3 Electromagnetic current transducer . . . 33

5.1 Motor Application Concept . . . 35
5.2 Mechanical Concept . . . 37
5.3 Mechanical Implemenation . . . 37
5.4 Mechanical Implemenation . . . 38
5.5 EOS and Encoder . . . 39
5.6 Mechanical Setup . . . 40
5.7 Hardware Concept . . . 43
5.8 Supply Concept . . . 43
5.9 Schematic Port Extension . . . 44
5.10 Supply Schematic . . . 46
5.11 Analog Schematic . . . 47
5.12 Current measurement . . . 48
5.13 Inverter schematic . . . 49
5.14 Overvoltage protection . . . 50
5.15 Supply schematic . . . 51
5.16 EEPROM addressing schematic . . . 52
5.17 B6 Power Inverter with TLI4970 Layout . . . 53
5.18 Hardware . . . 54
5.19 Firmware requirements . . . 55
5.20 Firmware structure . . . 57
5.21 USB communication . . . 59
5.22 USB communication . . . 60

5.23 Commutation sequence 60
5.24 Block commutation 62
5.25 FOC commutation 63
5.26 GUI 65
5.27 GUI 66
5.28 GUI 67

6.1 TLE5012 accuracy 69
6.2 TLE5012 accuracy 70
6.3 Hall estimation accuracy 70
6.4 Hall estimation accuracy 71
6.5 Inverter output 72
6.6 Inverter output 72
6.7 Sinusoidal commutation current 73
6.8 Sinusoidal commutation current 74
6.9 Sinusoidal commutation current 75
6.10 Speed jitter 76
6.11 Speed step 77
6.12 Load change 78
6.13 FOC torque controller 79
6.14 FOC controller load 80
6.15 FOC controller load step 81

List of Tables

1.1 Electric motor applications influence on efficiency [1, p. 14,38-47] 2
1.2 Electric motor comparison [2, p. 7] 8

2.1 Block commutation sequence 14

3.1 Comparison of the accuracy of different encoders [3, p. 122], [4, p. 23] . 20

5.1 Parameters of selected motors according to the datasheets [5], [6] 36
5.2 Motor operating mode possibilities with the demonstrator 63

6.1 Measurement results of Encoder-TLE5012 comparison 69
6.2 FOC controller parameters 76

Glossary

ABS - Antilock Braking System
ARM - Advanced RISC Machines
ADC - Analog to Digital Converter
AMR - Anisotropic Magneto-Resistive
AC - Alternating Current
BLDC - Brushless DC
BLAC - Brushless AC
CCW - Counter-clockwise
CSV - Comma Separated Values
CW - Clockwise
DAC - Digital to Analog Converter
DC - Direct Current
EEPROM - Electrically Erasable Programmable Read Only Memory
EMF - Electromotive Force
EPS - Electric Power Steering
FET - Field Effect Transistor
FOC - Field Oriented Control
GCC - GNU Compiler Collection
GMR - Giant Magneto-Resistive
GUI - Graphic User Interface
IC - Integrated Circuit
IDE - Integrated Development Environment
MCU - Microcontroller Unit
MOS - Metal Oxide Semiconductor
MY - Model Year
PCB - Printed Circuit Board
PM - Permanent Magnet
PMSM - Permanent Magnet Synchronous Motor
PWM - Pulse Width Modulation
RCS - Rotor Coordinate System
RTOS - Real Time Operating System
SCS - Stator Coordinate System
SIB - Sensor Interface Bus
SICI - Serial Inspection and Configuration Interface
SNR - Signal to Noise Ratio
SPI - Serial Peripheral Interface
SRM - Switched Reluctance Motor
SVM - Space Vector Modulation
TMR - Tunnel Magneto-Resistive
TPMS - Tire Pressure Monitoring System
USB - Universal Serial Bus

1

Introduction

1.1 Motivation

One of the key targets for a newly developed vehicle is to increase the fuel efficiency and to reduce the pollutant emissions, especially as it gets more and more difficult to meet the increasing specifications. These requirements are set by the customers who demand a higher fuel efficiency as well as the governments which are reducing the limits e.g. for CO_2, NOx emissions. In order to fulfill these high specifications, sophisticated mechanisms have to be applied. This approach results in a higher demand of intelligent electronics in a modern vehicle. Figure 1.1 shows the target emission limits for passenger cars in the NEDC drive cycle until 2020.

1.1.1 Electrification of vehicles

The increasing requirements for fuel efficiency and pollutant emission reduction result in electrification of the vehicle. This means that the former belt driven actuators are consequently changing to intelligent controlled systems. With this change, new applications for electric motors in a vehicle occur. The number of motors used in an average car is currently already around 50 and in premium cars up to 150. This trend for electrification of the actuators is increasing the number of high power electric motors in a car (e.g. Audi A8 - MY2017: +28 Motors compared to MY2014) [8, p. 4]
There are a lot of applications for a electric motor which can influence the efficiency of the car. Typical Applications for electric motors in a modern car are: power steering motors, starter motor, alternator, engine cooling fan, windscreen wiper, washer pump,

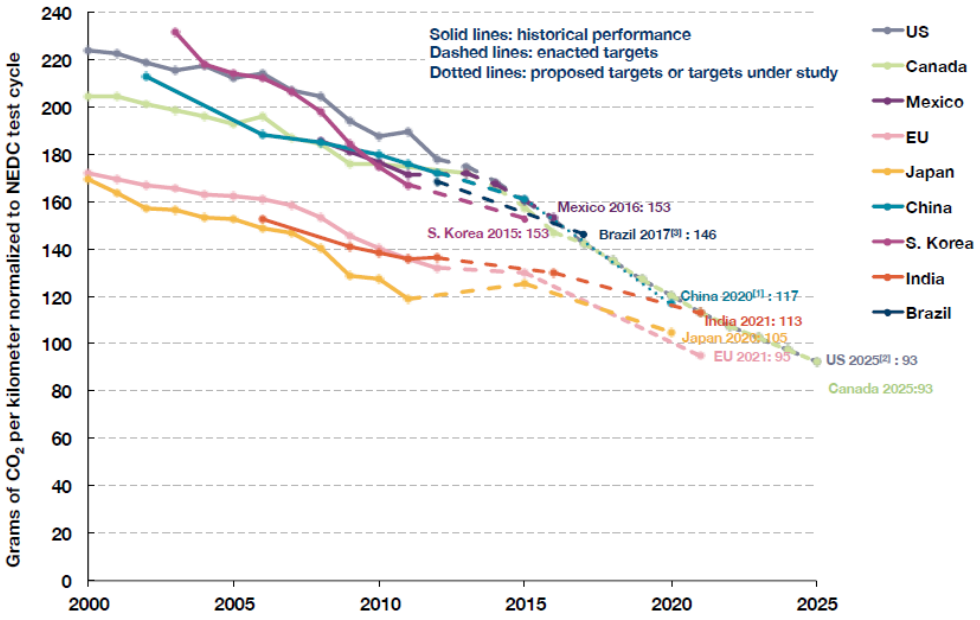

Figure 1.1: Emission Limits - CO_2 target emission limits in the NEDC drive cycle until 2020 (Weight-based corporate average values) [7, p. 4]

fuel pump, window actuation, heat and air conditioning motors, seating position motor, sunroof motor, ABS pump, engine water pump, headlight positioning, automatic closing aid, powertrain and more. Not all of these applications have a direct influence on the efficiency but many of them do. Other applications result from different requirements, e.g. Hybridization - with implementing a start/stop funcionality, several functions have to be active during the stop state as well (Cooling on demand - waterpump, brake booster, gearbox). Table 1.1 shows different electric motor applications and the affect on fuel efficiency and CO_2 emissions [1, p. 14,38-47].

Application	fuel efficiency	CO_2 reduction
Electric Power Steering (EPS)	1.3 mpg	5.9 g/km
Start/Stop with high efficient generator	2.76 mpg	16 g/km
Double clutch transmission (with BLDC)	0.7 mpg	3.2 g/km
Electric water pump (BLDC)	1.4 mpg	6.4 g/km
Fuel Pump	0.34 mpg	1.6 g/km

Table 1.1: Electric motor applications influence on efficiency [1, p. 14,38-47]

Efficiency or hybridization is only one reason for the electrification of vehicles - as discussed before, different new motor applications can include comfort functions as well. With this increasing sockets for electric motors in a modern vehicle, the demand on high efficient semiconductors and control algorithms for motor controls is increasing. For implementing the high efficient control algorithms, accurate and reliable sensing techniques are required as well as efficient electronics. An overview of motor applications with power range and ambient temperature in a modern vehicle can be seen in figure 1.2.

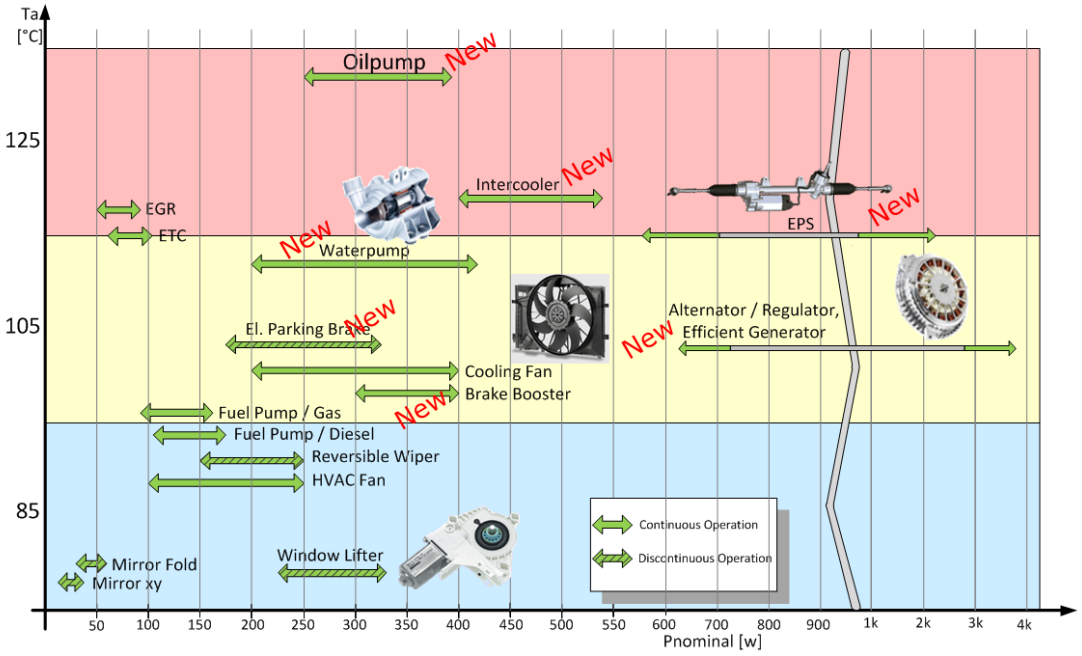

Figure 1.2: Motor Applications - different motor applications in a modern car [8, p. 5]

1.1.2 Electric motor types

For all new applications in a modern car discussed in chapter 1.1.1, different motor types can be used to fulfill the desired functionality. The selection of the motor type has an impact on the efficiency as well as on the complexity of the electronics. Figure 1.3 shows a classification overview of different motor types. The main focus of this thesis will be the Brushless DC Motor.

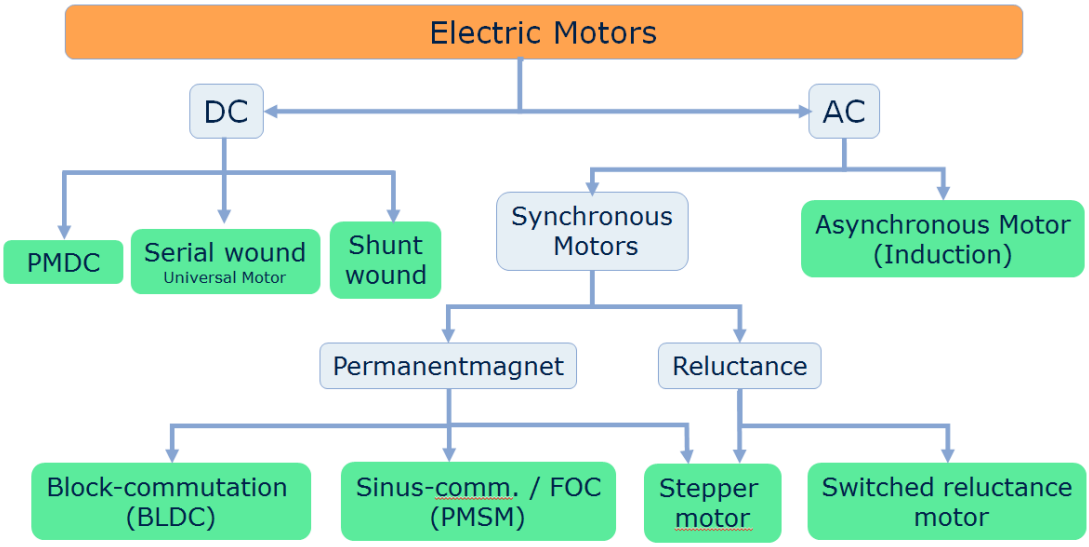

Figure 1.3: Motor Types - different motor types - classification [8, p. 9]

1.1.2.1 Brushed DC Motor

The brushed DC motor is the most traditional motor type used in automotive environments. Figure 1.4 shows the mechanical construction of a brushed DC motor. The most noticeable point is that it consist of a mechanical commutator with brushes. These brushed DC motors have efficiencies of 75-80% [9, p. 17]. With this principle, the direction of the field in the stator is constant and the mechanical commutator keeps the current switching in the rotor winding, to keep the rotor turning. The switching of the field in the rotor windings is called commutation. [10, p. 1] With a switching sequence, the generated field of the rotor is readjusted in a way that a force is always applied to the rotor in order to keep it turning. Currently around 60% of automotive motor applications are covered with this motor type [8, p. 10]. The main advantages of brushed motors are the low costs and the simple control algorithms. The main disadvantages are the low efficiency and the degradation of the brushes, especially in high temperature environments. With this degeneration, the brushed DC motor is not maintenance free over lifetime for some applications. In addition to that, there is a potential sparking of the brushes, which makes this motor type not suitable for all applications (e.g. fuel pump).

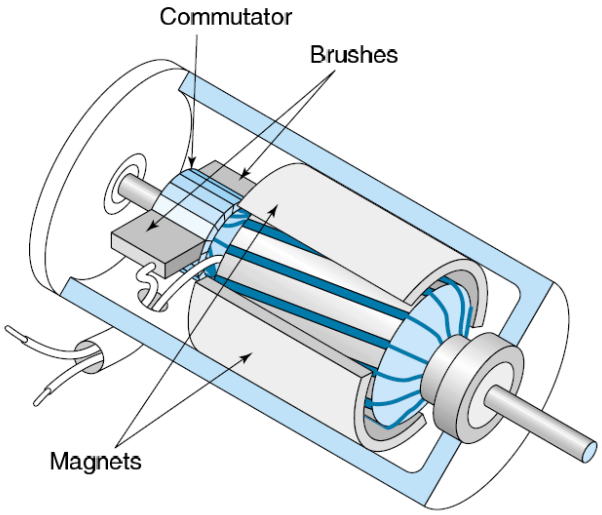

Figure 1.4: DC Motor - Principle construction of a brushed DC motor [11, p. 25]

1.1.2.2 PM Motors

Permanent magnet motors can be basically divided into three subsections: DC commutator motors with permanent magnet, brushless motors (dc and ac synchronous) and stepping motors [12, ch. 1.2]. The mechanical construction of a DC commutator motor with permanent magnets can be seen in figure 1.4. The advantages of using a brushless PM motor are the better mass/power ratio, higher efficiency, longer lifetime, lower torque ripple which results in a more silent drive and the flexible partitioning (rotor can be inside or outside). The main disadvantages are the higher cost for the motor and the more complex control algorithm, as well as the dependency on rare earth materials (if using neodymium magnets). Brushless motors have a typically efficiency of 85-90% [9, p. 17]. Figure 1.5 is showing the mechanical construction of a BLDC motor. This thesis is focusing on brushless motor drives, which will be discussed in chapter 2.

1.1.2.3 Switched Reluctance Motors

From a construction point of view, the switched reluctance motor is the simplest of all electrical machines. The mechanical setup is similar to the brushless permanent magnet motors with concentrated (toothed) windings, the main difference is that no

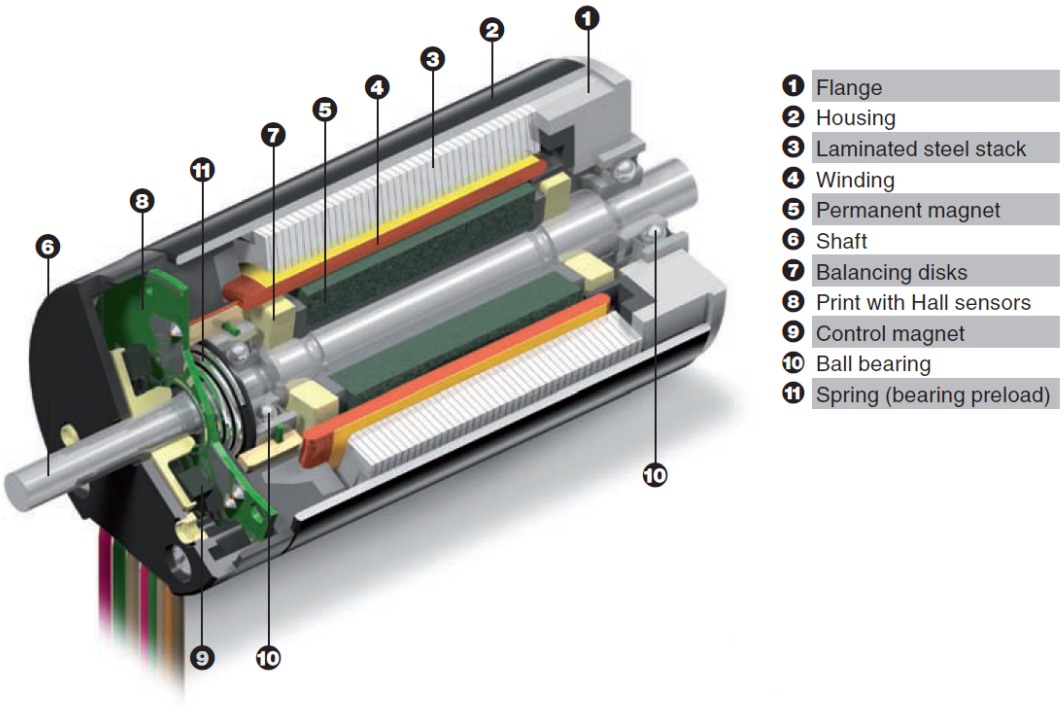

Figure 1.5: BLDC Motor - construction of a brushless DC motor [13, p. 26-27]

permanent magnets are needed on the rotor, instead the rotor is made of iron. The stator consists of coils which are used to generate the movement of the rotor. When one stator phase is energized, the rotor moves into the position of maximum inductance. Now the next phase will be energized and the rotor moves again to the position of maximum inductance - the rotor follows the field applied to the stator [14, p. 2-3]. Figure 1.6 shows the commutation sequence for a SRM. The main advantages of a SRM are the simple and robust design, the low cost and the independence of rare earth materials (for permanent magnets). The efficiency of a SRM is in the range of 73-82% [15, p. 8]. The high torque ripple, the audible noise (generated by the deformation of the stator iron due to magnetic forces and the torque ripple) and the complex control algorithms are the main disadvantages of SRMs.

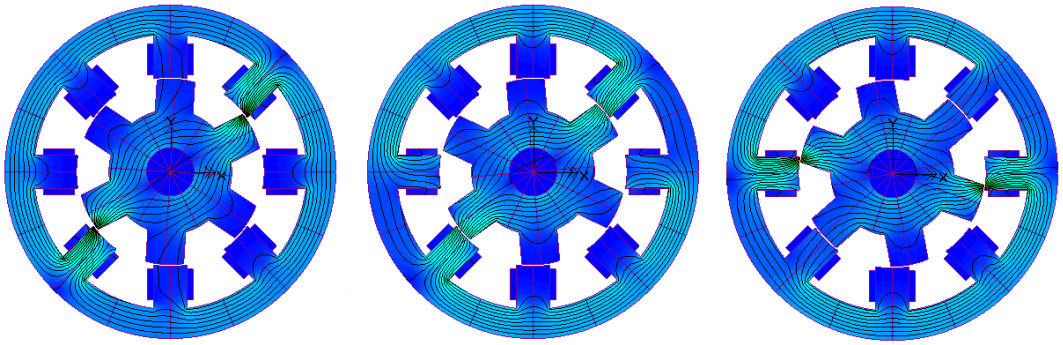

Figure 1.6: Switched Reluctance Motor - commutation sequence for a SRM [16]

1.1.2.4 Comparison of motor types

Table 1.2 shows a comparison between the different motor types discussed in this chapter. The simplest machine from a control perspective is the brushed DC motor. From a construction point of view, the SRM is the simplest machine but has the highest torque ripple. Another disadvantages is the requirement of a complex control logic but on the other hand the machine is maintenance free over life time. The BLDC motor has the same benefits as the SRM but has a lower torque ripple. The main disadvantage is the dependency on rare earth materials for the permanent magnets, if not using ferrite magnets.

Feature	Brushed DC Motor	BLDC Motor	Switched Reluctance Motor
Commutation	mechanical	electronic based on rotor position	
Maintenance	required periodically	Less required due to absence of brushes.	
Lifetime	Shorter	Longer	Longer
Speed/Torque Characteristics	Moderately flat	Flat	high torque ripple
Efficiency	Moderate	High	Moderate-High
Cost of Building	Low	Higher	Low
Control	Simple and inexpensive	Complex and expensive	

Table 1.2: Electric motor comparison [2, p. 7]

1.1.3 Application of sensors

With the increasing complexity of intelligent controls in a modern car, the demand on sensing technologies increases as well. The sensor IC market is one of the fastest growing segments in the electronics market today. For example, a new car features now besides other sensor techniques, up to 80 magnetic sensor applications [17, p. 3]. Figure 1.7 is showing examples of different applications for sensors in a modern vehicle, e.g. throttle position, pedal position, crank/camshaft speed, airbag pressure sensing or tire pressure monitoring system. An accurate and reliable sensing technique is a prerequisite for most efficient systems. This thesis issues drive systems and therefore covers the two main sensing applications for drive systems: rotor position and current sensing.

1.1.3.1 Rotor Position sensors

Figure 1.8 shows an overview of different rotor position techniques used in motor applications. The traditional sensing methods are the optical and inductive sensors. The benefit of using the inductive or magnetic method is that the absolute angle position is known at any time, whereas optical incremental encoder only support one index

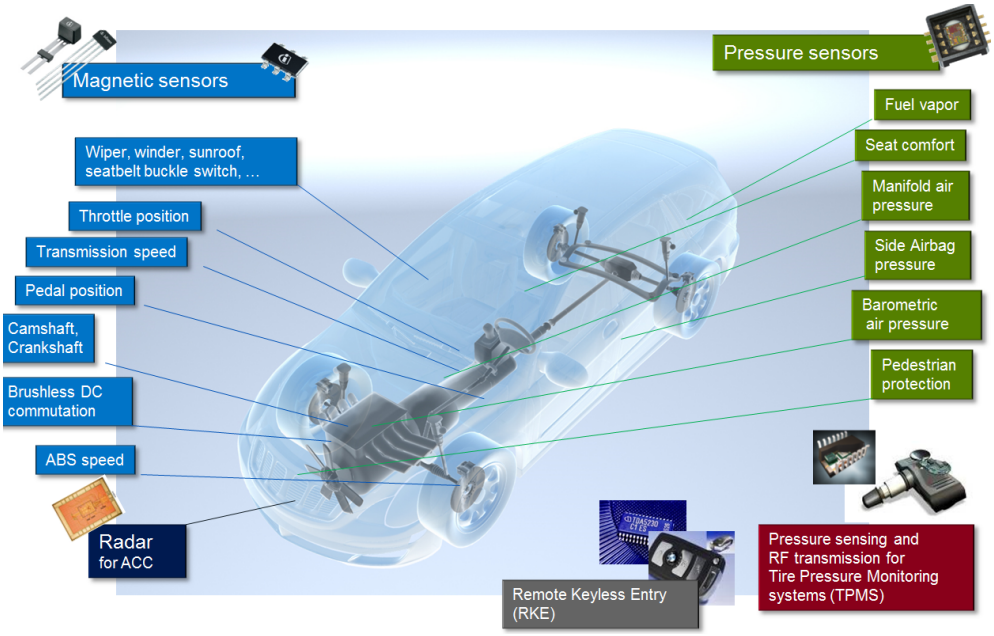

Figure 1.7: Sensor Applications - different sensor applications in a modern vehicle [17, p. 6-8]

pulse per revolution. Another way to determine the position of the rotor is using hall switches. These switches are distributed in a 120° distance around the shaft, which results in a update of the rotor position every 60°. A similar update rate can be achieved with measuring the back-EMF voltage of the motor. For this method, one phase should not be energized and the induced voltage on this phase will be measured. With a zero crossing detection of this voltage, the position of the rotor is known. This technique is one method for a so called sensorless control and has the benefit that no additional components are needed. The disadvantage is that this technique is not suitable for low speeds, as the back-EMF voltage is proportional to the speed of the rotor and could be too low for a reliable zero crossing detection. For a highly efficient control algorithm, the update rate of hall switches or back-EMF measurements are too low, as the position has to be interpolated between the known points, especially for low speed.

1.1.3.2 Current sensors

For an efficient control of a motor, the stator phase currents have to be measured. With the phase currents and a proper motor model, the generated torque can be calculated.

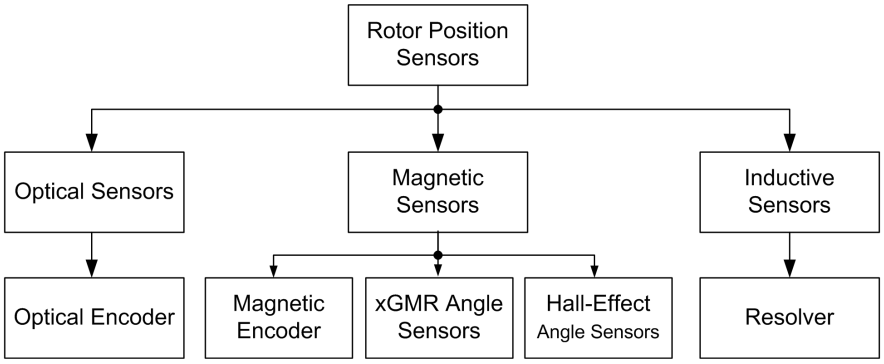

Figure 1.8: Rotor Position Sensors - Overview of the rotor position sensor principles

The phase currents can be measured either direct in the phase or indirect in the inverter output stage. Figure 1.9 shows an overview of different current sensing techniques. Current sensing techniques can be categorized in these physical principles[18]:

- Ohm's law of resistance (Shunt resistor, Trace-resistance Sensing)
- Faraday's law of induction (Rogowski coil, Current transformer)
- Magnetic field sensors (hall-effect, Fluxgate-principle, magneto resistance effect)
- Faraday effect (Fiber-optic current sensors)

The main requirement for a current sensor used in drive applications is the bandwidth of the sensor, as it has an influence on the performance of the control.

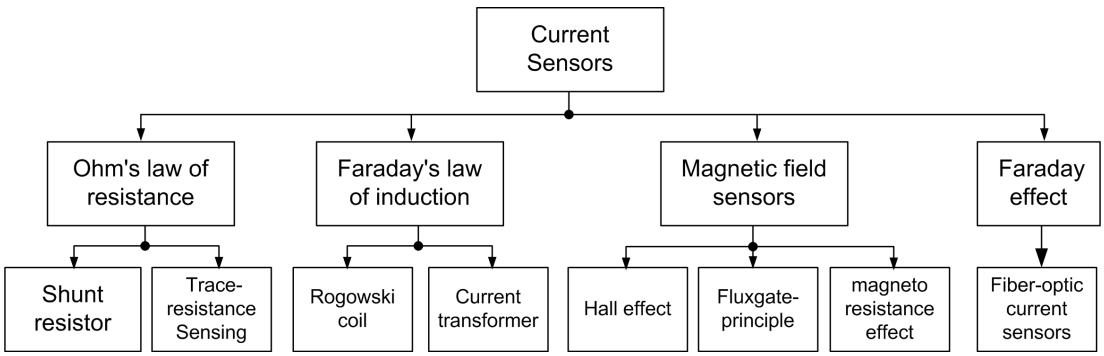

Figure 1.9: Current Sensors - Overview of current sensing principles

2

Brushless DC Motors

2.1 Mechanical Construction

Brushless motors are a type of synchronous machines, which means that the generated field in the stator is rotating synchronous to the rotor. BLDC motors do not have the "slip" as induction motors have. There exist single-phase, 2-phase and 3-phase configurations of BLDC motors, which represent the number of stator windings. The most popular configuration is the 3-phase motor were the windings are connected in a star fashion [2, p. 1]. These three windings are placed in the stator of the BLDC motor and the rotor contains the permanent magnets, either buried or on the surface of the rotor. The number of permanent magnets and the number of pole-pairs on the rotor of the machine can vary. Depending on the required magnet field density, the material of the magnets can be ferrite or a neodymium alloy. The advantage of using an alloy is the higher magnetic density per volume but on the other hand the costs are increasing. Ferrite magnets have the advantage that they are independent from rare earth materials. Figure 2.1 shows a cross-section of the principle construction of a BLDC motor with three phases and six poles. [2, p. 1-4]

2.1.1 Difference BLAC - BLDC

There exist basically two types of brushless machines: the BLAC and the BLDC motors which differ in the construction of the stator windings. Motors with a sinusoidal back-EMF are typically called BLAC motors and those with a trapezoidal back-EMF are named BLDC motors. This distinction is caused by the different structure of the stator

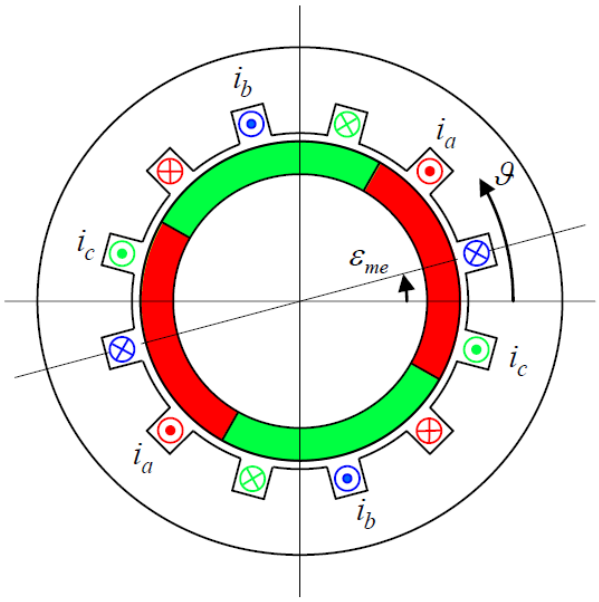

Figure 2.1: BLDC - principle mechanical configuration of a BLDC motor with two pole-pairs [19, p. 26]

windings in combination with the magnetization of the magnets and the shape of the airgap (in case of burried magnets). The back-EMF is the voltage which is induced in the stator windings when the rotor is turning. This voltage depends on the velocity of the rotor, the magnetic field of the permanent magnets and the stator windings. The voltage is increasing with increasing speed, magnetic field of the PMs or number of turns in the windings. Figure 2.2 shows the difference between a sinusoidal and a trapezoidal back-EMF.

2.2 Theory of operation

In order to generate a movement on the rotor, torque has to be applied on it. This torque is generated by the interaction between the field generated in the stator and the magnetic field of the permanent magnets in the rotor. Torque on the rotor is generated due to the Lorentz force on a current carrying wire according to equation 2.1. The magnetic field B is generated by the permanent magnets and the current I flows through the stator windings (length l). The peak torque occurs when both fields

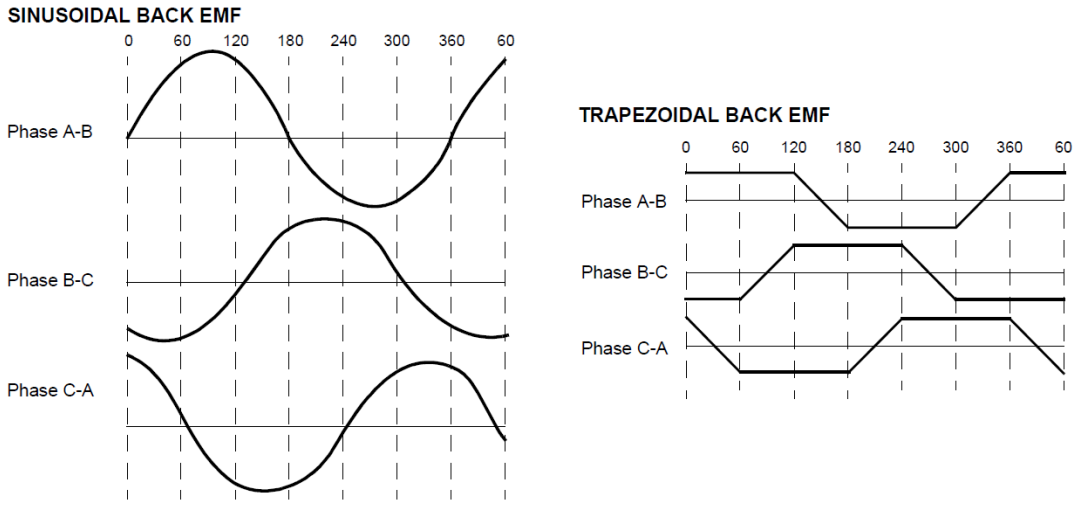

Figure 2.2: Back-EMF - examples for sinusoidal and trapezoidal back-EMF [2, p. 2]

are 90° shifted to each other. If now the stator field is rotating, the rotor is trying to catch up with this field and the motor is turning. Besides the magnetic field in the rotor, the current in the stator is generating a magnetic field as well and is influenced by the induced back-EMF voltage of the rotor in the stator windings. [2, p. 5]

$$F = I \cdot l \times B \tag{2.1}$$

2.3 Operating Modes

As discussed in chapter 2.2, to create a movement on the rotor, the stator field has to rotate. This rotation of the field can be achieved by different commutation algorithms. The simplest commutation algorithm is the block commutation, followed by the sinusoidal commutation but the most sophisticated way is the field oriented control.

2.3.1 Block commutation

Block commutation is the simplest method for driving a BLDC motor. Usually this commutation technique is done using hall-sensors or back-EMF position sensing method. In block commutation mode, one phase is positive energized, one negative and one phase is floating. When the hall switch pattern changes, the next phase will be energized and

another one is floating. This principle is shown in figure 2.3. In this sequence, every hall pattern results in a defined output pattern for the motor phases, shown in table 2.1 for one direction. In order to change the velocity of the rotor, the amplitude of the applied voltage has to be changed. A higher amplitude results in a higher velocity of the rotor. This is typically done with pulse width modulation of the "high" amplitude. When the three windings are connected in a star configuration, applying a positive voltage U on one phase and ground on another phase, the current will flow through both windings and if neglecting the back-EMF voltage, this would result in a star point voltage of $\frac{U}{2}$. This way one winding is positive and the other one is negative energized.

Hall Sector	H1	H2	H3	U	V	W
3	1	1	0	X	L	H
2	0	1	0	H	L	X
6	0	1	1	H	X	L
4	0	0	1	X	H	L
5	1	0	1	L	H	X
1	1	0	0	L	X	H

Table 2.1: Block commutation sequence

2.3.2 Sinusoidal commutation

The main difference between the block commutation and the sinusoidal commutation is that instead of just applying static voltages on the windings, a sinusoidal voltage is used. This results in a smoother movement of the rotor as it reduces the torque ripple but increases the switching losses in power stage. The frequency of the sinusoidal voltage is defined by the speed of the rotor. For this commutation method, the position of the rotor has to be known more precisely. If using hall sensors or sensorless rotor position sensing (e.g. with a back-EMF estimation, as the phases are never floating in sinusoidal commutation), the angle between the fixed points have to be interpolated, which is affecting the efficiency of the motor. Figure 2.4 is showing the voltages applied to the phase inputs and the mathematical difference between them, which results in a sinusoidal voltage across the windings.

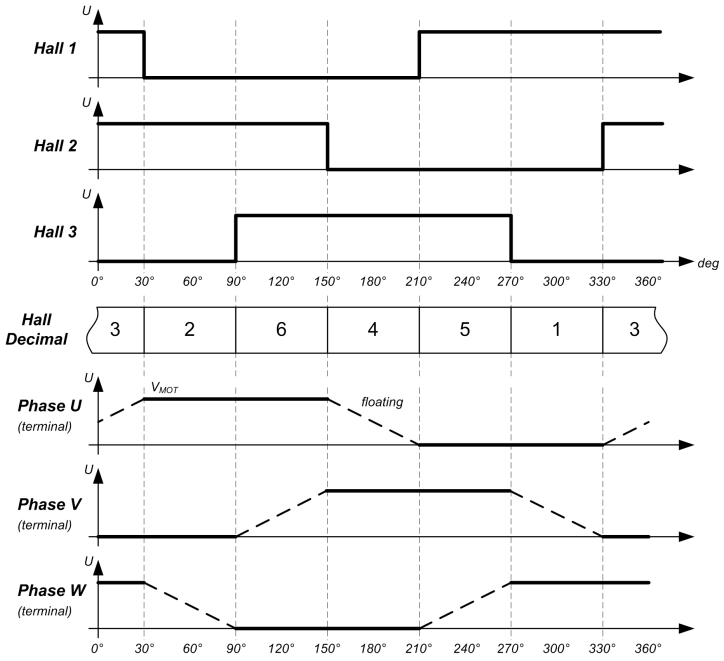

Figure 2.3: Block commutation - commutation sequence depending on the hall switch state

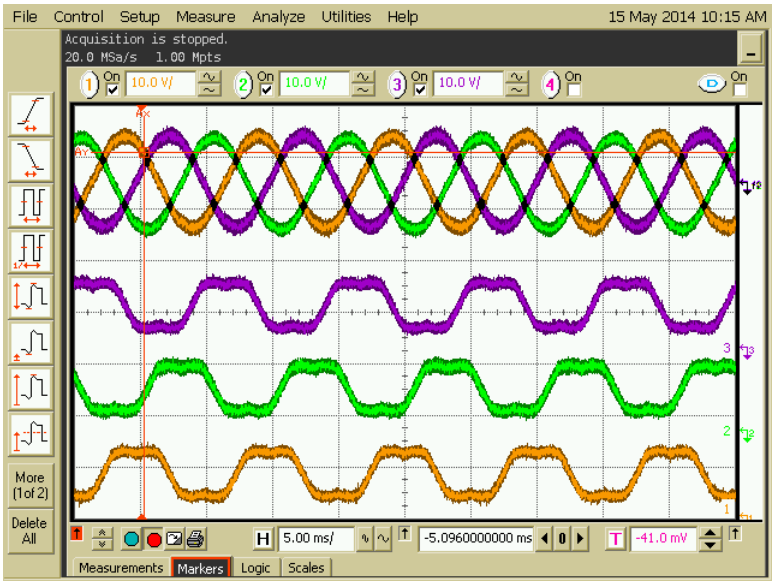

Figure 2.4: Sinusoidal commutation - sinusoidal commutation sequence

2.3.3 Field Oriented Control - FOC

Field Oriented Control is the most advanced control method for brushless DC motors. With FOC it is possible to implement a torque or position control as well as a speed control. FOC is the most efficient way to control a motor, but requires the most mathematical processing power. The basic idea behind FOC is that the three phase signals will be converted into two rotor referenced values. The output itself is similar to the sinusoidal commutation, as it generates sinusoidal voltages on the windings. The goal of FOC is to separately control the torque building and magnetic flux generating stator current components [20, p. 4-5]. In order to decouple these components, several mathematical transformations are necessary. Figure 2.5 shows an overview of the blocks, which are needed for a field vector control. As it can be seen the phase currents and the rotor position have to be known for FOC.

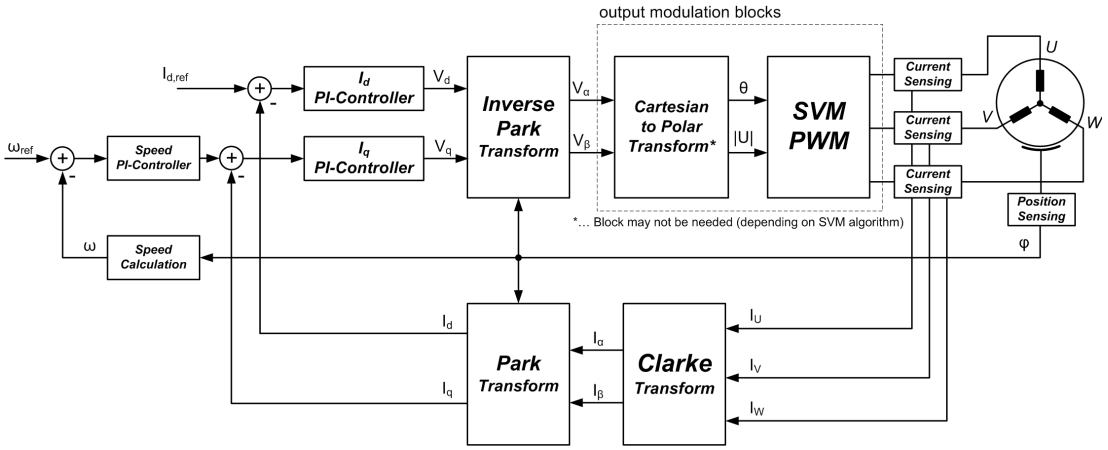

Figure 2.5: FOC commutation - Principle concept of a FOC control

The first coordination transfrom is called the "Clarke" transform and is moving the three-axis and two-dimensional coordinate system into a two-axis system. The transform removes the redundancy of the three phase system and this resulting two-axis system is keeping the same reference - the stator. Figure 2.6 and equation 2.2 is showing the transform of the individual phase currents into the α, β domain. [21, p. 8]

$$\begin{aligned} i_\alpha &= i_u \\ i_\beta &= \frac{1}{\sqrt{3}}\left(i_u + 2i_v\right) \\ i_u + i_v + i_w &= 0 \end{aligned} \tag{2.2}$$

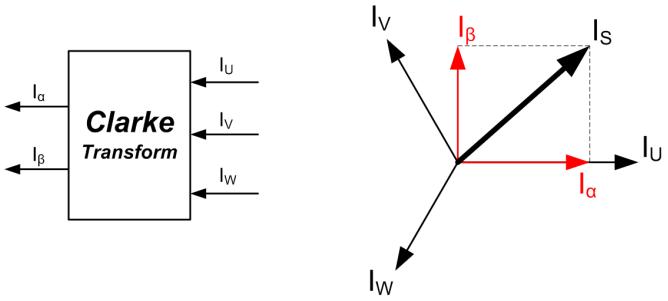

Figure 2.6: Clarke Transform - transformation into two dimensional α, β domain

The next step is the Park transformation, shown in figure 2.7 and equation 2.3. With the Clarke transform, the stator currents are represented in a two axis and stator referenced orthogonal coordinate system. With the Park transformation, this stator coordination system (SCS) is rotated with the angle of the rotor and is then referenced by the rotor. This rotor coordinate system (RCS) is called the d-q axis and φ is the rotor angle. Figure 2.8 shows the location of the d-q axis in the rotor with 2 poles. For constant speed and constant torque operation, the currents I_q and I_d are stationary in the RCS and therefore easy to control. The inverse Park transform is used for a conversion from the RCS to the SCS. Equation 2.4 shows this relationship from the d-q system to the α, β system. [21, p. 8] [22, p. 8]

$$\begin{aligned} i_d &= i_\alpha \cos(\varphi) + i_\beta \sin(\varphi) \\ i_q &= -i_\alpha \sin(\varphi) + i_\beta \cos(\varphi) \end{aligned} \tag{2.3}$$

$$\begin{aligned} V_\alpha &= V_d \cos(\varphi) - V_q \sin(\varphi) \\ V_\beta &= V_d \sin(\varphi) + V_q \cos(\varphi) \end{aligned} \tag{2.4}$$

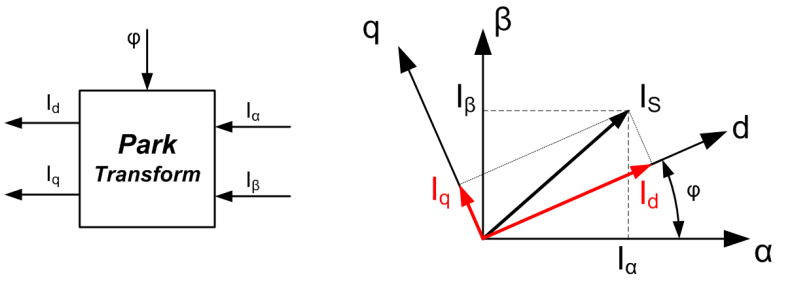

Figure 2.7: Park Transform - transformation from SCS to RCS

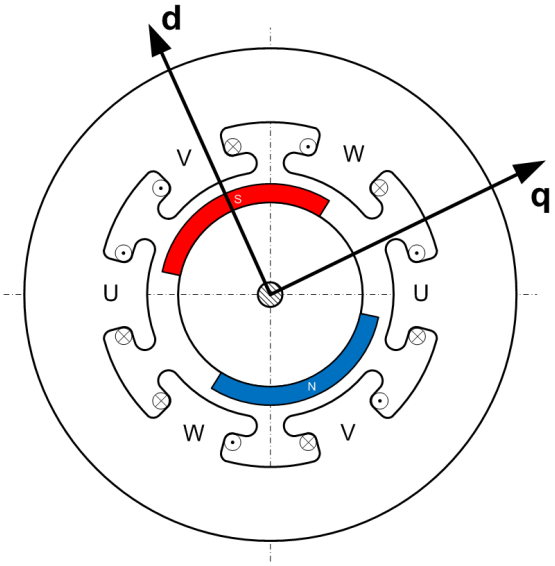

Figure 2.8: RCS - location of the d-q axis in the rotor with 2 poles

As I_q and I_d is stationary in the RCS, they can be easily controlled with PI controllers. I_q is the torque generating current in the rotor as it is orthogonal to the PM magnetic field. For a maximum torque per ampere control if $L_d = L_q$, I_d is controlled to 0. It is also possible to control the I_d to negative values. This mode is called "Field weakening mode" and is used to extend the operating speed of the motor. Equation 2.5 shows the mathematical representation of the PI controllers. The input signal $e(t)$ is the error signal, which is the deviation between the reference value and the actual value. [22, p. 9-10]

$$U(t) = K_p \cdot e(t) + K_i \cdot \int_0^t e(\tau)d\tau \tag{2.5}$$

The final step in the FOC process is the output modulation, which applies the voltages on the phases according to the input voltage vector U_S. One of these modulation schemes, is the Space Vector Modulation SVM. Depending on the implementation of the SVM, it could be necessary to calculate the vector from the V_α and V_β values with the Cartesian to Polar coordinate system transformation shown in equation 2.6.

$$\begin{aligned} |U_S| &= \sqrt{V_\alpha^2 + V_\beta^2} \\ \Theta &= \arctan\left(\frac{V_\beta}{V_\alpha}\right) \end{aligned} \tag{2.6}$$

For applying these voltages on the windings, pulse width modulation is used. The SVM calculates the appropriate duty cycle values for each phase output stage. The space vector diagram shown in figure 2.9 is describing the six possible sectors of the output stage. The desired output vector U_s can be generated by superposition of two phase voltages. The energized phases are determined by the sector of the output vector (Sector A-F). As shown in the figure, the maximum output voltage of a SVM could be in a hexagonal shape. For a sinusoidal output, the amplitude of the voltage vector U_s has to be limited to fit a circle in this hexagon. Using the maximum output voltage of the SVM (hexagonal shape) is called over-modulation and could generate a higher torque. Using over-modulation results in a higher torque ripple and higher losses in the machine, as the output voltage is not sinusoidal. The two passive vectors exist, if all phases are shorted, either with the high-side or the low side switches of the output inverter.

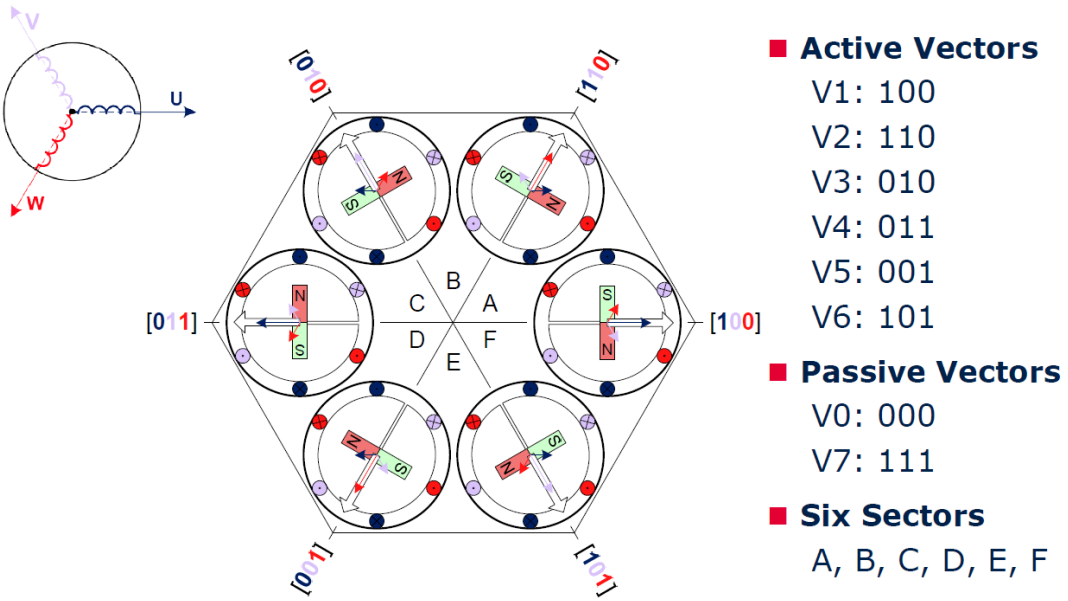

Figure 2.9: SVM - Space Vector Diagram [22, p. 16]

3

Sensing - angle

As discussed in chapter 1.1.3.1, a reliable and precise rotor position sensing is essential for an efficient control of a brushless motor. As shown in figure 1.8, angle sensors can be classified by their measuring principle. There exist optical, magnetic and inductive measurement methods, which are used in motor control applications. The accuracy requirements depend on the motor application and is shown for the different sensing techniques in table 3.1. Optical encoders cause higher costs but do also have a higher accuracy (absolute encoders) than other sensing methods [3, p. 122]. The rotor position sensing can be either in the motor, or externally on the motor shaft. Another distinction can be made with absolute and relative encoders. With absolute encoders, the position of the rotor is known at any time. With relative encoders, the rotor angle is only known once per revolution and has to be calculated from the incremental steps in between.

Encoder type	Principle	Accuracy
Resolver	Inductive	$\pm 0.16°$
Encoder	Optical	$\pm 0.16°$
Sin-Cos absolute encoder	Optical	$\pm 0.03°$
TLE5012	Magnetic	max. $\pm 1°$

Table 3.1: Comparison of the accuracy of different encoders [3, p. 122], [4, p. 23]

3.1 Resolver

The resolver makes use of an electromagnetic inductive sensing principle and consists of a single-phase rotor winding and depending on the number of pole-pairs, two-phase stator windings. Figure 3.1 shows the construction and cross-section of a resolver. With the coupling between the rotor and the stator phases, the angle of the rotor shaft can be calculated. Resolvers are supplied and evaluated by an electronic circuit but do not need any additional electronic components. Due to this fact, resolvers are very robust compared to other sensing techniques, especially in high temperature and vibrational environments. Another advantage of the resolver is that it is supplying the absolute angular position information of the rotor immediately at start-up. The requirement for this is that the number of pole-pairs in the resolver has to be an integer multiple of the number of pole-pairs of the motor. The information of the rotor position is included in the induced sinusoidal voltages on the stator which are shifted by 90°. The angle of the rotor can be calculated with equation 3.1. [3, p. 122-124]

$$\varphi_m = tan^{-1}\left(\frac{V_{sin}}{V_{cos}}\right) \tag{3.1}$$

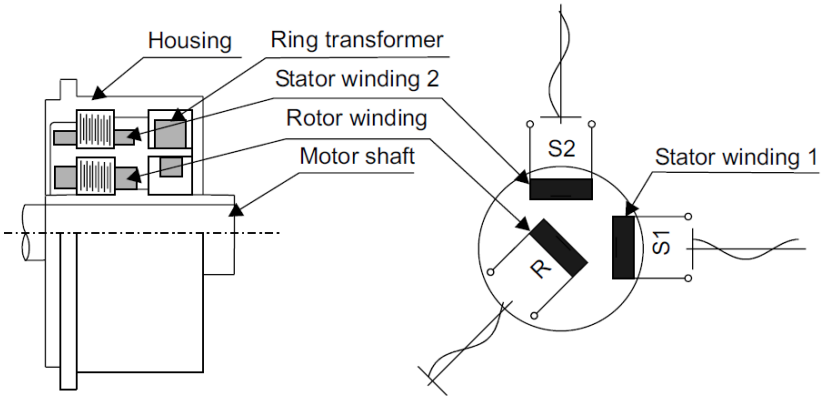

Figure 3.1: Resolver - principle construction and cross-section [3, p. 123]

3.2 Incremental Optical Encoder

The incremental encoder uses an optical technique for detecting the rotor position. This technique provides electrical pulses if the rotor is moving. On the shaft of the optical

encoder, a rotor disc is mounted with optically transparent slots or a reflective pattern. On one side of the disc, a light source is emitting a light beam, which is then sensed on the other side of the disc with optical sensors or on the same side of the disc if a reflective pattern is used. Figure 3.2 is showing the principle mechanical construction of an optical incremental encoder with transparent slots. If the disc is rotating, the light beam is modulated and generates rectangular pulses on the output as shown in figure 3.3. In order to detect the direction of the rotation, there is a second light-beam and sensor placed with an angular offset (light source A and B in figure 3.2). Depending on which signal is leading, the direction of the rotation can be determined. With the A and B tracks, only a relative movement of the rotor can be detected. In order to have a reference of the absolute position of the rotor, another track is implemented on the rotor disc. This track has only one slot and one light source - sensor pair and is called the index track (light source Z). With this single pulse per revolution, the absolute position of the rotor is known. The resolution of the encoder is determined by the number of slots in the rotor disc. [23, p. 287-289]

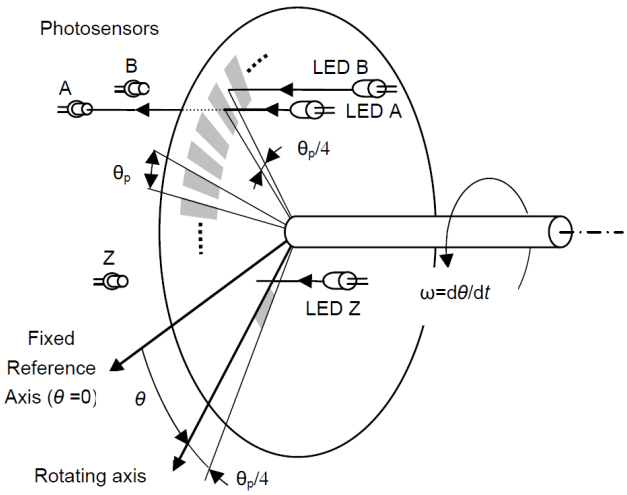

Figure 3.2: Incremental Encoder - principle construction of an optical incremental encoder [23, p. 288]

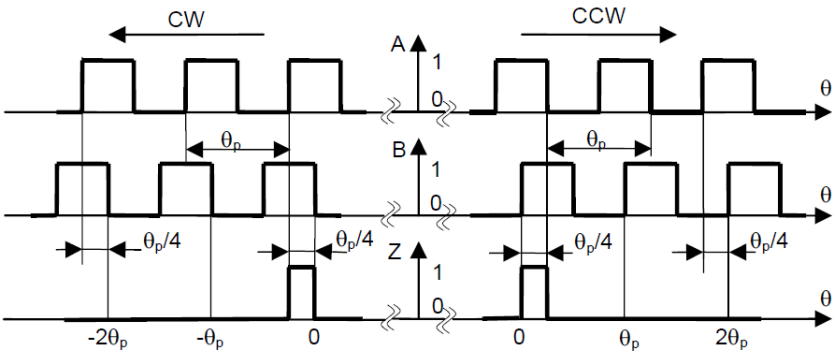

Figure 3.3: Incremental Encoder - output signals generated by a incremental encoder for clockwise CW and counter-clockwise CCW direction [23, p. 289]

3.3 Magnetic Angle Sensing

Another principle for measuring the rotor position is the magnetic angle sensing. The main technique of this principle is to measure the orientation of a magnetic field. This magnetic field is generated with a permanent magnet and is linked to the rotor. This magnetic sensor could use a hall or magneto resistive effect (xMR) based technique.

3.3.1 Hall effect

The hall effect is one of the most widely used effect in sensing magnetic fields. Figure 3.4 is showing the principle of the hall effect. If a magnetic field is applied perpendicularly to an, electrical current carrying thin sheet of material, this field creates a transverse force on the moving electrons and is pushing them on one side. The charges of positive polarity will be pushed to the other side. This generates a measurable voltage across the thin material according to equation 3.2. I is the current flowing through the thin material, B is the applied magnetic field, n is the charge carrier density, e is the elementary electronic charge ($1.602 \cdot 10^{-19}$ C) and d is the thickness of the material. Figure 3.5 shows the measuring principle of a hall effect angular position sensor. [24, p. 36-37]

$$V_{Hall} = \frac{I \cdot B}{n \cdot e \cdot d} \tag{3.2}$$

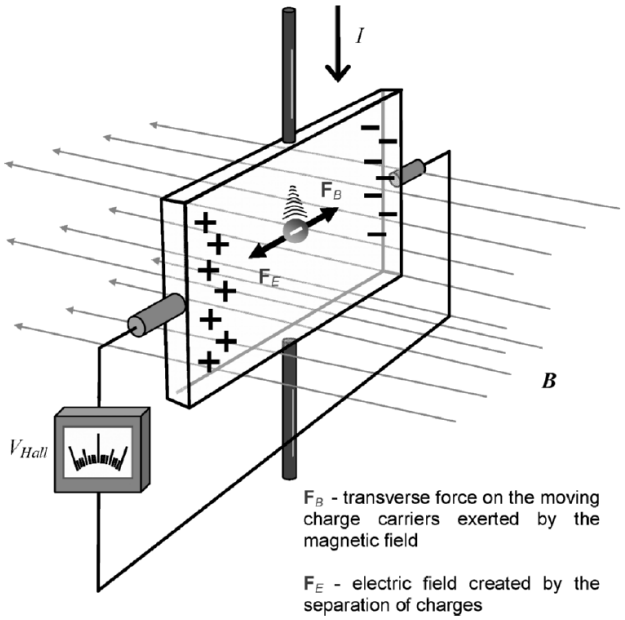

Figure 3.4: Hall effect - principle of the hall effect [24, p. 37]

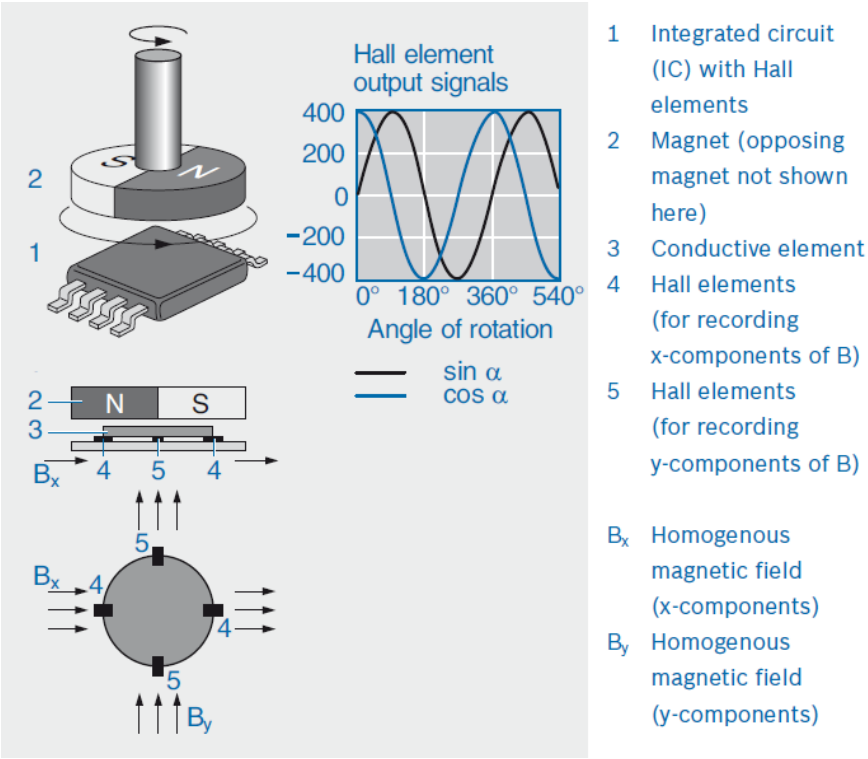

Figure 3.5: Hall effect - position sensor with hall effect [25, p. 329]

3.3.2 Magneto-Resistive Effect

Magneto-Resistive effect means that an applied magnetic field results in a change of resistance of a ferromagnetic material. [26, p. 583-584]

3.3.2.1 AMR

The anisotropic magneto-resistive (AMR) effect is the dependency of the resistance of a material on the angle α between a current in a ferromagnetic material and the magnetization as shown in figure 3.6. The relationship between the resistance and the angle of the magnetic field can be described as stated in equation 3.3. The maximum resistance is reached at $\alpha = 0°$ and the minimum at $\alpha = 90°$, but the overall resistance change $\Delta R_{AMR} \sim 2 - 3\%$. Angle sensors which use the AMR principle have only a angle detection capability of 180°. [26, p. 583-584] [27, p. 2]

$$R_\alpha = R_0 + \Delta R \cos^2 \alpha \tag{3.3}$$

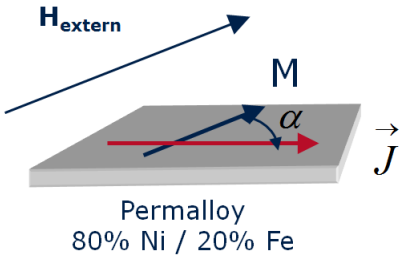

Figure 3.6: AMR - principle of the anisotropic magneto-resistive effect [27, p. 2]

3.3.2.2 GMR

For the giant magneto-resistive (GMR) effect, a layered system is needed. This system consists of two magnetic iron layers (FM1 and FM2) separated by a thin non-magnetic layer (NM). Depending on the thickness of this isolation layer, the magnetic orientation of the two outer layers is either parallel or anti-parallel. With the anti-ferromagnetic layer (AFM), the magnetic direction of the reference layer FM1 is fixed. The magnetization direction of the upper free layer can be influenced by an external field and can rotate. This rotation of the external field changes the direction of the magnetic field

of these two layers from parallel to anti-parallel, which changes the resistance of the system as shown in figure 3.7 due to the GMR effect. If the electric charge carriers hit obstacles or are deflected (scattered) the resistance of a material increases. The charge carriers of a materials can either have a spin-up or spin-down state. If the material is now ferromagnetic, one of these carriers are a majority and the other one are the minority. If the number of spin-up and spin-down carriers is equal, the material is not ferromagnetic. Usually the spin of an electron does not influence the transportation of electric current but in narrow geometries, it has an influence, especially with the presence of a magnetic field. As the GMR layers are only a few nanometres thick, the ability of charge carriers to scatter and thereby switch the spin decreases. If now electrons are moving through this GMR layers, a spin-up electron can strike a layer containing a predominance of spin-down electrons. If this occurs, a scattering on the interface occurs at a high probability and will increase the resistance. If the charge carrier and the GMR layer have the same magnetization vectors, there will be almost no scattering, resulting in a lower resistance. This effect is shown in figure 3.8. The number of GMR layers can increase the resistance change, more layers result in a higher ΔR. [28, p. 88-89] [29, p. 56]

The sensitivity of GMR effect sensors, which dependent on the rotation of the magnetic field is higher than the AMR effect sensors and in a range of $\Delta R_{GMR} \sim 4 - 10\%$. The minimum resistance is reached when both fields are in parallel direction at $\alpha = 0°$ and the maximum resistance can be achieved at an angle $\alpha = 180°$. The dependence of the resistance on the magnetic direction is shown in equation 3.4. Angle sensors which are using the GMR effect have an unambiguous 0...360° angle detection capability if using two GMR cells, which are oriented orthogonal to each other. For measuring the resistance two Wheatstone bridges are used for the sin and cos outputs, as shown in figure 3.9. [26, p. 584] [27, p. 2]

$$R_\alpha = R_0 + \frac{\Delta R(1 - \cos\alpha)}{2} \tag{3.4}$$

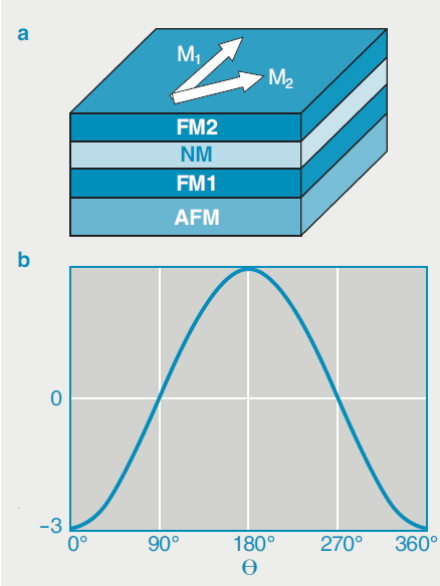

Figure 3.7: GMR - dependence of the resistance on the orientation of the magnetic field [29, p. 56]

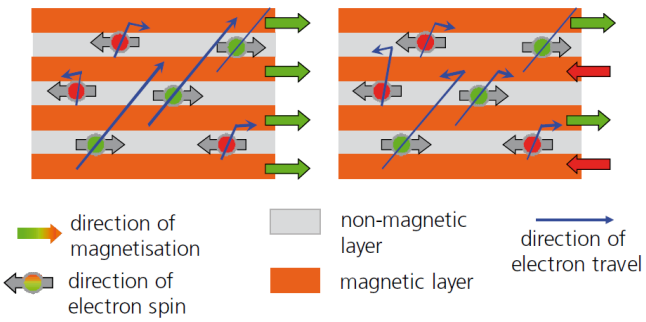

Figure 3.8: GMR - Resistance change of the GMR system depending on the charge carrier spin [28, p. 89]

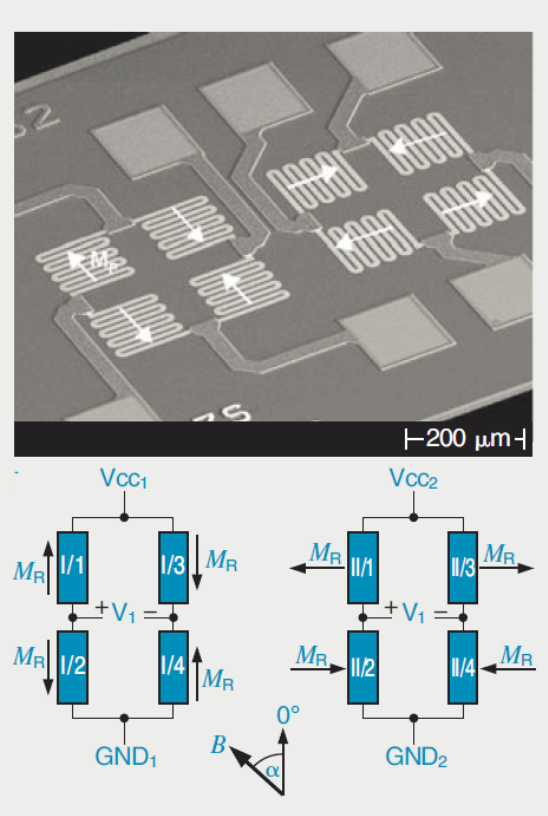

Figure 3.9: GMR - angle sensor using the GMR principle with two measurement bridges. [29, p. 57]

3.3.2.3 TMR

In a Tunnelling Magneto-Resistive (TMR) cell, the intermediate non-magnetic layer of a GMR system is replaced with a thin insulating layer of metal oxide as shown in figure 3.10. With the quantum-mechanical tunnel effect, small currents can flow through the insulating layer when an appropriate voltage is applied on the outer layers. This tunnel current depends on the spin of the tunnelling charge carriers. This spin is dependent on the relative magnetization of the two outer magnetic layers. A parallel magnetization leads to a higher current than anti-parallel magnetization. This results in a change of the electrical resistance depending on the direction of the outer magnetic field. The benefit of TMR elements over GMR elements is the higher sensitivity but on the other hand, the higher complexity in manufacturing is the main disadvantage. The relationship between the angle of the field and the resistance is the same as in a GMR sensor (according to equation 3.4) but the sensitivity is much higher: $\Delta R_{TMR} \sim 50 - 200\%$. [28, p. 89] [27, p. 2]

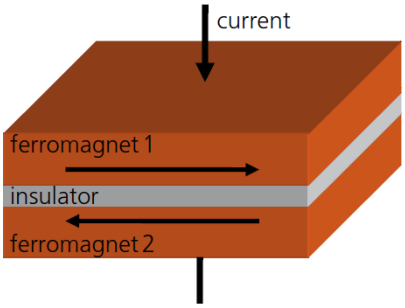

Figure 3.10: TMR - construction of a TMR cell [28, p. 89]

3.3.3 End of shaft angle sensing

As discussed in the previous chapter there exist several methods for measuring the angle of a magnetic field. This field is usually generated with a diametrically magnetized permanent magnet. If this magnet pill is positioned at the end of the rotor shaft with a sensor on top of it, it is called end of shaft angle sensing. The mechanical set-up of a end of shaft sensing method is shown in figure 3.11. The main disadvantage is that one end of the rotor shaft has to be available, which is sometimes not possible from a mechanical point of view.

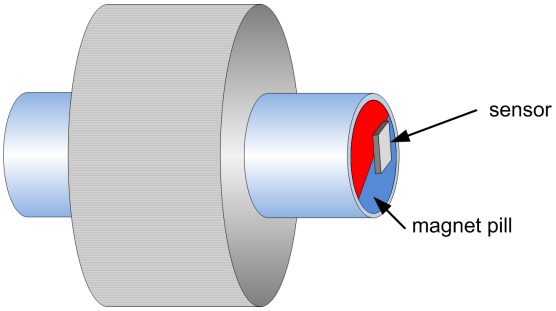

Figure 3.11: End of shaft - position sensing technique

3.3.4 Out of shaft angle sensing

The other method for measuring the angular position of the rotor is the out of shaft angle sensing method. This method is using a diametrically magnetized permanent magnet ring which is placed on the rotor shaft as seen in figure 3.12. The sensor itself is out of the axis of the rotor shaft and measures the field of the ring magnet. This solution has the advantage that no end of the rotor shaft has to be accessible but needs more computing power and is more susceptible to stray fields.

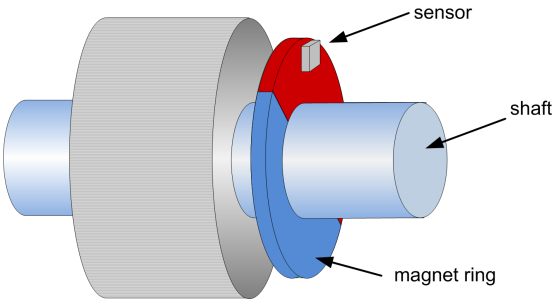

Figure 3.12: Out of shaft - position sensing technique

4

Sensing - current

4.1 Methods

Besides the angular position of the rotor, another information is needed for an efficient motor control - the phase currents as discussed in chapter 1.1.3.2. For measuring the current, different techniques could be used.

4.1.1 Precision Resistor

The most traditional method for current sensing use a precise power resistor. The voltage drop across this resistor is amplified with an operational amplifier and the voltage is then measured with an analog-digital converter of a microcontroller. The tolerance of the resistor value, the temperature dependence and the influence by the inductance of the resistor are defining the accuracy and bandwidth of this measurement. The value of the resistance of the shunt resistor depends on the desired current measurement range and the amplification factor. A higher gain and a lower resistance would result in an increase of noise on the signal. On the other hand higher resistance values and lower gain would improve the signal to noise ratio SNR but the power losses would increase. Therefore this trade-off has to be considered when dimensioning the system. Another drawback is that a shunt-measurement is not galvanic isolated for the case that special isolation requirements are needed. Depending on the voltage levels of the shunt resistor, the operational amplifier has to be selected appropriately (common-mode range). To keep this voltages at low level, a current measurement with precise resistors is usually

done in the low-side path. One big advantage is the lower cost of this sensing principle but sometimes a shunt-current measurement is not possible or impractical due to the disadvantages discussed before. Figure 4.1 shows the current measurement with a precision shunt resistor in the low side path with filtering and offset compensation.

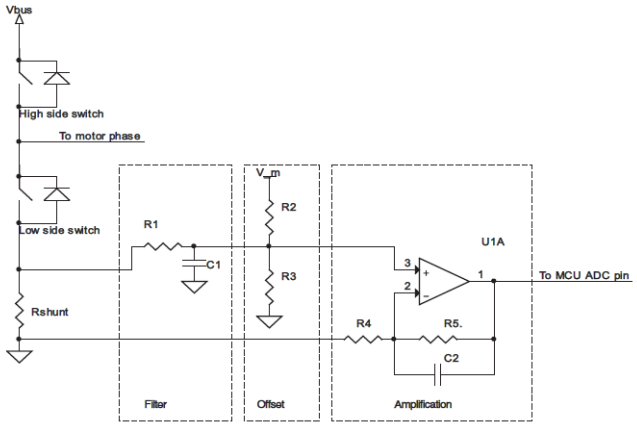

Figure 4.1: Shunt current measurement - principle of a current measurement with precision resistors in the low side path of an inverter[30, p. 1]

4.1.2 Electromagnetic Current Transducer

Electromagnetic current transducers use a magnetic circuit to concentrate the magnetic field created by a current through a wire. This magnetic field is proportional to the current and can be measured with secondary windings or with a hall element. In figure 4.2 the concentrated field is measured with a hall element. The hall voltage is proportional to the current and can be measured easily. One benefit of this method is the galvanic isolation and no insertion losses are implemented with this technique. The main disadvantage of this method is that a magnetic core is needed and therefore the overall mechanical size is higher. [31]

4.1.3 Coreless Hall Effect Sensor

Another principle is to directly measure the magnetic field generated by the current without the flux concentrator. This magnetic field can be measured with a magnetic sensor, e.g. hall plates. With this sensing technique the size of the sensor can be significantly reduced and the sensor does not have the hysteresis effect of a core. A

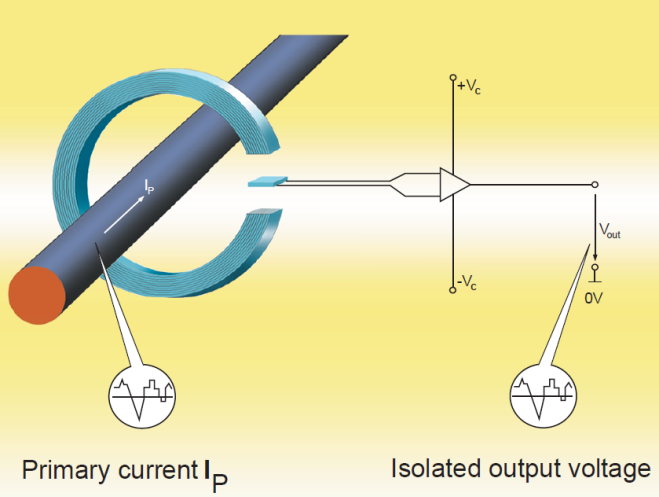

Figure 4.2: Electromagnetic current transducer - principle of the LEM open-loop hall-effect transducer [31, p. 1]

galvanic isolation between the current rail and the interface is possible as well. Figure 4.3 shows the structure of a coreless hall effect current sensor in a SMD package.

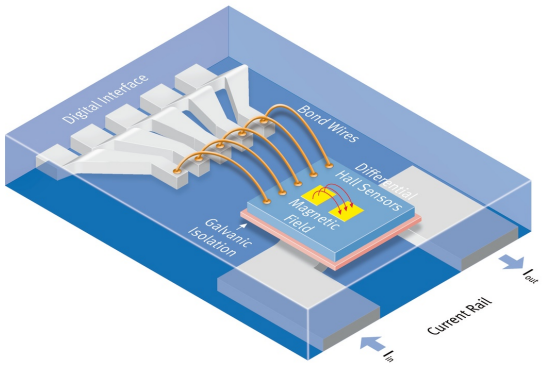

Figure 4.3: Electromagnetic current transducer - principle of the Infineons coreless hall-effect current sensor [32]

5

Implementation

5.1 Scope

The scope of this project is to develop an electric drive demonstrator for Infineon advanced sensor solutions for high performance motor drive implementations. Besides the demonstration effect for different sensing technologies, the development of the demonstrator shall also help to develop system expertise in the area of motor control, especially with respect to feature set and performance requirements of the individual sensors. As a side aspect, the demonstrator can be used to evaluate new concepts for sensing solutions.

5.2 Requirements

The drive demonstrator shall consist of two individually controlled and coupled BLDC motors. One of these motors is used as an active brake and shall feed back into the DC current rail. Furthermore the control of the testbench, as well as the selection of different commutation methods, shall be possible in graphic user interface (GUI). Different rotor position and phase current sensing techniques shall be used in the demonstrator. For including a reference angle measurement, an optical incremental encoder shall be implemented as well. The demonstrator shall be sized so, that it can be used for trade shows and customer visits, thus the mechanical outlines, selected voltage levels, weight and power demand shall be sized to enable a simple installation and operation of the demonstrator.

5.2.1 General Conept

The general concept of a motor control application is shown in figure 5.1. The system consists of a hardware with a microcontroller unit (MCU), a pre-driver with measurement signal conditioning unit and a power stage. The main sensor application in this system is the phase current measurement and the angular position sensing. The pre-driver is the interface between the MCU and the output power inverter. For the demonstrator two of these systems are required, one for the drive motor and another one for the load motor. These two motors are coupled with an auxiliary shaft, which can be used for implementing other sensing techniques.

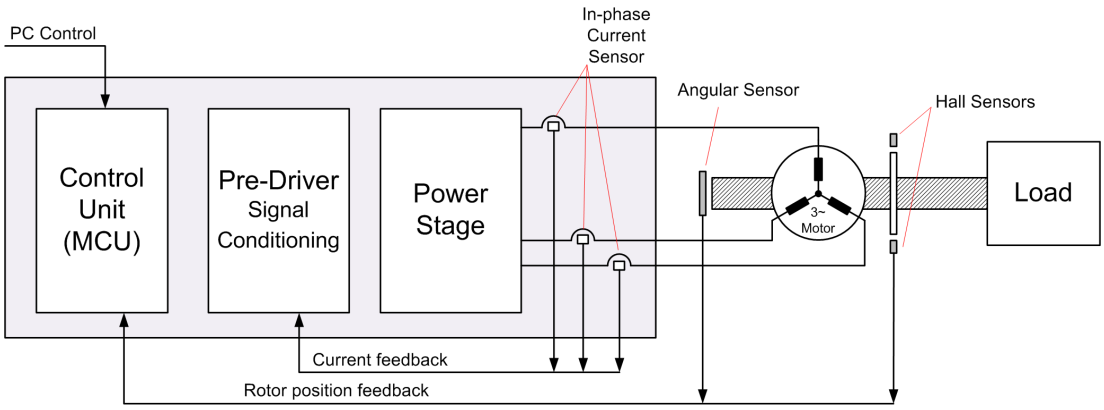

Figure 5.1: Motor Application Concept - General application concept of a motor system

5.3 Motor Selection

For selecting the motor, different parameters have to be considered. First of all, the mechanical size of the complete testbench should be portable for trade shows and customer visits. The nominal voltage of the motor should be in the safety extra-low voltage range, which requires no special isolation. The nominal current range of the motor is defined by the demonstrated current sensor and should be in the range of $50A$. The maximum speed of the motor should be in a range of $3000-4000rpm$. Furthermore the motor should have a double shaft configuration. With these requirements, the selection of suitable motors is narrowed. Two different appropriate motors have been selected:

1. Dunkermotor BG75x50
2. Ohio Electric Motors - Frame 42

Table 5.1 is showing the parameters of both motors.

Parameter	Dunkermotor BG75x50	Ohio Electric Motor 42
Nominal Power	500W	740W
Configuration	double-shaft	
Weight	2,2kg	12,3kg
Magnets	neodymium	ferrite
max. speed	3700rpm	3600rpm
Nominal current	21,2A	52A
pole-pairs	4	2
Nominal Voltage	24V	

Table 5.1: Parameters of selected motors according to the datasheets [5], [6]

5.4 Mechanical Implementation

5.4.1 Requirements

With the selection of the motors, the overall size of the testbench is determined. The motors shall be mounted on a base plate which allows the flexibility of different motor configurations. Furthermore the motors shall be coupled with elastic shaft couplers and shall support the insertion of a sensor setup onto an auxiliary shaft. All rotating parts shall be covered with a transparent cover.

5.4.2 Concept

Figure 5.2 shows the mechanical construction concept with the two coupled motors on a base plate.

5.4.3 Actual Implementation

Figure 5.3 shows the mechanical construction of an Ohio Electric Motor and a Dunkermotor mounted on the baseplate. The baseplate is made of a aluminium strut profile

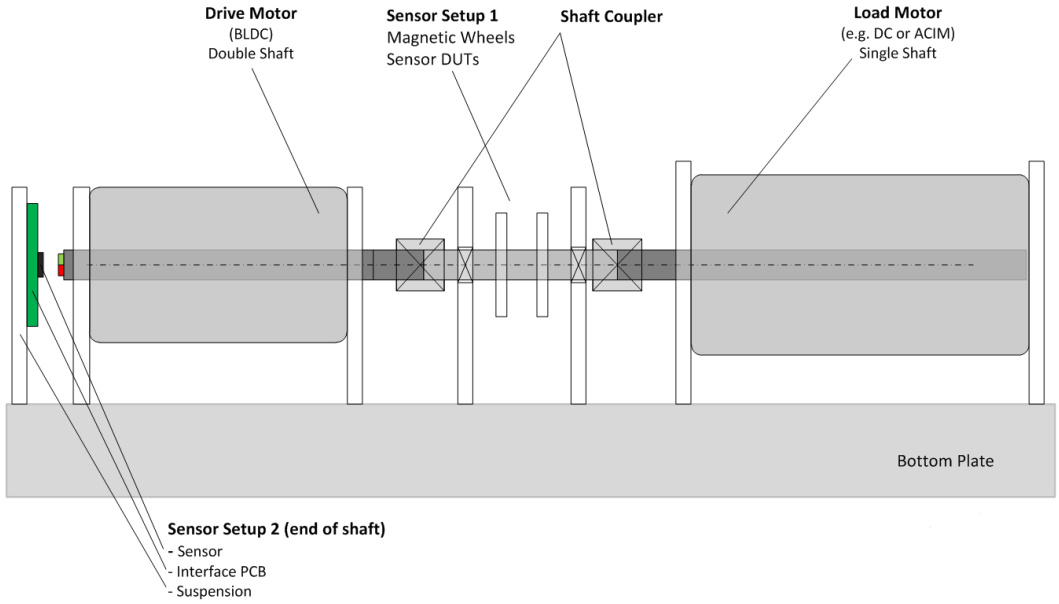

Figure 5.2: Mechanical Concept - Concept of the construction

which allows flexible motor configuration. The Dunkermotor and the bearings are suspended with aluminium brackets. The protective cover is indicated with blue color. The rear shaft of the Dunkermotor is used to mount the encoder and End-of-Shaft rotor position sensor, which will be discussed in chapter 5.4.3.1. Another configuration with two coupled Dunkermotors is shown in figure 5.4. To compensate mechanical alignment tolerances of the whole system, flexible shaft couplers are used. These couplers only compensate misalignment but they support a torsion proof connection.

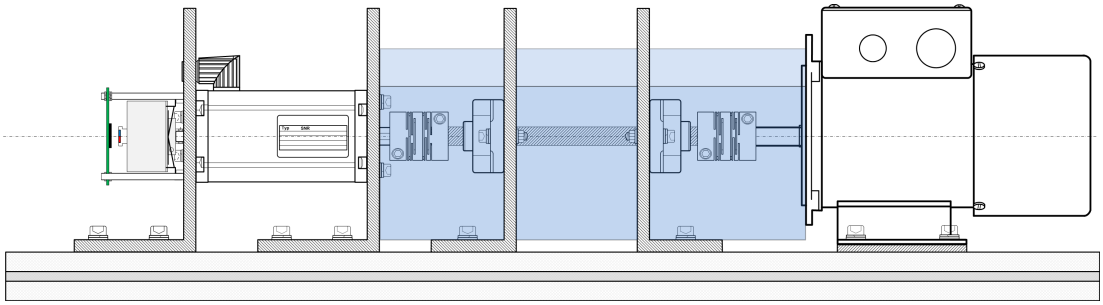

Figure 5.3: Mechanical Implemenation - Dunkermotor and Ohio Electric Motors configuration with protective cover

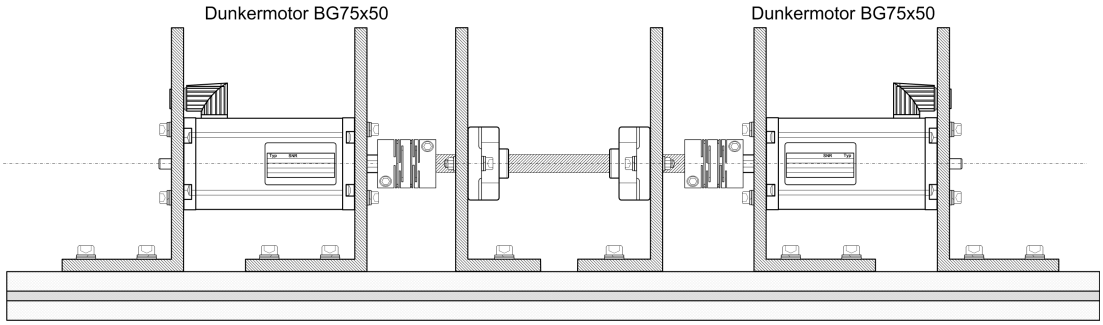

Figure 5.4: Mechanical Implemenation - with two Dunkermotor

5.4.3.1 EOS Encoder

Special care had to be taken for the end of shaft and encoder angle sensing on the rear shaft of the Dunkermotor as the available space is limited. The overall construction can be seen in figure 5.5. For the rotor angle position reference sensing, a Baumer GI342 incremental encoder with 2048 pulses and a hollow shaft has been chosen. The rear shaft of the motor has been extended with an aluminium interface, which is holding the magnet for the end of shaft angle sensing. The PCB is hold in place with threaded rods, which allow a variation of the airgap between sensor and magnet.

5.4.3.2 Final Setup

The final setup shown in figure 5.6. The setup consists of the Dunkermotor on the left side and the Ohio Electric motor on the right side. Two individual hardware sets are mounted on the bottom of the testbench.

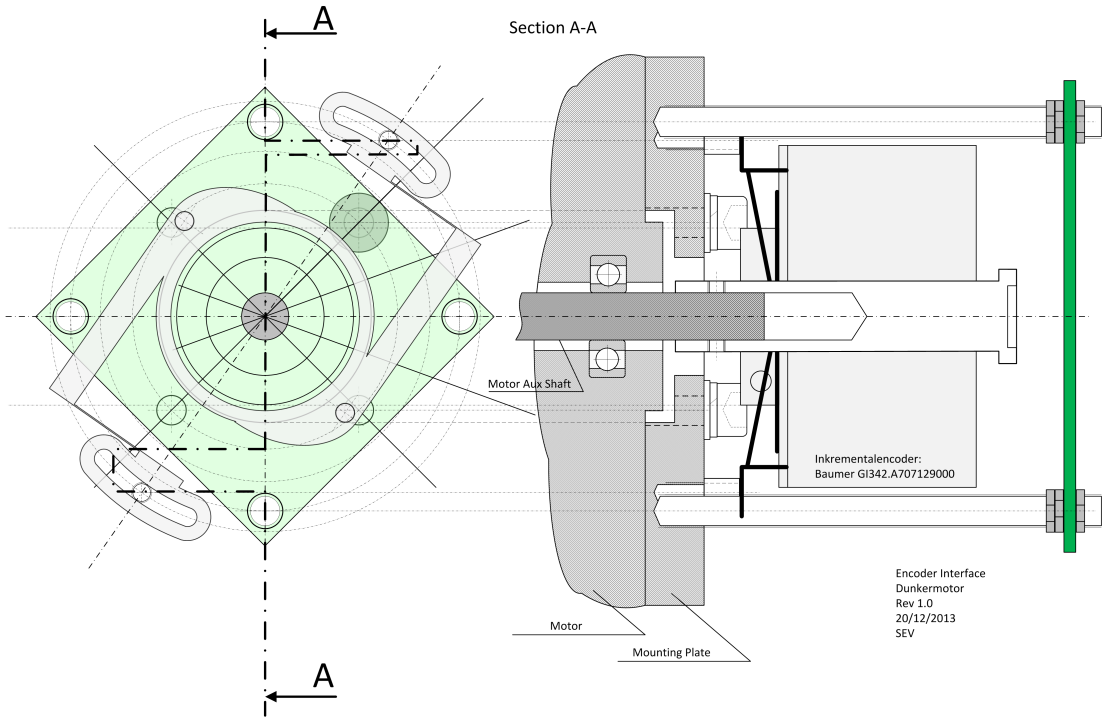

Figure 5.5: EOS and Encoder - mechanical construction of EOS sensing and encoder

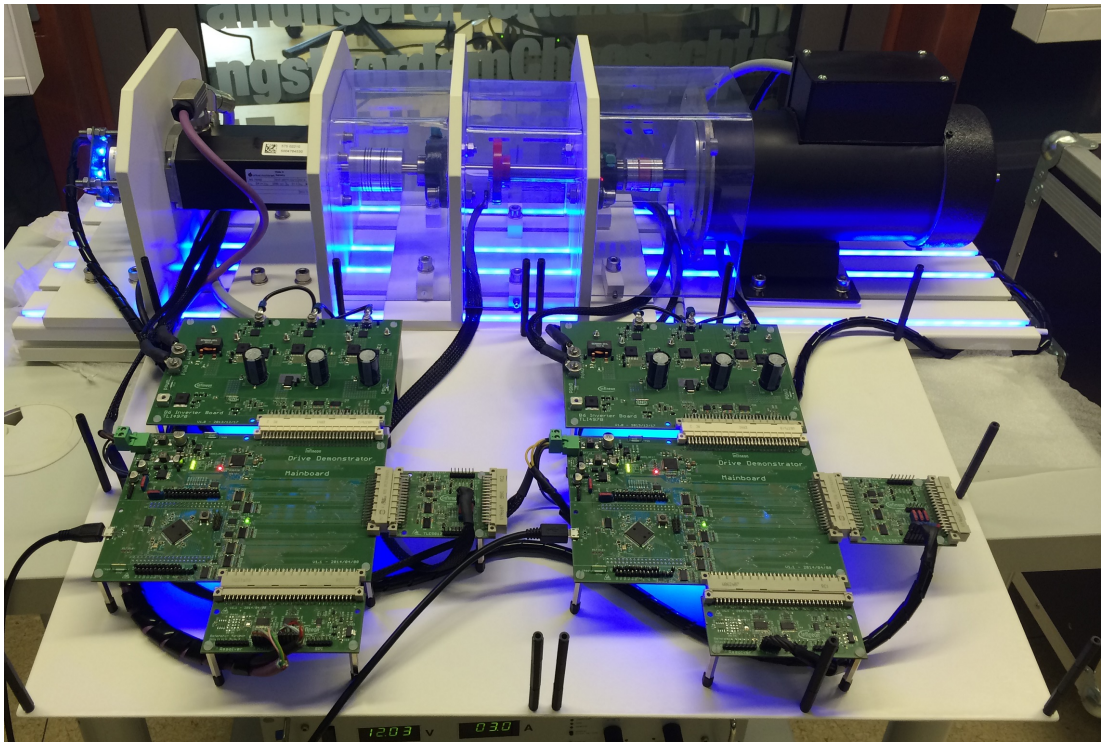

Figure 5.6: Mechanical Setup - the mechanical construction of the Dunkermotor and the Ohio Electric motor

5.5 Hardware

5.5.1 Requirements

The motor bench consists of two BLDC motors, therefore two individual hardware setups are needed. As one of this motor should be used as load motor, the output stage should allow to feed back the current into the supply rail. The key focus on the testbench is to evaluate different sensing principles in drive applications. The different sensing applications are: angular position sensing, rotor position sensing with hall switches and phase current measurement. To enable a full flexibility in terms of power capability and sensor interfaces, both the output power stage as well as the sensor interface boards shall be implemented on separated boards that connect to the mainboard through a standardized connector. The configuration management shall be performed by the mainboard. With the selection of the motor, discussed in chapter 5.3, the voltage capability of the output power stage should be $24V$ and the current capability $50A$.
In order to maximize the flexibility, a spare general purpose sensor interface bus (SIB) shall be implemented on all boards for extendability. The SIB should support interconnections between the sub-boards, as well as connection to the MCU.

5.5.2 Concept

The general hardware partitioning is shown in figure 5.7. The mainboard is connected and controlled via a USB connection to the PC. The pre-driver which generates the gate signals for the B6 power inverter stage is also placed on the mainboard. The PWM output signals and an SPI connection is used to interface the pre-driver. The pre-driver includes operational amplifiers for shunt current measurement signal conditioning as well. The output B6 power stage is implemented on a separate board which is connected to the mainboard. Different current sensing methods require the insertion of different sensor elements into the high current loops. Therefore the current sensing is implemented on the B6 inverter board and different interfaces are foreseen. For supplying the high currents to the inverter stage, the B6 output board has an own supply interface.
In order to automatically detect the different sub-boards which are connected, each subboard includes an EEPROM. In this EEPROM the board type will be programmed

and should be read out by the mainboard on startup. Therefore on each sub-board an I^2C interface is needed to read out the EEPROM.
The speed sensor board is the interface board for the hall switches and the reference speed measurement. An interface for a resolver is foreseen, but not used in the demonstrator, as an incremental encoder is used. The hall switches of the motor will also be interfaced with this board.
The general purpose connector is used for interfacing different sensor sub-boards. The boards should be connected in daisy chain configuration, which allows a maximum extendability. For the end of shaft measurement which should be implemented, an additional interface board is used.
As the implemented current sensor only supports the SPI interface, but should be read out as often and fast as possible a separate SPI interface is used for the inverter board. For the communication with the other boards, a second SPI interface is used.

5.5.2.1 Supply Concept

With the different voltage domains used in the demonstrator, special considerations have to be taken for the supply concept. Figure 5.8 shows the supply concept of the demonstrator. Signals which are going off-board, shall be buffered with an auxiliary voltage of $5V$. These voltages are generated with a voltage tracker device. The microcontroller has a supply voltage of $3.3V$ and therefore voltage level translators have to be used for all communication signals. Another level shifter is needed on the sensor boards to translate the bus voltage to the levels needed by the sensor. With this topology maximum flexibility is achieved as the signals are translated to appropriate voltage levels directly at the sensor board. As the demonstrator should work with only one supply voltage level, a DC/DC converter is used to generate a $9V$ supply rail. A $9V$ rail is used because this voltage is in the operating range for the PSI5[1] interfacing protocol.

[1] PSI5 is a common interface protocol developed for airbag ICs

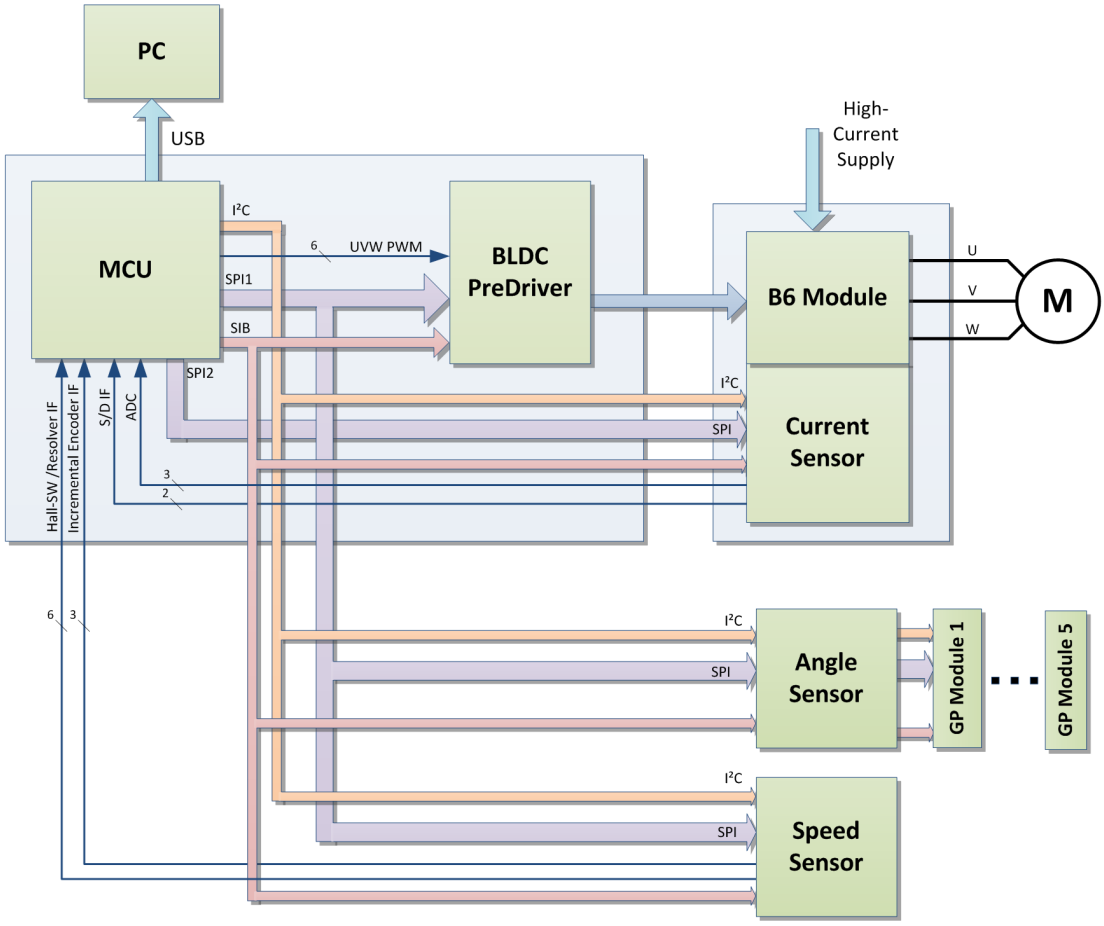

Figure 5.7: Hardware Concept - general hardware partitioning

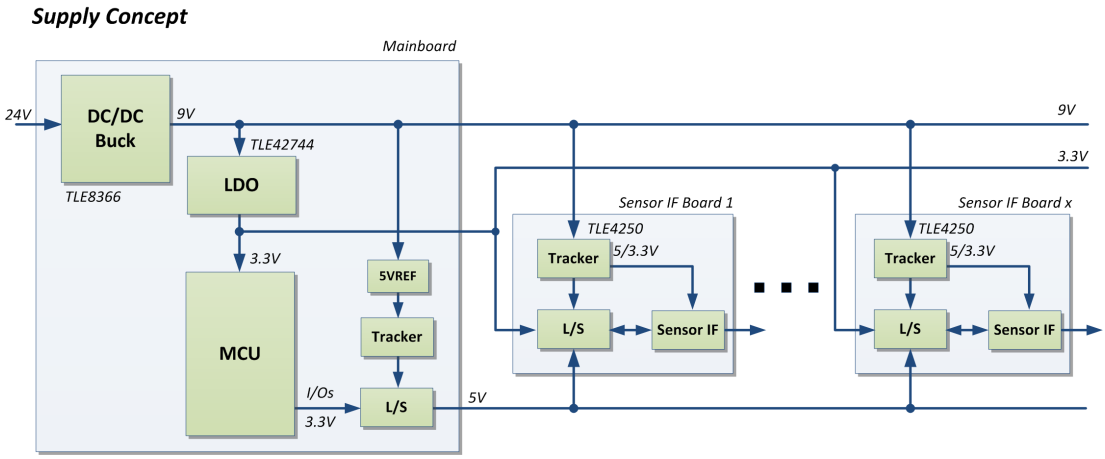

Figure 5.8: Supply Concept - general supply partitioning

5.5.3 Actual Implementation

5.5.3.1 Microcontroller

One central part of the drive demonstrator hardware is a powerful microcontroller. Infineon Technologies offers a wide range of different controllers but for this system, the XMC4500 is used. The XMC4500 has a powerful 32bit ARM Cortex-M4 core which is running at 120MHz clock frequency. 1024KB on-chip flash memory and 64KB on-chip high-speed data memory is included as well as a USB 2.0 interface and various ADCs and DACs. The computing power of the controller is more than sufficient for the complexity of the software. The controller only needs one 3.3V supply voltage and one crystal oscillator. [33]

As the number of I/Os is not sufficient for the complexity of the application, a port extension for outputs and inputs is needed. Due to the serial to parallel conversion, the access time on these ports is relatively high. Therefore these ports are only used for non time critical functions. The serial to parallel logic is interfaced with an SPI interface of the MCU as shown in figure 5.9. U6 and U11 are the serial to parallel shift register for the output extension and U7 is used for parallel to serial conversion for the inputs. As the MISO Line of an SPI interface is usually an open-drain line, a TriState Buffer (U8) has to be implemented.

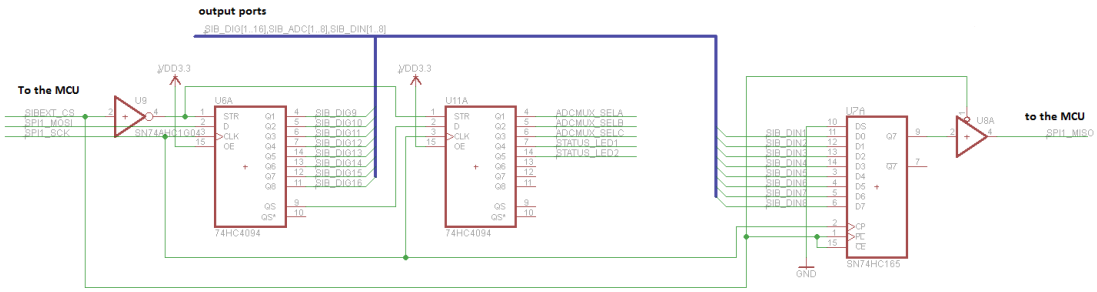

Figure 5.9: Schematic Port Extension - schematic of the port multiplexer

5.5.3.2 PreDriver

Another essential component of the mainboard is the pre-driver device. The Infineon TLE9180 - 3-Phase Bridge Driver IC has been selected. It is completely configurable via the SPI interface, supports 100% duty cycle output and has an operation voltage up to

60V. Furthermore it also includes three flexible operational amplifiers for shunt current measurement signal conditioning. With the TLE9180 several protection functions are implemented as well, e.g. voltage supply monitoring or failure detection of the output stage. [34]

5.5.3.3 Supply

As discussed in chapter 5.5.2.1 different supply domains are used in the demonstrator. Figure 5.10 shows the schematic of the power supply on the mainboard. The 9V rail is realized with a DC-DC Step-Down Voltage Regulator TLE8366, which supports an adjustable output voltage and a maximum output current of $1.8A$. [35] The voltage can be adjusted according to equation 5.1.

$$V9 = 0.6V \cdot \frac{R6 + R7}{R7} = 0.6V \cdot \frac{12k + 820}{820} = 9.38V \tag{5.1}$$

The general $3.3V$ supply voltage for the mainboard is generated with a linear voltage regulator TLE42744 (U3). The regulator is supplied either from the $9V$ supply rail or if an additional supply is not present, via the USB interface. The sensor interface bus is using $5V$ signal levels and therefore a voltage tracker has been foreseen. The used voltage tracker TLE4254 (U18) supports an adjustable output voltage. This $5V$ rail is generated with respect of the $3.3V$ as the tracker supports a higher output voltage than the reference voltage. The output voltage can be calculated according to equation 5.2.

$$V_{BUS} = 3.3V \cdot \frac{R8 + R9}{R9} = 3.3V \cdot \frac{2.7k + 5.1k}{5.1k} = 5.05V \tag{5.2}$$

As the sub-boards could use either a $5V$ or $3.3V$ supply voltage, an additional voltage tracker is used to buffer the $3.3V$ voltage reference for the voltage supply on the sub-boards. As $5V$ reference the SIB bus voltage is used.

5.5.3.4 Bus voltage level translation

All digital I/Os are level shifted from the $3.3V$ MCU supply voltage to the $5V$ bus supply voltage and vice versa. One limitation is that the selected level shifters (TI SN74LVC8T245) are only unidirectional, this means that data on one port can only be transmitted or received. For the analog inputs a protection circuit is implemented

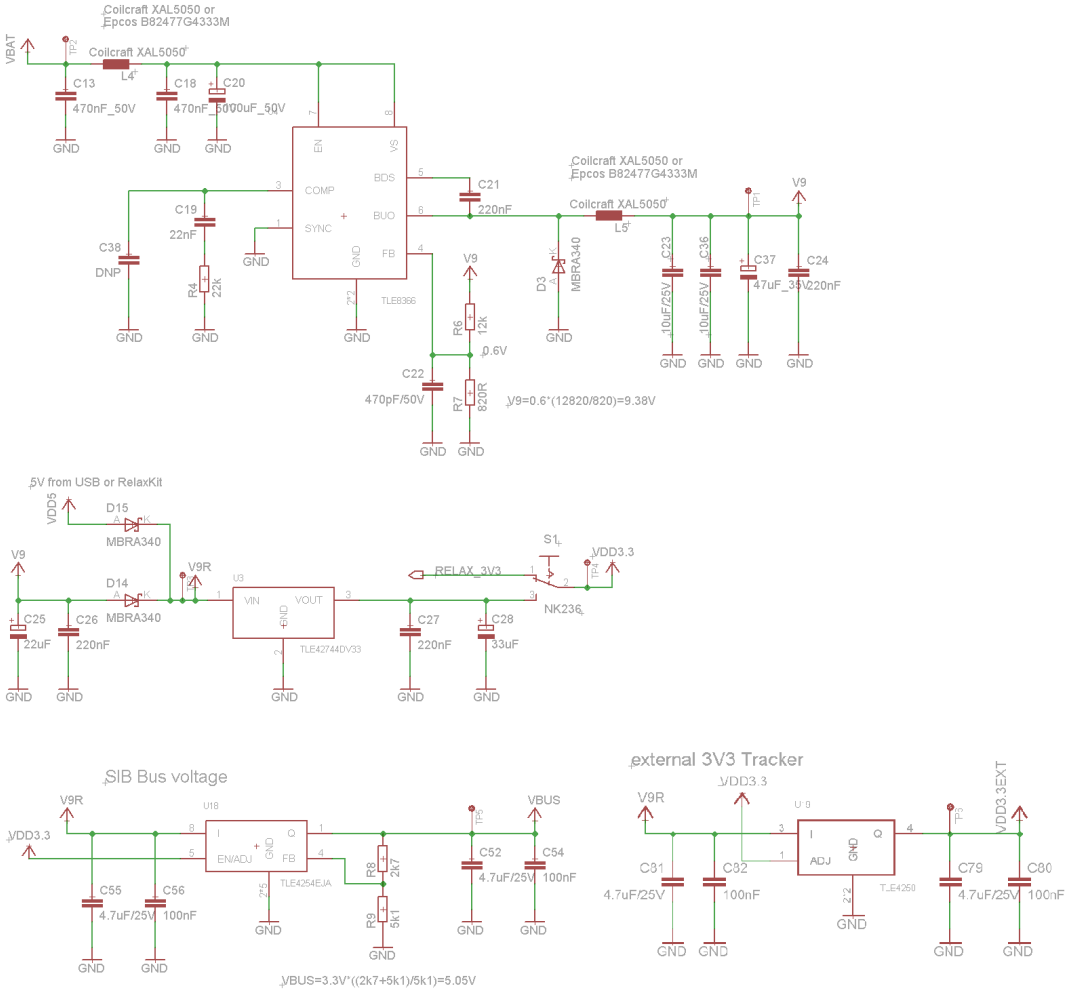

Figure 5.10: Supply Schematic - mainboard supply schematic

to protect the microcontroller from voltages higher than $3.3V$ as well as voltages lower than $0V$. The protection circuit realized with Schottky diodes and additional low-pass filters can be seen in figure 5.11.

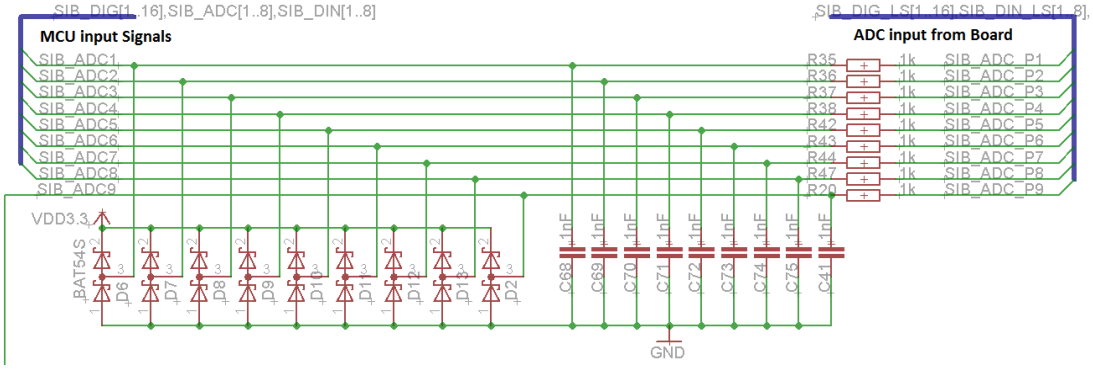

Figure 5.11: Analog Schematic - analog inputs protection and filtering

5.5.3.5 B6 power inverter sub-board

In order to address different current measurement techniques, two separate B6 inverter boards are created. One board uses the shunt current measurement and the other one uses an in-phase current measurement with current sensors. The different options for a current measurement can be seen in figure 5.12. Boards for option 1 and option 3 have been developed for the demonstrator. Option 1 shows the principle of the shunt current measurement in the low-side path of the inverter. With this method the current in the phase is measured indirectly and have to be calculated depending on the switching state of the output MOSFETs. With option 3 the phase currents are measured directly with the Infineon TLI4970 hall effect current sensor.

Figure 5.13 shows the schematic of the B6 inverter board with shunt current measurement. The measured voltage from the shunts are filtered and will be amplified in the pre-driver. Three $1000\mu F$ electrolytic capacitors are used to buffer the supply voltage. The power inductor L1 and the capacitors C40 and C41 form a Pi-Filter. With this filter noise caused by the fast switching of the inverter MOSFETs is filtered. The MOSFET used in the inverter stage is the Infineon IPLU300N04S4-R7, which is specified for a $V_{DS} = 40V$ and an $R_{DS,on} = 760\mu\Omega$. [36]. For limiting the slew-rate $(\frac{dV}{dt})$ of the switching MOSFETs, gate series resistors are used. The capacitors between

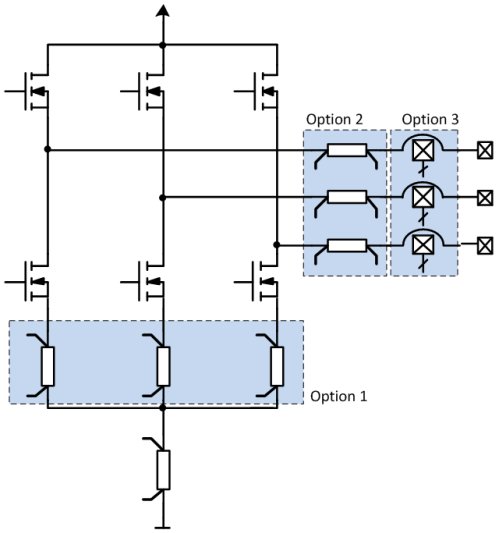

Figure 5.12: Current measurement - general hardware partitioning

the gate-source and gate-drain terminals of the inverter MOSFETs (e.g. C2, C11 at MOSFET Q1) can be used for further decreasing the slew-rate, but are not used in the current hardware. In order to be able to decrease the deadtime, which is the time between the switching of the high-side and low-side FETs, a non-symmetric discharge circuitry is used. The switching time to the ON-state of the FET is limited by the series resistance and the switching to the off-state is done faster via the diodes parallel to the resistors.
The other B6 inverter board is very similar to the first one, but instead of using three shunt resistors in the low side path of the inverter, three current sensors are directly measuring the phase currents. For the current sensor the coreless Infineon TLI4970 is used, which supports a measuring range of $\pm 50A$ within an accuracy of $\pm 1\%$ [32]. The current sensor can be read out via an SPI protocol, but for programming the device, the Serial Inspection and Configuration Interface (SICI) has to be used. Therefore the SICI interface is implemented as well.

As the B6 inverter stage is also used for the load motor to feed back to the DC current rail, a overvoltage protection has been included. During dynamic speed changes of the drive motor and due to the inertia of the whole system, it could be possible that current is fed back to the supply rail without energy absorption by the drive motor. If this state occurs, the voltage of the DC rail could raise and damage the system.

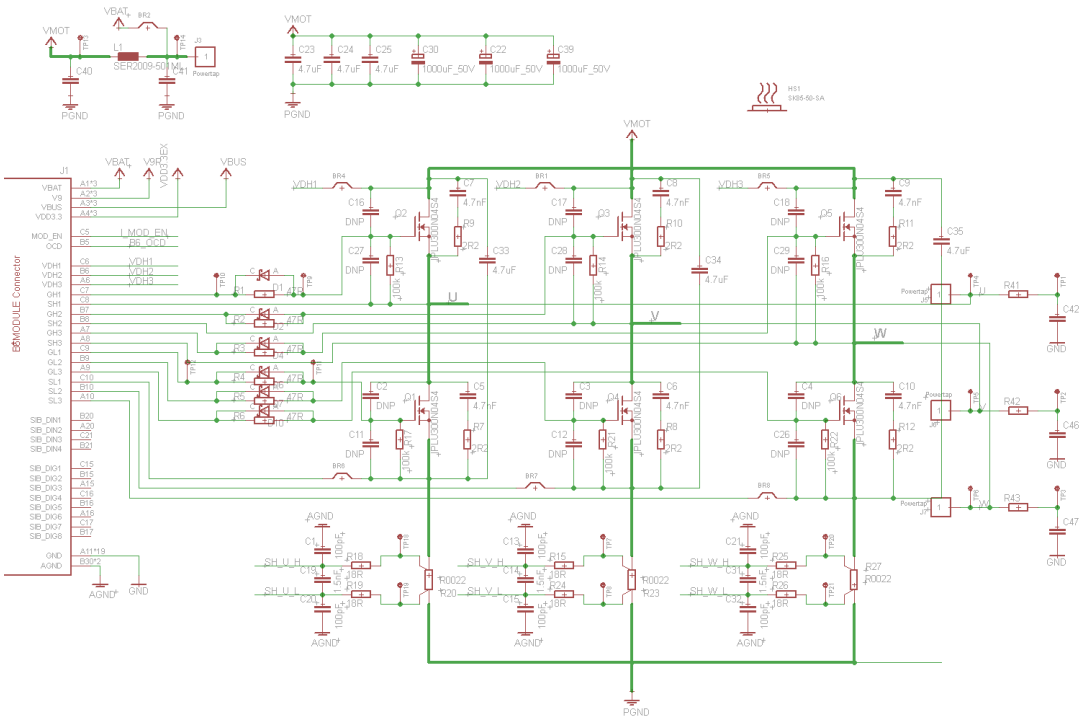

Figure 5.13: Inverter schematic - B6 output stage with shunt current measurement

To prevent this, the rail will be loaded with a resistor by the overvoltage protection circuit, if the voltage exceeds a defined value. Figure 5.14 shows the schematic of the overcoltage protection. If the supply voltage exceeds the zener voltage of diode D3 and D5, the power MOSFET Q7 will be switched on. A hysteresis prevents an oscillation of the switch. The protection circuit is implemented on the B6 inverter board, but has not been tested.

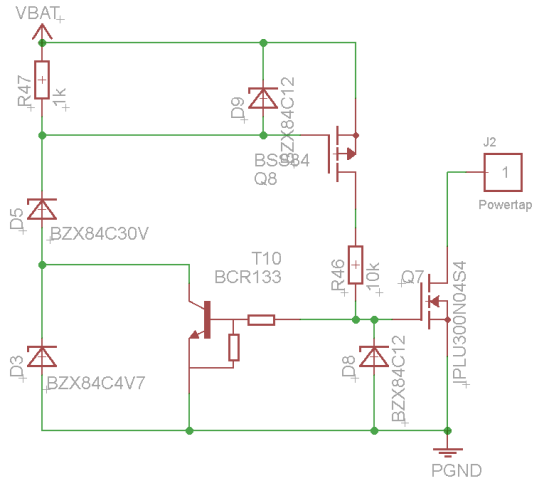

Figure 5.14: Overvoltage protection - circuitry for protecting the supply rail from ramp-up

5.5.3.6 Speed Sense Sub-board

The Speed Sense sub-board is used for interfacing the incremental encoder and the hall-switches of the motor. To enable the operation of the sub-board, the module has to be activated, in order to enable the power supply of the sub-board. Depending on the reference voltage of the voltage tracker, the sub-board could be either supplied with $3.3V$ or $5V$. Figure 5.15 shows the schematic for the power supply of the sub-board. This supply schematic is the same for all sub-boards, except the speed sense board where the additional $12V$ rail is generated for supplying the incremental encoder.

5.5.3.7 Angle Sense Sub-board

For interfacing the different sensors, several boards can be connected on the General Purpose connector. One of these general purpose boards is the angle sense sub-board,

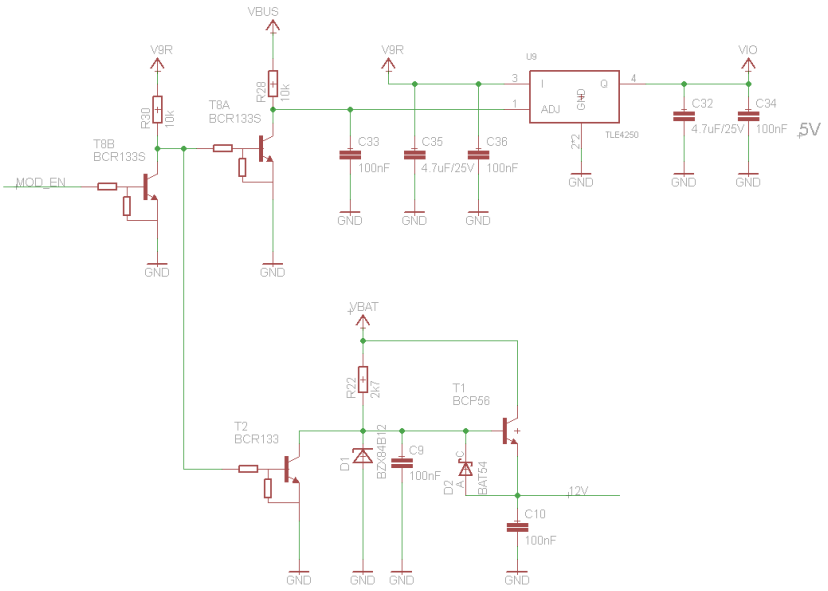

Figure 5.15: Supply schematic - sub-board supply schematic

which is used to interface the angular position sensors Infineon TLE5009 and TLE5012. Both sensors are using the GMR principle discussed in chapter 3.3.2.2. The difference between these two sensors is that the TLE5009 has an analog output and the TLE5012 a selectable digital output. For a fast readout of the angle the incremental interface mode of the TLE5012 is used.

As several sub-boards could be connected to the general purpose port, the MCU should be able to detect the connected sub-boards. Therefore a circuitry for addressing the EEPROMs is implemented. The schematic for one sub-board is shown in figure 5.16. U5 is a D Flip-Flop and forms a shift register with other connected boards. On the Mainboard a high level will be set on the DET_DIN pin and the DET_CLK starts pulsing. The DET_SENSE pin is connected via a wired "OR" from all boards and is read back from the MCU. If the DET_SENSE signal turns to "low" state, the MCU stops the clocking. The number of pulses sent until DET_SENSE turns to "low" state determines the number of connected boards on the general purpose connector. Connected to the DET_CLK is a counter on each sub-board. If the shifted "high" level is reaching the sub-board, the counter will stop counting. This way the first sub-board in the chain has the highest count value and the last one, the lowest. The output of the counter

is then used as device address for the EEPROM. The EEPROM supports up to eight addresses, but two are needed for the Speed Sense and Inverter board. This results in a maximum of six additional connected general purpose boards.

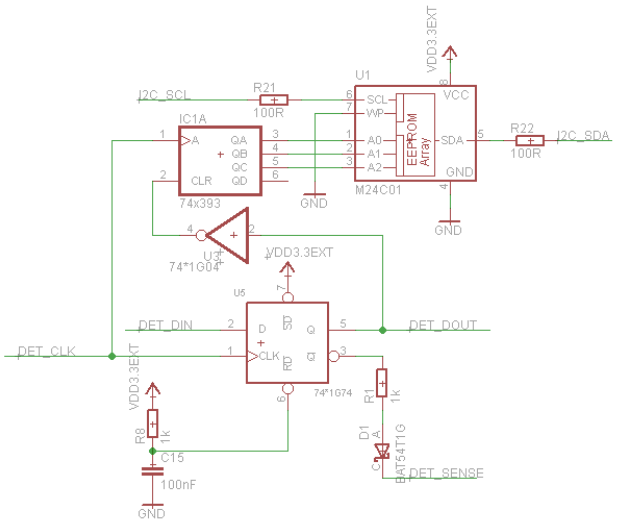

Figure 5.16: EEPROM addressing schematic - sub-board incremental addressing

5.5.3.8 Layout of B6 power inverter sub-board

Special attention has been paid on the layout of the power inverter stage, as the current capability should be around $50A$. There are no special requirements regarding the isolation as the output stage is designed for a $24V$ application. In order to distribute the current evenly a four layer board with $70\mu m$ thick outer copper layers is used. The buffer capacitors are placed as close as possible to the inverter stage. For cooling the power devices, a heatsink is mounted at the bottom of the PCB. For a better thermal conductivity, thermal vias are placed around the power MOSFETs and current sensors. Figure 5.17 is showing the layout of the inverter stage. The high current paths of the inverter are indicated and are held as short as possible in order to reduce the inductance of the output stage. One of the bottle necks of the output stage is the common shunt resistor in the low side path of the circuit. The manufacture and assembled drive demo PCBs can be seen in figure 5.18.

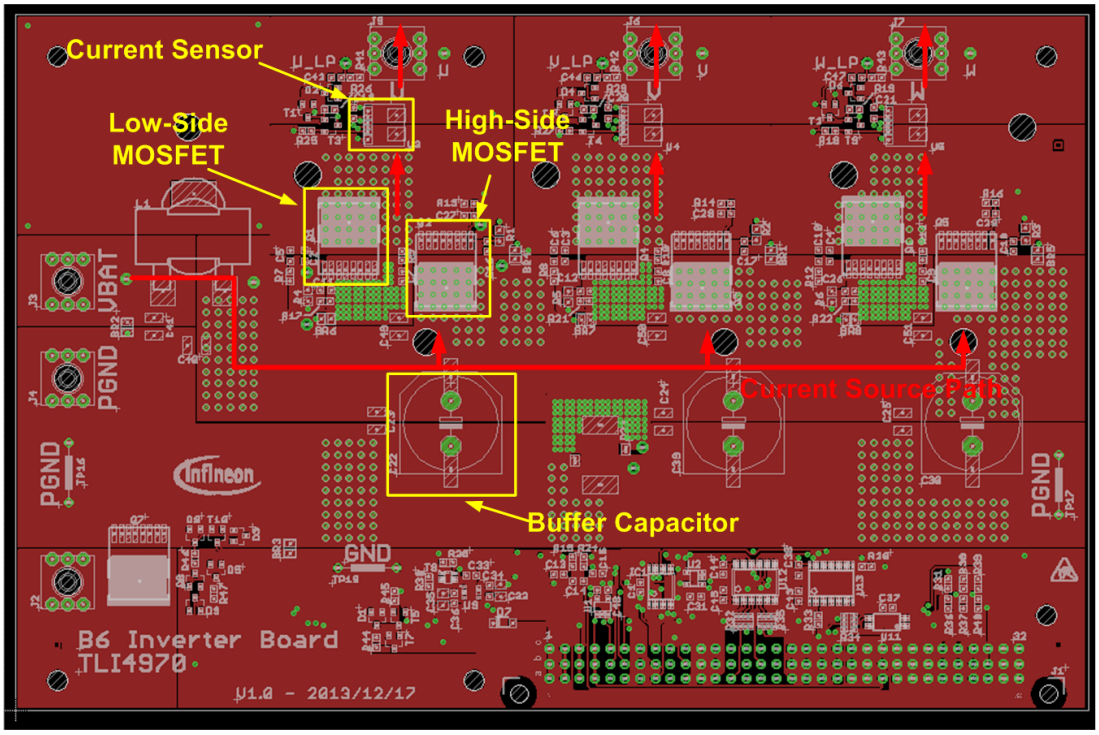

Top Layer

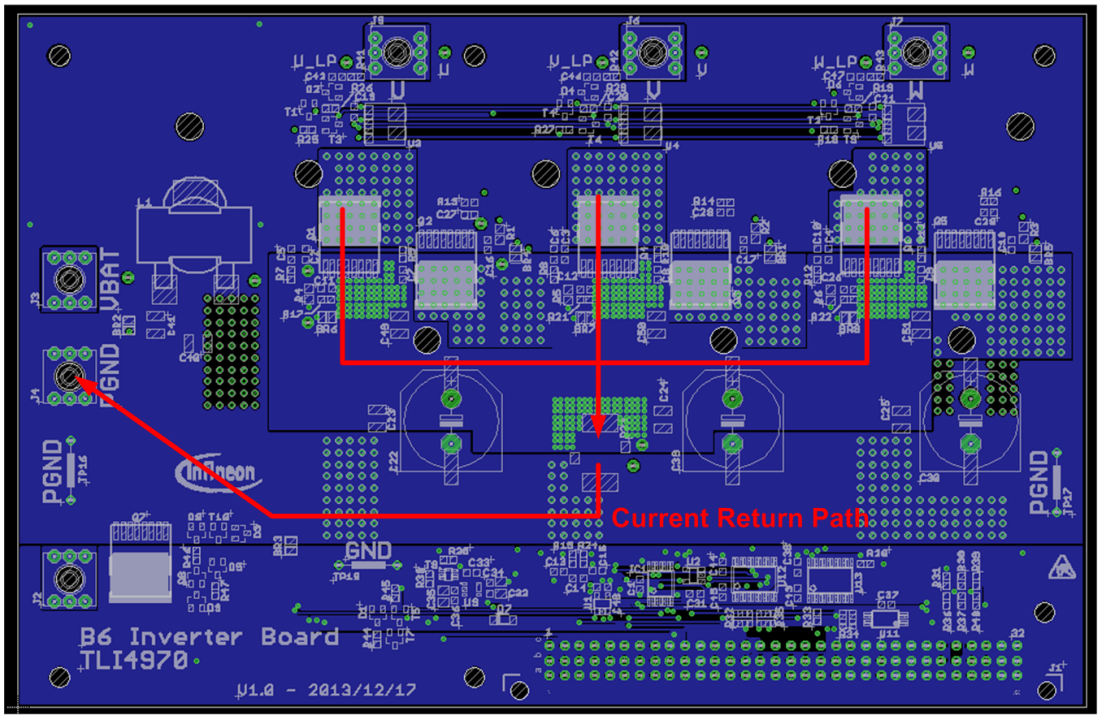

Bottom Layer

Figure 5.17: B6 Power Inverter with TLI4970 Layout - top and bottom layer with current path of the inverter stage

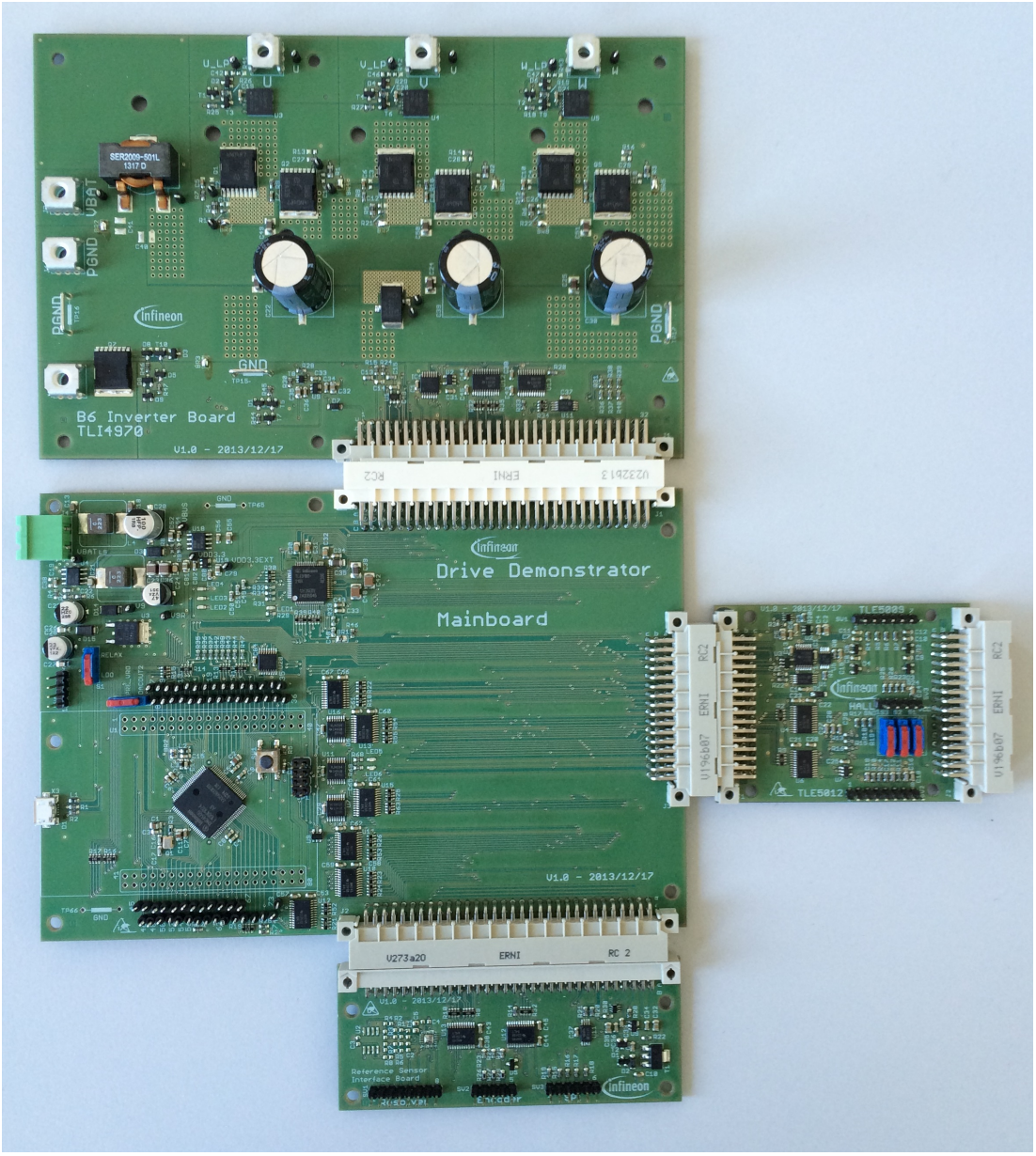

Figure 5.18: Hardware - picture of finished hardware

5.6 Software

5.6.1 Requirements

5.6.1.1 Firmware

The firmware shall be implemented in a modular way. Since the drive demo has to support multiple hardware configurations, all hardware components shall be abstracted through a separate hardware abstraction layer that provides low-level driver functions to the upper control layers. The configuration management shall detect the available hardware components and shall enable the required low level functions to provide the required functionality to the higher software layers. In case multiple hardware selections are available for a particular sub-function (e.g. both encoder and end-of-shaft measurement are available for rotor position measurement), the configuration management shall ensure that a default setup is selected, prevent from potential hardware conflicts on the main board and allow for alternative input selections through the GUI interface layer.

The firmware shall be based on a generic real-time operating system (RTOS) layer for functions which are not time critical (e.g. USB communication). On the drive application layer, the firmware shall support both speed control as well as position control as shown in figure 5.19. The loading of the drive motor is determined by the load motor. Four quadrant controls (drive/brake forward/reverse) shall be implemented, as the same hardware is used for the drive and the load motor. All relevant parameters for the individual control loops (PI Controllers) shall be adjustable through the GUI interface.

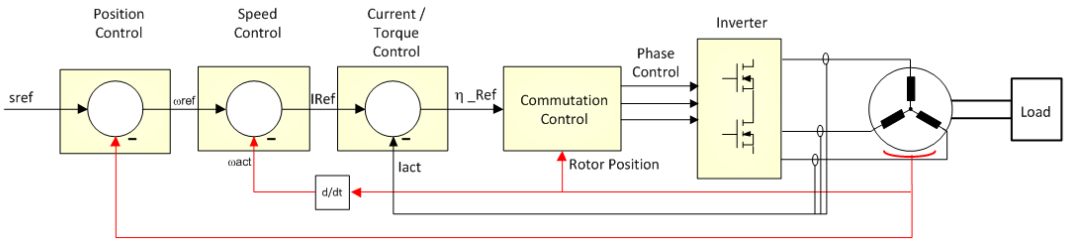

Figure 5.19: Firmware requirements - structure of the modular firmware

5.6.1.2 PC GUI Configuration Control

The configuration control section of the GUI shall provide all information regarding the current hardware configuration. In case multiple selections are possible (multi-purpose hardware), the GUI shall enable a selection of the individual options.
The following parameters shall be configurable through the Configuration window:

- PID control parameters for all control stages (FOC, speed, position controller)
- Limit parameters for all controllers (angular speed, torque, current)
- Operating modes (Block, Sinusoidal, FOC)

The Stimulus Control section shall be used to control the drive and load motor. The primary input to the system is the drive control mode. The following control modes shall be selectable:

- (Angular) position control
- Speed Control
- Duty Cycle Control
- Current / torque control (FOC)

In Angular position control mode, an absolute angle can be entered. Once acknowledged the rotor will be driven into the requested angular position. In Speed Control mode, the RPM speed of the drive shaft is controlled. In this mode, the GUI shall display the requested and current speed value as well as the drive motor current information. In case of FOC, Id and Iq shall be displayed, too.
To enable automatic operation of the system, the GUI shall provide an auto-drive mode. Depending on the selected mode of operation (Position or Speed control) minimum and maximum values for angular position or speed can be entered. The GUI shall then generate a stimulus to operate the drive system in the selected range.

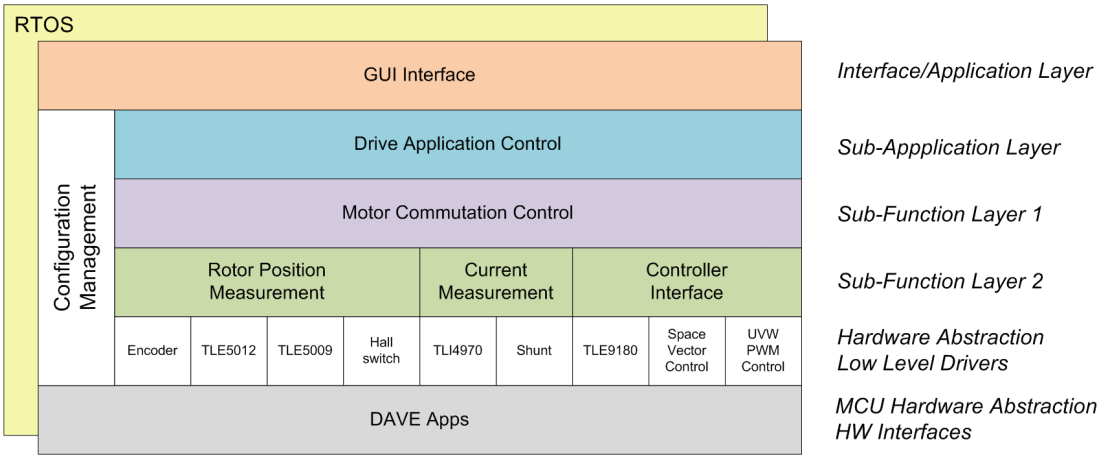

Figure 5.20: Firmware structure - topology of the firmware

5.6.2 Concept

5.6.2.1 Firmware Structure

As discussed in chapter 5.6.1.1, the firmware shall have a layered structure in order to maximize flexibility. Figure 5.20 is showing the layered approach of the software.

The bottom layer is the MCU abstraction layer and consists of the basic routines for accessing the hardware of the microcontroller. The next layer comprises the low level device drivers and is another hardware abstraction layer. In this layer all components and modules are abstracted, e.g. the different angle sensing techniques, current measurements or power inverter output. The sub-function layer 2 manages the handling of the different modules of the hardware abstraction layer and provides a unified interface for the upper application layers. This layer together with the hardware abstraction layer are the main layers to support the flexibility in the hardware as well as the software configuration. For implementing a new sensing technique, a new block is implemented in the hardware abstraction layer and the sub-function layer 2 has to be adapted for interfacing the new technique.

In the sub-function layer 1, the motor commutation control is implemented. All different operating modes (Block, sinusoidal and FOC) are implemented here and can be controlled from the application layer. This layer contains the speed and position controllers and is used to control the motor commutation. The communication with the PC is realized in the GUI interface layer. This layer contains the routines of the

USB command handler, which distributes the incoming command and returns desired data.
Besides all the stacked layers, there exist the configuration management layer, which can interface all of the other layers. In this layer, functions of all sub layers are configured and the sub-board management is done. This includes for example the configuration of the output functions (SVM, PWM control) for different sensing techniques (e.g. current sensor, three-shunt measurent, single-shunt current measurement) as well. Furthermore this layer consists of different diagnostic functions, e.g. data loggers or real-time feedback to the PC GUI.
If applicable, functions from theses layers are implemented in a RTOS environment in order to maximize the flexibility. The RTOS is used as a platform for non time critical functions, e.g. the USB communication or data loggers.

5.6.2.2 USB Commands

The USB communication between the MCU and the PC GUI, is bidirectional and can be initiated either by both sides. The USB interface is realized via a VirtualCOM port, which is emulating a serial interface on the USB physical layer. With this approach it is possible to communicate with the MCU with different programs or programming languages as the serial port interface is widely supported (e.g. Matlab, LabView, C# , Visual Basic, ...).
The serial port is using a byte-wise communication and a dataframe consists of one ID byte and a variable number of data bytes. A typical structure of a communication frame is shown in figure 5.21. All command frames have a predefined length, except a status message frame, which is used for displaying status messages on the PC GUI. This frame has a variable number of data bytes (up to 100 bytes).

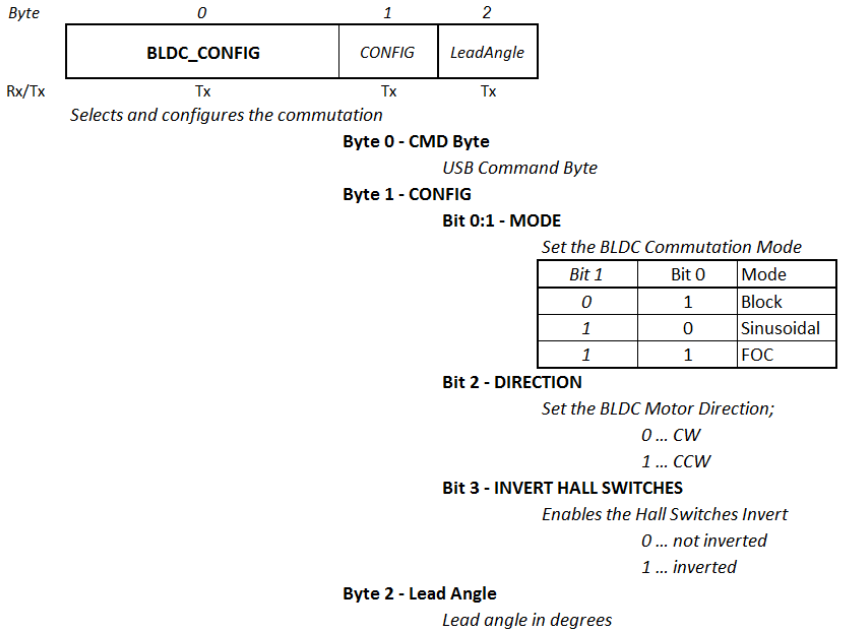

Figure 5.21: USB communication - structure of a dataframe

5.6.3 Actual Implementation

For the implementation of the firmware, Infineon IDE Dave 3 is used. The code is written in C and is compiled in Dave with ARM GCC. It comprises a MCU abstraction with so-called "Dave Apps", which are available for various different applications. These apps can be configured via a graphical interface in the IDE. For example the USB VirtualCOM, ADC, SVM or the RTOS is implemented with a Dave app.
The windows GUI software is written in *C#* . Microsoft Visual Studio Express 2014 *C#* is used as IDE for the Windows Forms project.

5.6.3.1 USB Communication

Figure 5.22 shows the structure of the USB communication between the demonstrator and the GUI. On the PC side, the sub functions can transmit the data via the virtual serial port driver to the MCU. On the MCU side the Virtual serial port Dave app is receiving the data and after processing the command, the requested functions will be executed. For transmitting data from the MCU to the PC the same method applies on the firmware side. In the GUI, a separate thread is polling the serial interface and invokes a function in the main form. This function processes the incoming data und

executes the requested function. The receive thread also separates the data frames from the byte stream of the interface. Therefore the number of data bytes in each frame has to be known. When receiving a status message frame ID, the stop byte is the carriage return.

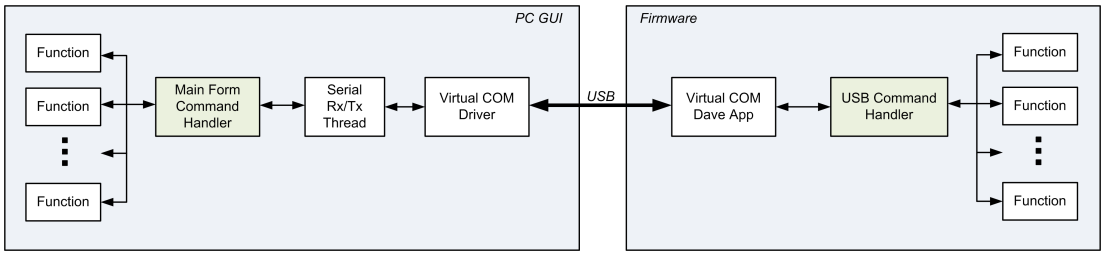

Figure 5.22: USB communication - structure of the USB communication

5.6.3.2 Commutation sequence

The primary part in the firmware is the commutation of the BLDC motor. The output of the sinusoidal signals is done via the SVM - PWM app from Dave. A PWM frequency of $20kHz$ and a 7-segment SVM generation is selected. In a 7-segment SVM scheme, all three phases are switching and the passive vectors are equally distributed. Furthermore the current measurements are triggered from the SVM module. The commutation routines are executed every PWM period. Figure 5.23 shows the commutation sequence, which will be executed every PWM period from the Sub-Application layer.

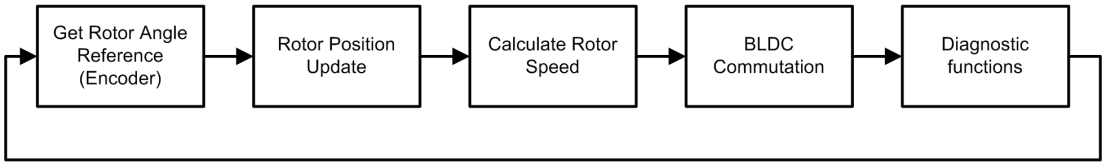

Figure 5.23: Commutation sequence - functions will be executed every PWM period

For determining the reference rotor position of the encoder, the position interface of the MCU is used. This basically maps a counter on the phase A and B inputs and counts with every edge of the signals. The counter will be cleared on every index pulse. The count value of the counter is now proportional to the angular position of the rotor. As the incremental interface is selected from the TLE5012, the same procedure is done for the angular position sensing with the TLE5012. The calculation of the rotor

speed in incremental mode is done via counting pulses of the encoder. The time taken for counting 100 pulses is measured and with this information the rotor speed can be calculated.
When the hall sensors are used for rotor position sensing, the angle is only known at specific points. Therefore the angle has to be interpolated between the known points. As the signal of the hall sensor jitters, a moving average filter for the interpolation is used. With every hall sensor change, the angle is synchronized. This results in a non-monotonous angle function, but best performance in commutation. The time between a full hall pattern sequence is measured and used for calculating the rotor speed.

5.6.3.3 Block Commutation

Figure 5.24 is showing the structure for block commutation. In the first step the field angle is calculated and the lead angle is added. In the next step the current hall state is calculated from the angle. If clock wise (CW) direction is selected, the hall pattern is inverted. When the hall state or the duty cycle value changes, the inverter output pattern is updated accordingly.

5.6.3.4 Sinusoidal Commutation

For sinusoidal commutation, the PWMSVM Dave app is used to output the according PWM values. The input values for the SVM unit are the field angle and the amplitude value.

5.6.3.5 Field oriented control (FOC)

For the FOC, the Motorlib is used from Dave. In this library, the park, clarke, PI-controller and coordinate conversions are already implemented. The FOC commutation is implemented as discussed in chapter 2.3.3. The actual structure programmed in the firmware for speed control is shown in figure 5.25.

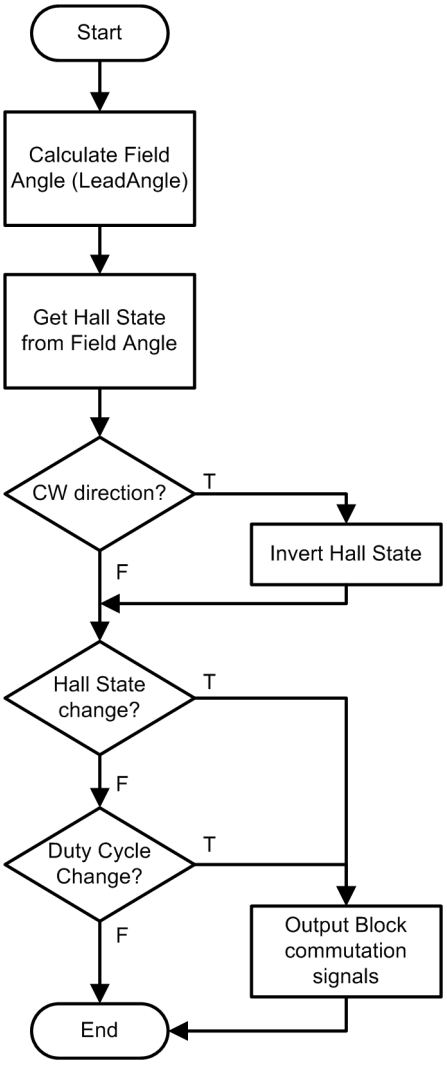

Figure 5.24: Block commutation - structure

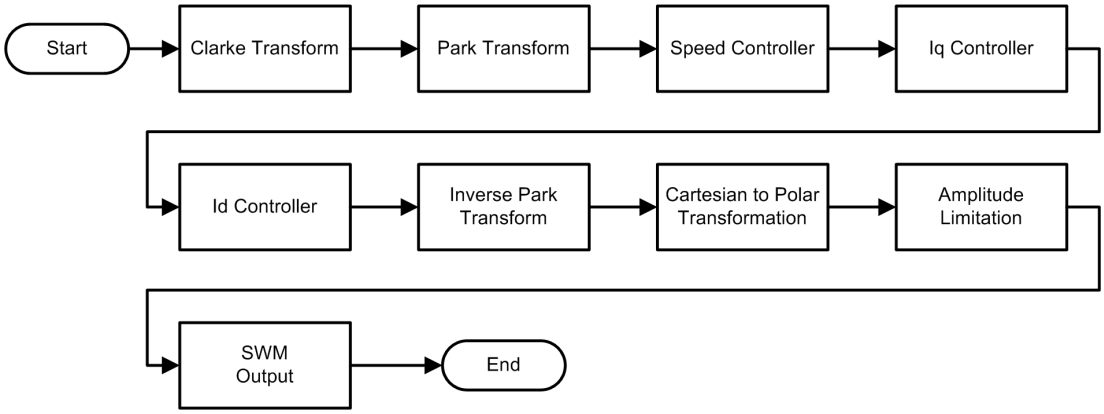

Figure 5.25: FOC commutation - structure

5.6.3.6 GUI interface

An overview of the possible operating modes of the motor with the demonstrator is shown in table 5.2.

Commutation method	Operating modes	Control options
Block commutation	target voltage	Speed Control, Speed - DC Link current control
Sinudoidal commutation	target voltage	Speed Control, Speed - DC Link current control
	FOC	Speed Control, Torque (I_q, I_d) Control, Position Control

Table 5.2: Motor operating mode possibilities with the demonstrator

Figure 5.26 is showing the graphical user interface for the drive demonstrator. The functions of the different controls are:

(A) With these buttons, the motor can be started or stopped.

(B) The direction of the motor can be selected (clock-wise CW or counter clock wise CCW) here. The other option here is the possibility to invert the hall switches, depending on the hall switch interface of the motor.

(C) The Lead Angle can be set here for non-FOC operating mode.

(D) With the PWM duty cycle control the voltage applied to motor can be set. This is used if no speed controller is active and non-FOC mode is used.

(E) With this control the commutation method can be selected. It can be chosen between block-, sinusoidal- and FOC operating mode. The FOC operating mode supports three options: Speed Control, Torque Control (Id, Iq - control) and Position Control.

(F) In this control, the Rotor Sense Mode is selected.

(G) In non-FOC mode, a speed controller or a speed with inner DC-link current control can be selected and parametrized. The inner current DC link controller can be useful for limiting the current taken from the power supply. The benefit of only using the speed controller is that for this method, no current measurement is needed.

(H) With these sliders, the set speed and set position for the different controllers is selected.

(I) These controls are used in FOC torque operating mode. With Iq the generated torque can be controlled and with Id field weakening is possible.

(J) In this area, status messages are displayed. The source of these messages could be either the GUI or as well the MCU.

Figure 5.27 is showing the general control interface for the drive demonstrator:

(A) With these controls the drive demonstrator serial port can be selected and the connection to the demo can be established.

(B) This button opens the configuration window. In this window, e.g. the shunt resistor current measurement, the position offset of the encoder and TLE5012 or the PI controller parameters for FOC control can be configured. Furthermore it is possible to select the output of the DAC.

(C) With these buttons the pre-driver can be initalized and enabled. In the PreDriver Status Window, the diagnostic registers can be read out.

(D) With these controls the DataRecorder can be configured and initiated. This function is described in chapter 5.6.3.7.

(E) The real-time data logger is started and configured in this section (see chapter 5.6.3.7).

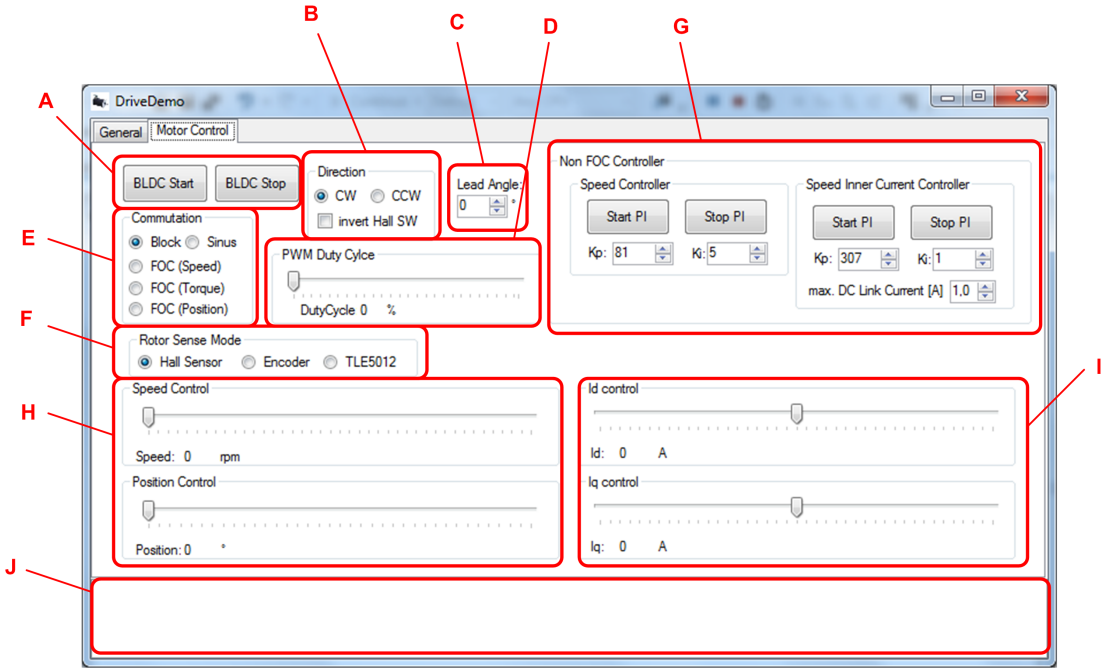

Figure 5.26: GUI - interface for motor control

5.6.3.7 Data recorders

In order to be able to display MCU internal variables and parameters, three different diagnostic tools are implemented:

1. DAC output:
   Can be used for displaying real-time data on a connected oscilloscope. Several output variables can be selected: e.g. rotor angle, calculated speed, phase currents, I_q, I_d. These variables are sampled and output on every PWM period: $50\mu s$.

2. Real Time Data Logger:
   With the real time data logger, the data sampling rate can be selected in the

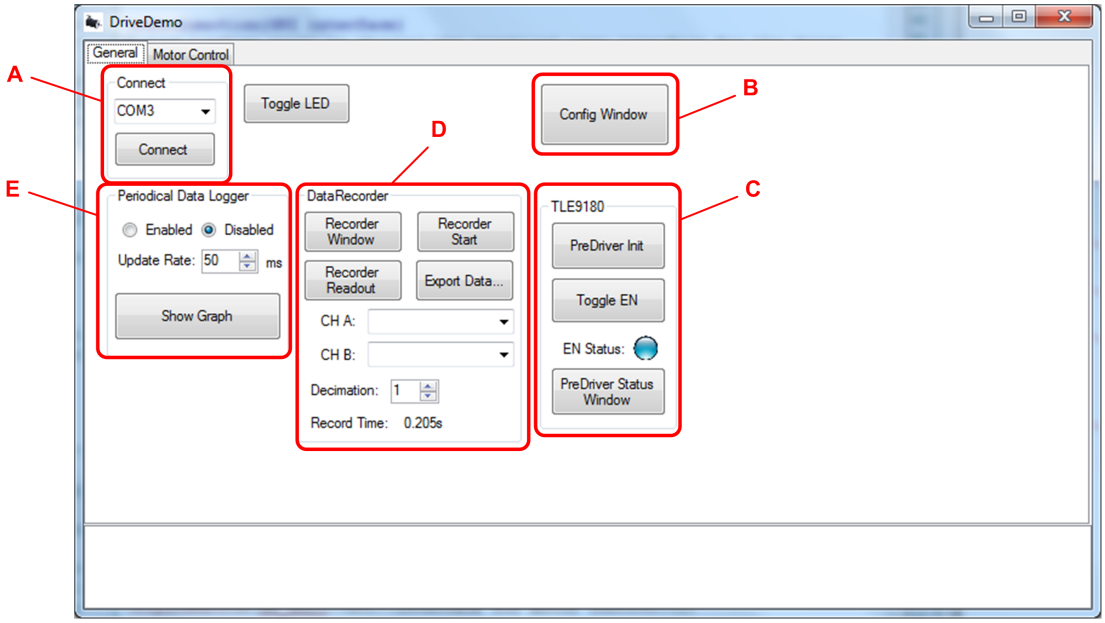

Figure 5.27: GUI - general interface for drive demonstrator

GUI with a minimum of $50ms$. In the periodical data logger graph, the set speed and current speed are displayed. Furthermore up to four different other internal signals (variables) can be selected. It has to be considered that this function is only sampling every $50ms$ and does not supply an averaged value. Figure 5.28 shows the graph window.

3. High-Resolution Data Recorder:
   Another option is the high-resolution data recorder, which can be initiated in the main form. Two different signals can be recorded with a maximum sampling rate of the PWM frequency ($20kHz$). The recording always starts at the zero crossing of the index pulse and 4096 samples are taken, which results in a recording time of 0.205 seconds. To increase the covered time span, a selectable decimation can be used, which decreases the sampling rate by that decimation factor (e.g. a decimation factor of 2 results in a recording time of $2 \cdot 0.205 = 0.41$ seconds). The recorder data is displayed in a graph in the GUI and can be exported to a CSV file.

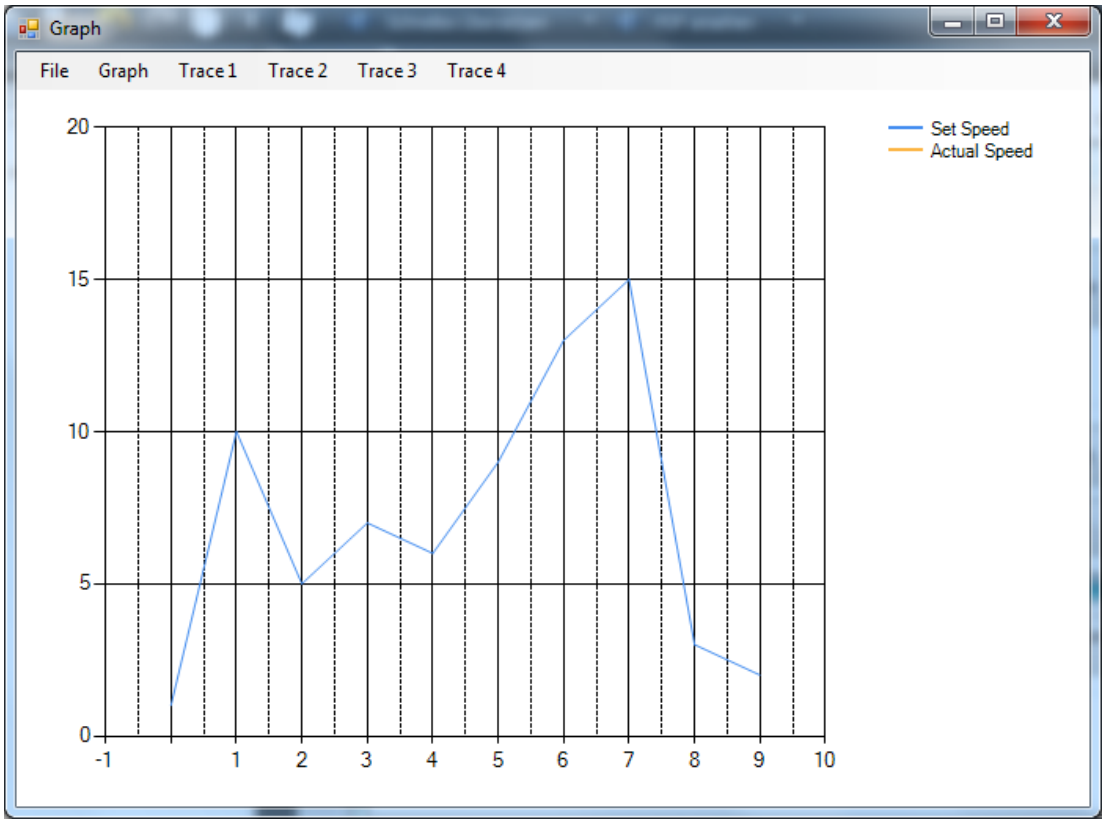

Figure 5.28: GUI - interface of the real time data logger

6

Results

6.1 Measurements

All following measurement results are recorded with one of the diagnostic tools discussed in chapter 5.6.3.7 or with an oscilloscope. All measurements are done at room temperature with a motor supply of $14V$. The Dunkermotor BG75x50 is used as drive motor for the test setup. The coupled motor is a DC motor, which is used as drive motor if the BLDC is used in active braking.

6.1.1 Accuracy of Angle Measurements

All measurements discussed in this chapter reflect the accuracy of the angle measurement compared to the reference measurement mounted on the testbench. As additional errors (e.g. mechanical mounting, accuracy of encoder or misalignments) occur, these results do not reflect the absolute performance of the sensing method, but give an indication of the performance of the demonstrator. Furthermore the accuracy of the Encoder is not considered and could influence the measurements.

6.1.1.1 Angle error of TLE5012

The accuracy of the TLE5012 compared to the optical encoder is measured with the high resolution data recorder. The TLE5012 is configured with enabled and disabled hysteresis mode and the measurement has been done at $500rpm$ and $1800rpm$. Figure 6.1 shows the angle error at 500rpm with and without activated hysteresis of the TLE5012 and figure 6.2 the results at 1800rpm. Table 6.1 shows the results of the

angle error. It can be seen that a different speed does not influence the accuracy of the sensor. The angle error of the TLE5012 compared to the encoder is ±0.107%.

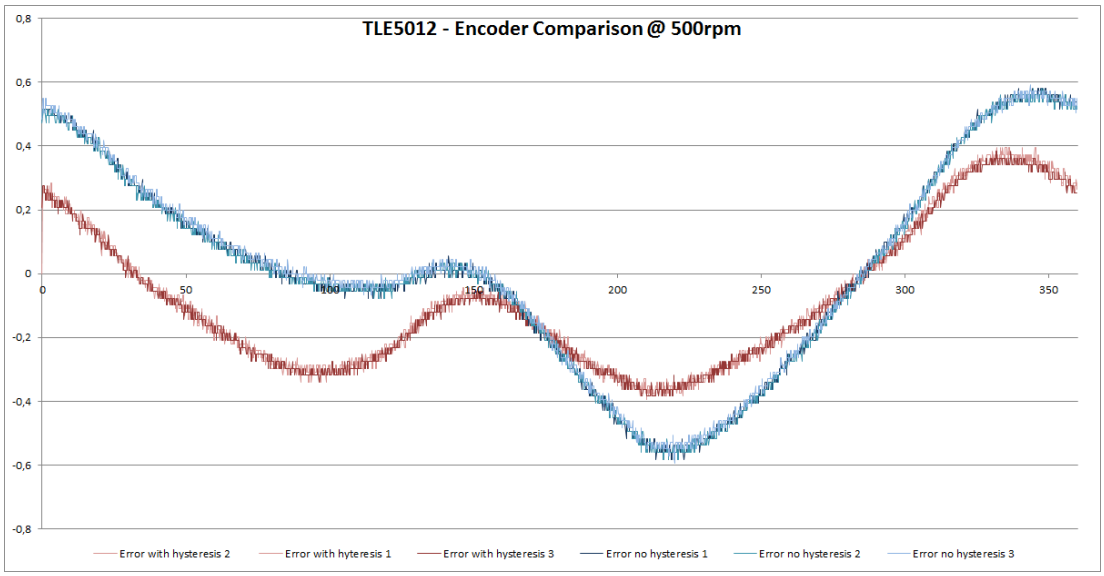

Figure 6.1: TLE5012 accuracy - angle error compared to encoder at 500rpm

TLE5012 Config	500rpm	1800rpm
hysteresis disabled	±0.5822°	±0.5822°
hysteresis enabled	±0.3845°	±0.3845°

Table 6.1: Measurement results of Encoder-TLE5012 comparison

6.1.1.2 Angle error of Hall switch estimation

As discussed in chapter 5.6.3.2, the angle of the rotor is only known at specific points when using the hall switches for angle estimation. Therefore the angle function is not monotonous and could have jumps at the synchronization points. Reasons for that could be e.g. the estimator is inaccurate, the hall switches jitter or the position of the hall sensors is not evenly distributed. Figure 6.3 is showing the hall estimator and the encoder angle and figure 6.4 shows the angle error. The measured deviation between the hall estimation and the encoder angle is ±4.79° = ±1.33%.

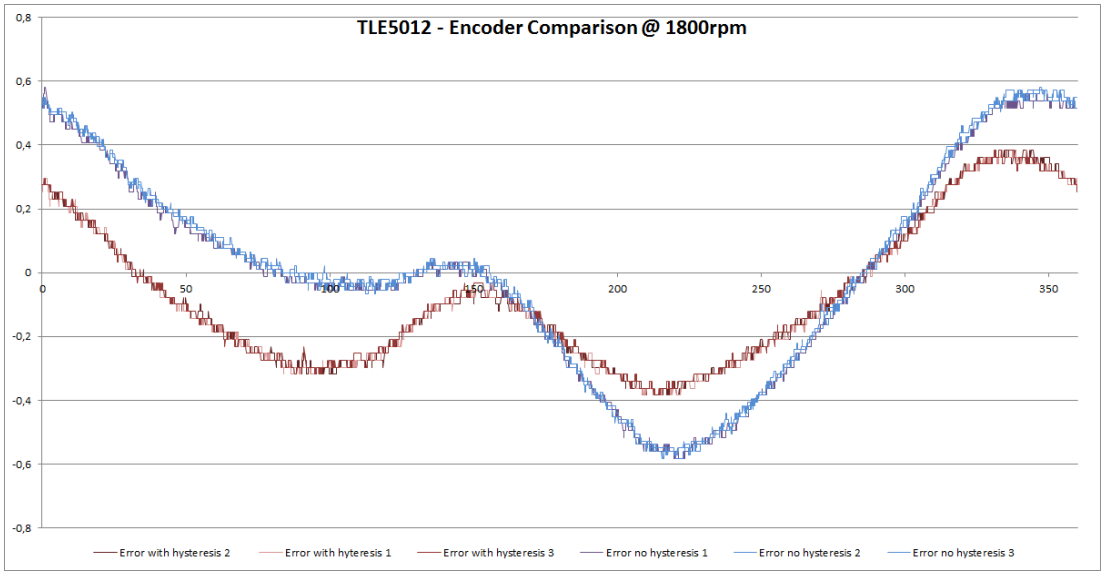

Figure 6.2: TLE5012 accuracy - angle error compared to encoder at 1800rpm

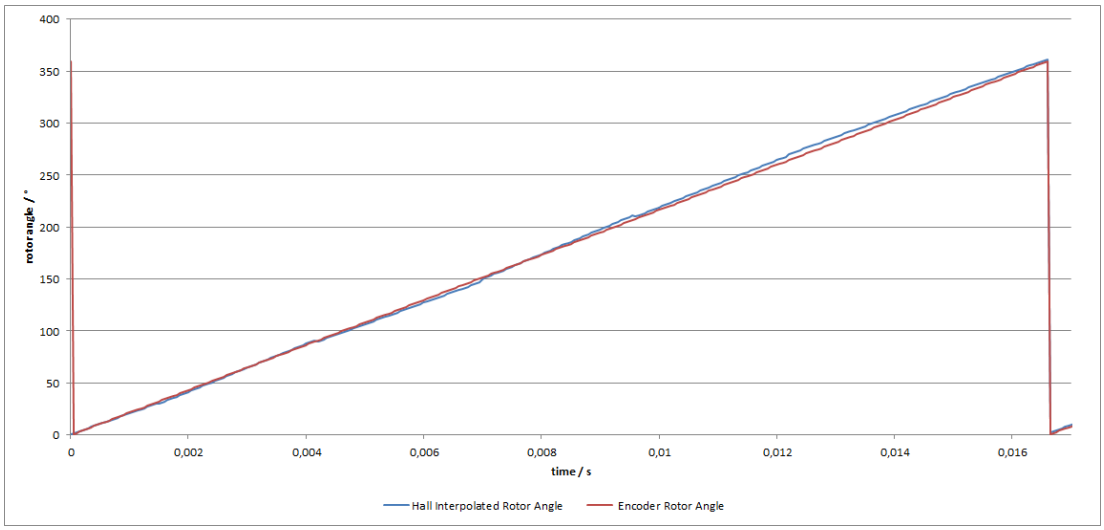

Figure 6.3: Hall estimation accuracy - angle error compared to encoder

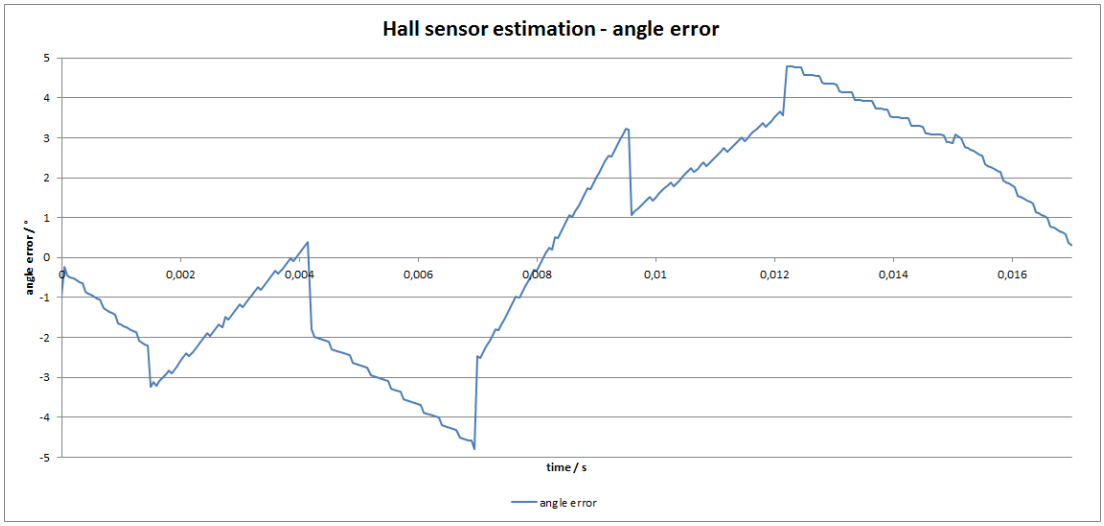

Figure 6.4: Hall estimation accuracy - angle error compared to encoder

6.1.2 Output stage

The two output modes of the power inverter is either the block or the sinusoidal mode. Figure 6.5 is showing the low pass filtered phase voltages in block commutation as well as the W phase current. In figure 6.6 the sinusoidal output is shown. In this mode the difference between the motor terminals result in the sinusoidal voltage. The voltage difference between the three phases is seen in the upper part of the figure.

The channels of the oscilloscope are:

- **Channel 1 (yellow)** - Voltage on Phase U
- **Channel 2 (green)** - Voltage on Phase V
- **Channel 3 (purple)** - Voltage on Phase W
- **Channel 4 (pink)** - Current of Phase W ($1V \widehat{=} 50A \widehat{=} 10A/Div$)

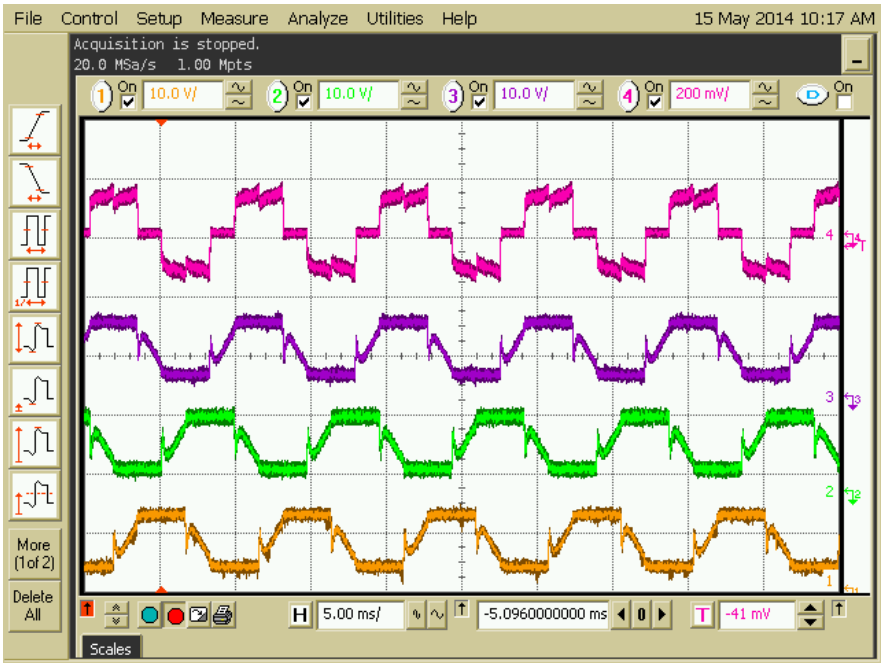

Figure 6.5: Inverter output - in block commutation

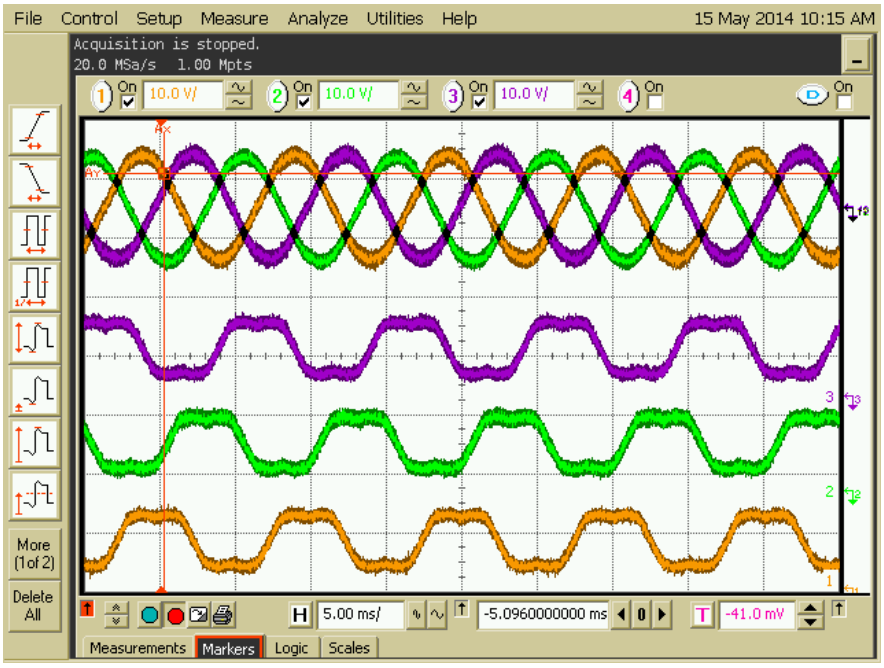

Figure 6.6: Inverter output - in sinusoidal commutation

6.1.2.1 Current Distortion

For a proper sinusoidal output, the rotor position has to be known precisely as shown in figure 6.7, where the encoder is used as angle sensing method. As discussed in chapter 6.1.1.2, the hall estimator results in an error of $\pm 1.33\%$. This error results in a distortion of the sinusoidal signal as shown in figure 6.8.

The channels of the oscilloscope are:

- **Function 1 (yellow)** - Voltage difference Phase U - Phase V
- **Function 2 (green)** - Voltage difference Phase V - Phase W
- **Function 3 (purple)** - Voltage difference Phase W - Phase U
- **Channel 4 (pink)** - Current of Phase W ($1V \widehat{=} 50A \widehat{=} 10A/Div$)

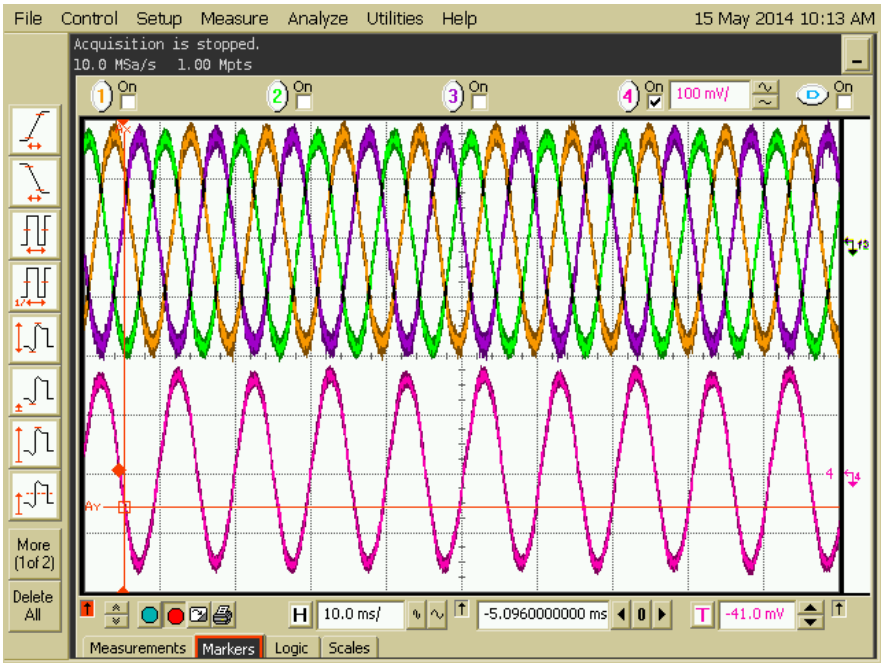

Figure 6.7: Sinusoidal commutation current - with encoder angle sensing

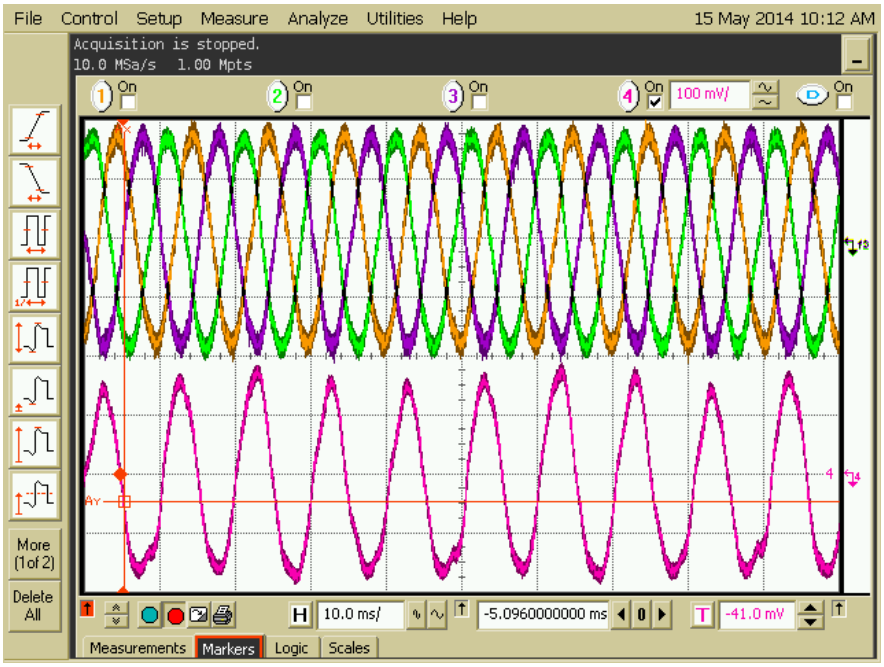

Figure 6.8: Sinusoidal commutation current - with hall estimator sensing

6.1.2.2 Phase currents in sinusoidal commutation

The phase currents in sinusoidal commutation are measured with the high-resolution data recorder. The TLI4970 current sensor is used to measure the currents on board. The motor is sinusoidal commutated with a fixed PWM duty cycle. Figure 6.9 is showing all phase currents in sinusoidal commutation mode. The currents are recorded separately as only two channels can be recorded simultaneously. This is possible, as the high resolution data recorder always starts with the index pulse of the encoder.

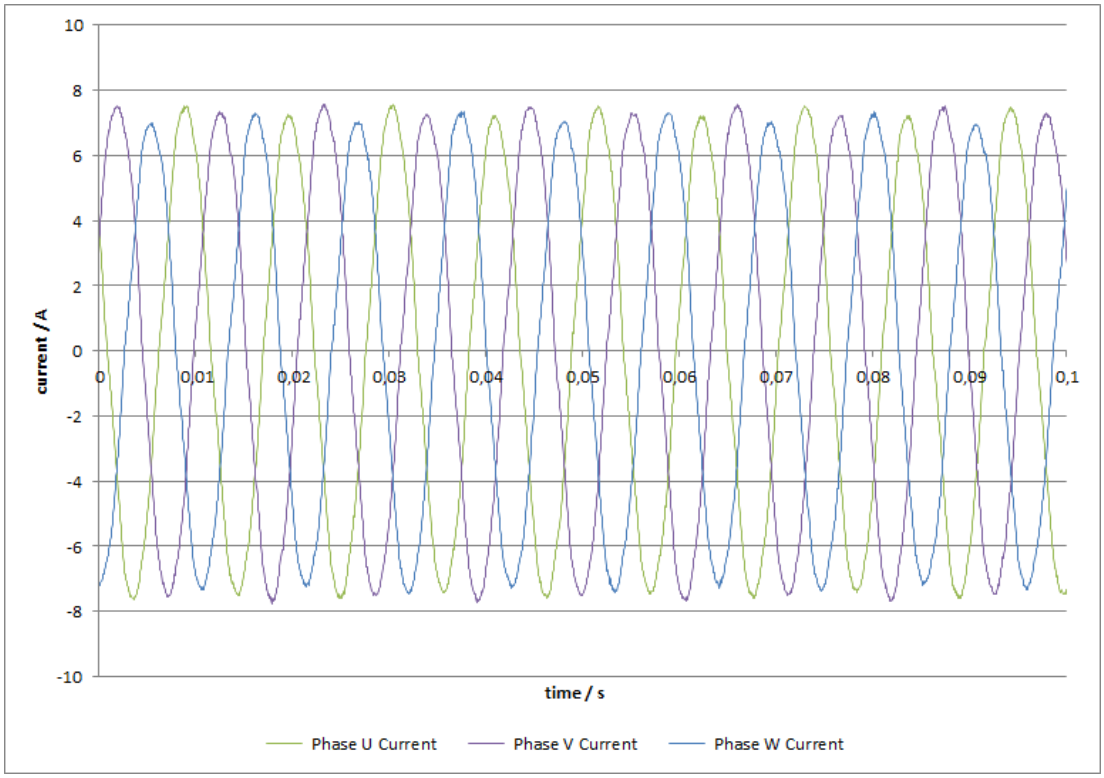

Figure 6.9: Sinusoidal commutation current - all phase currents measured with TLI4970

6.1.3 FOC drive measurements

The FOC controller parameters used for the following measurements is shown in table 6.2. All values are taken from the GUI - an internal conversion factor is not considered.

Controller	Parameter	Value
Speed Controller	K_p	150
	K_i	1
I_q Controller	K_p	25650
	K_i	65000
I_d Controller	K_p	25650
	K_i	65000

Table 6.2: FOC controller parameters

6.1.3.1 Speed controller jitter

The FOC commutation method is used with the speed controller. Figure 6.10 is showing the speed jitter with using the encoder. The desired speed of the controller is set to 1300rpm and results in a accuracy of $\pm 12 rpm \widehat{=} \pm 0.92\%$.

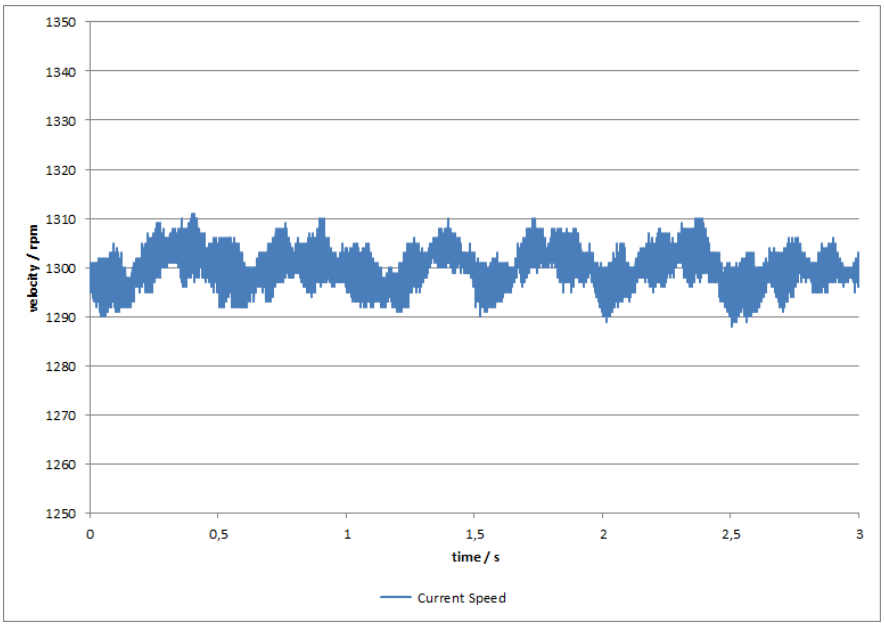

Figure 6.10: Speed jitter - when using FOC speed controller with encoder

6.1.3.2 Speed Step

Figure 6.11 is showing the FOC current I_q and the measured speed with an encoder. The reference speed input was a step function. It can be seen that the torque generating current I_q, which is controlled by the speed controller is increased very fast and settles to a steady value if the desired speed is reached.

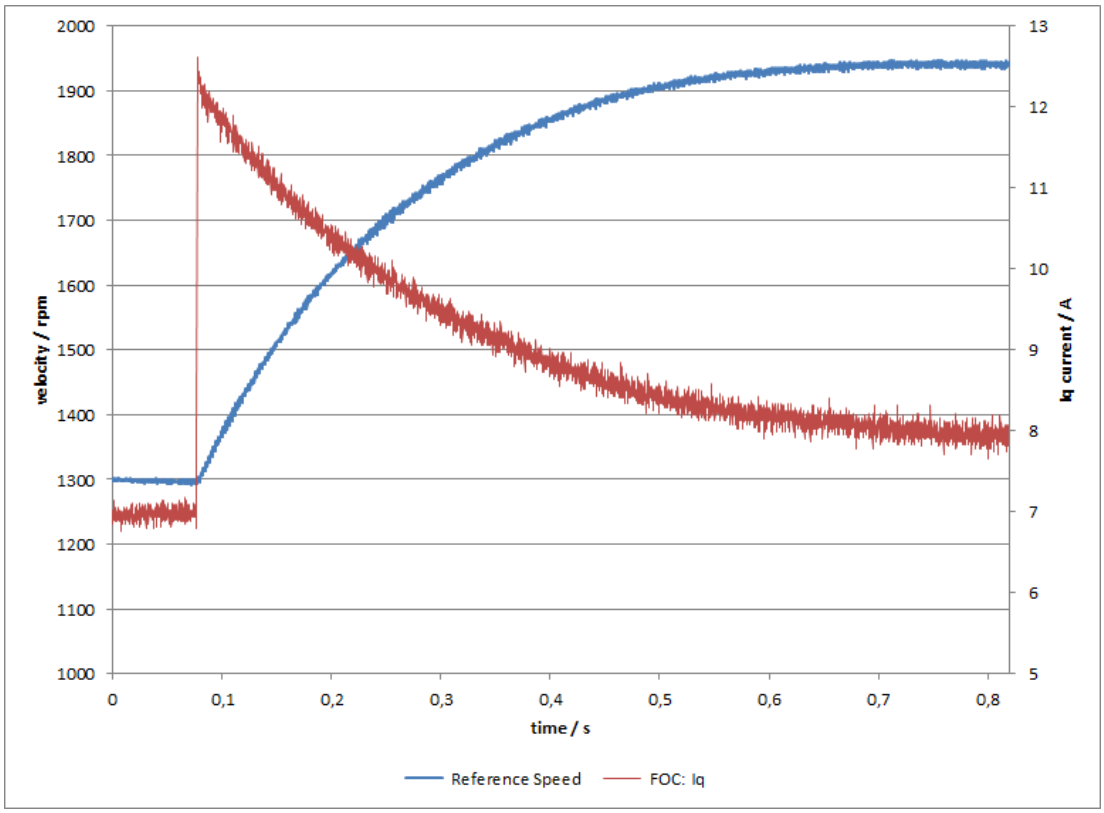

Figure 6.11: Speed step - FOC speed controller with reference speed step

6.1.3.3 Speed Controller Load

If a load is applied on the motor shaft, the speed controller increases the reference I_q until the desired speed is reached again. This behaviour is shown in figure 6.12. A defined load step could not be applied, as no second hardware setup for driving the load motor was available.

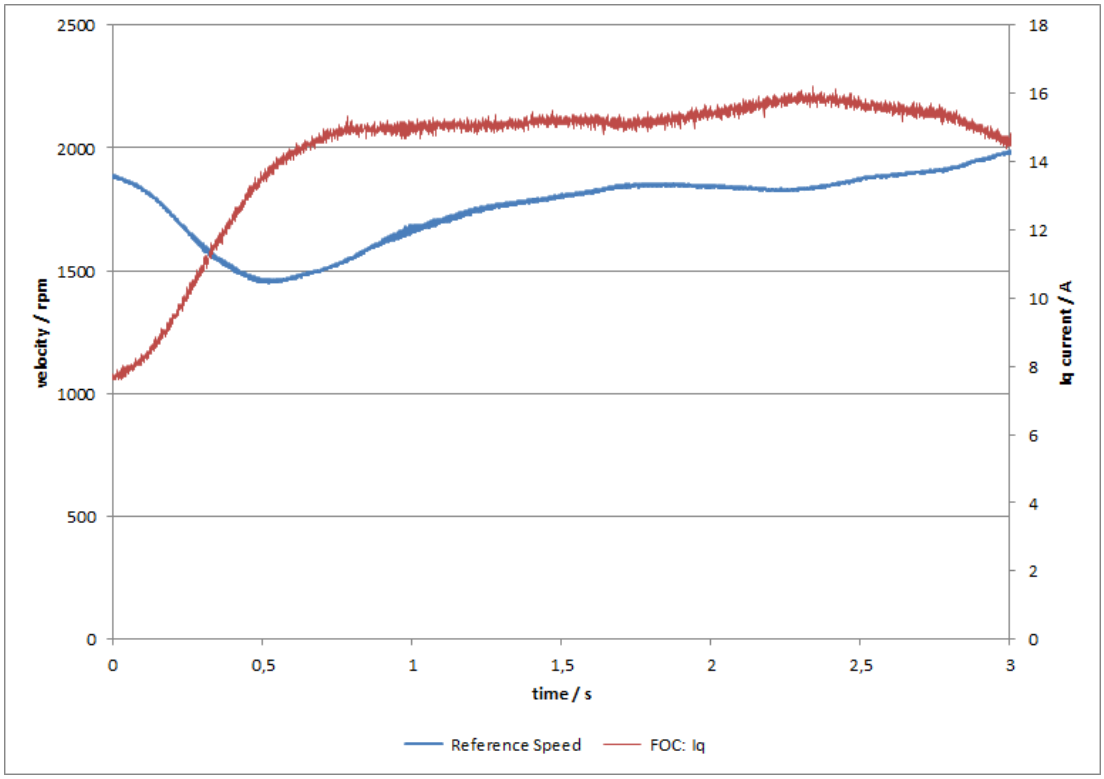

Figure 6.12: Load change - FOC speed controller with load change

6.1.3.4 Torque Controller Step

Figure 6.13 is showing the measured speed and FOC current I_q during a step function of $I_{q,ref}$. The reference step is changing from $1.5A$ to $2A$. With the change of the torque generating current I_q, the velocity of the rotor increases linearly. The maximum error of the I_q current controller in this measurement is $\pm 32.4mA \widehat{=} \pm 1.6\%$.

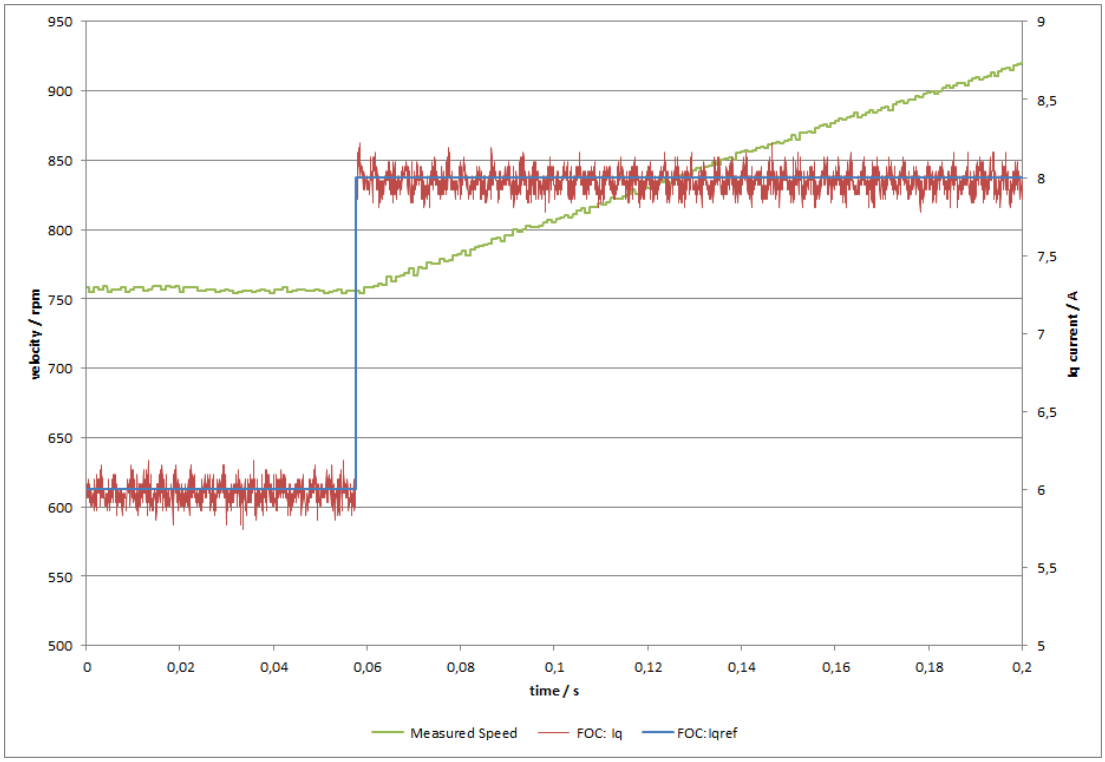

Figure 6.13: FOC torque controller - step of I_q

6.1.4 FOC load measurements

For this measurements the BLDC motor is used in brake mode and loads the DC motor. The DC motor is driven with a constant voltage source. The FOC commutation controller of the BLDC motor uses the same parameters as used in the drive measurement (see chapter 6.1.3). If the I_q is controlled to a negative value, the BLDC motor generates a torque in the other direction of the drive motor.

6.1.4.1 FOC load motor

Figure 6.14 is showing one phase current of the motor and the FOC I_q current. The reference of I_q is set to constant $-20A$. The maximum error of the controlled current I_q is $\pm 36.9mA \widehat{=} \pm 0.74\%$. The resulting torque can be calculated according to equation 6.1:

$$M = \frac{3}{2} \cdot p \cdot [\Psi_{PM} \cdot i_{sq}] = \frac{3}{2} \cdot 4 \cdot [7.831m \cdot 5] = 0.234Nm \tag{6.1}$$

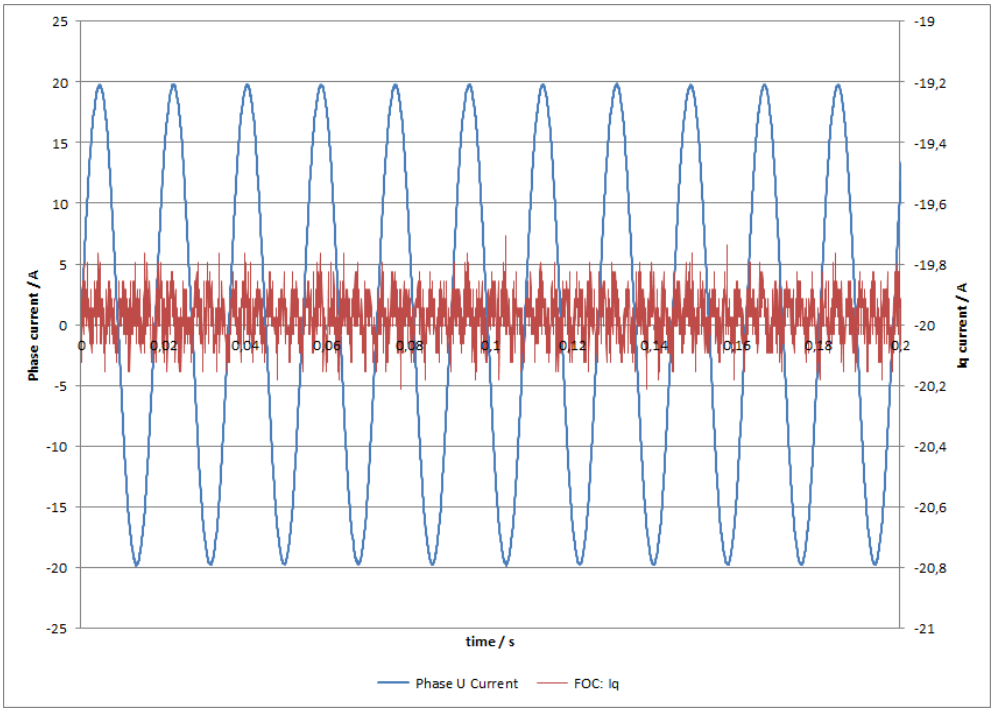

Figure 6.14: FOC controller load - BLDC motor used to generate constant torque

Figure 6.15 is showing a step function of the load from $I_q = 0A$ to $I_q = -20A$.

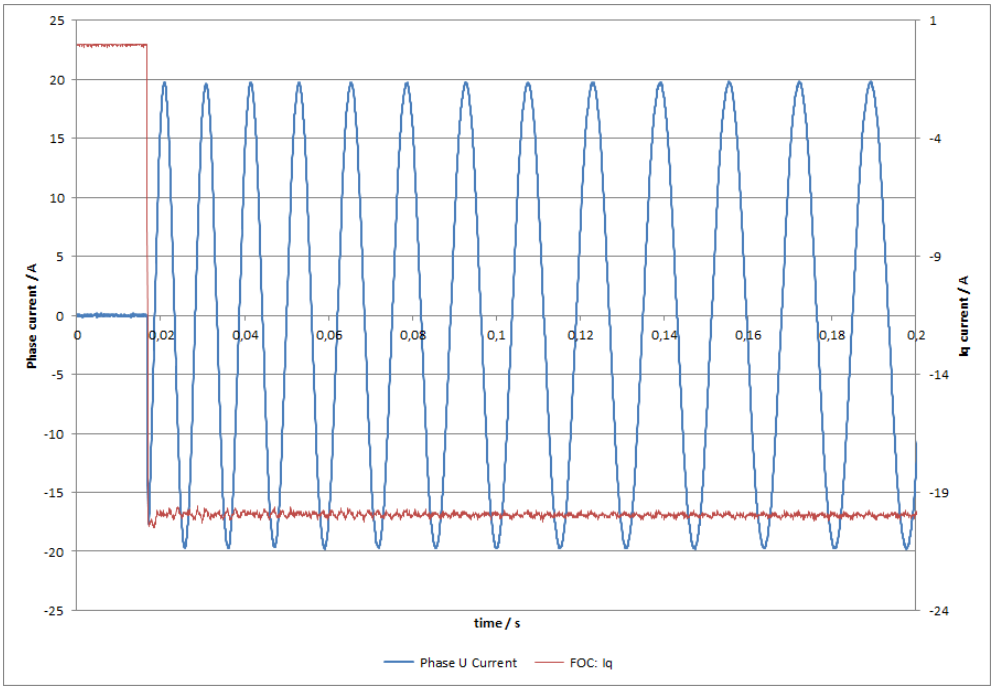

Figure 6.15: FOC controller load step - a load jump produced by the BLDC motor

7

Conclusion and Outlook

7.1 Conclusion

The main topic on this project was to develop and construct a flexible and extensible BLDC motor testbench. The testbench should help to develop system expertise in the area of motor control, especially with respect to feature set and performance requirements of the individual sensors. Furthermore the testbench should be used as demonstrator for Infineons advanced sensor solutions. As a side aspect, the demonstrator can be used to evaluate new concepts for sensing solutions.
In order to accomplish this task, knowledge in the area of BLDC motor control has been gained in the first step and available parts were evaluated. This evaluation has resulted in a requirement specification, which limits the available options. One of the main factors here was the current sensing technology. The testbench should be tailored to use the full scale range of the Infineon TLI4970 coreless hall effect current sensor, but the voltage range should stay in a reasonable low range. This has been the limiting factor for the motor selection, as usually the motor current is kept lower than $50A$ for $24V$ motors. Two suppliers for an appropriate motor were found, Dunkermotoren GmbH and Ohio Electric Motors.
The high currents were also the challenging factor in the hardware design. Therefore special considerations had to be taken for the layout of the power inverter. A heatsink has been added for cooling the inverter MOSFETs and the high current tracks are kept as short as possible.
For the angular sensing different interfaces are implemented. A reference measure-

ment is done with an optical encoder. In addition to that interfaces for the TLE5012, TLE5009 and a resolver are implemented. Furthermore the hall switches of the BLDC motor can be used for an angle estimation.
All hardware functions are partitioned on several sub-boards to support flexibility. Different sub-boards implement e.g. different current sensing techniques (shunt or current sensor). Furthermore a generic port interface is available for interfacing new modules or sensing techniques.
The software has been partitioned in a similar way as the hardware and follows the same flexible approach. For different sensing techniques, sub-blocks are used and are abstracted for upper layers. Therefore an extension for a new hardware or software block is simple. Furthermore the software makes usage of several Dave Apps, which are maintained and tested software blocks.
For controlling the demonstrator, a graphic user interface for Windows is implemented. With the GUI, all functions of the testbench are accessible and parametrized. Furthermore the GUI supports several diagnostic tools for displaying the measured or internal recorded data. These tools are: the real-time data logger, high resolution data recorder and the DAC output.
The accuracy of the angle measurement is limited by the mechanical precision of the testbench. With this limitations the testbench is not suitable for precise qualification of the devices. The test results discussed in chapter 6 are giving an indication on the performance of the overall setup and not of the individual device. Furthermore mechanical misalignment is influencing the accuracy of the end of shaft angle measurement and result in a higher error.
Comparison measurements with shunt current measurement and in phase current sensing were not possible due to a bug in the pre-driver. The bug in the pre-driver is influencing the accuracy of the built-in operational amplifiers for signal conditioning. Furthermore due to a bug, one of the operational amplifiers is not functional at all. As the pre-driver is currently under development and not released yet, a performance analysis can be done with the released and fully functional pre-driver.
All controllers are parametrized for using the Dunkermotor, as the Ohio Electric Motor was not available due to a long ordering and shipment process. The parameters in the GUI should give a starting point but have to be adjusted for the individual application

and setup (depend on the supply voltage, load).

7.2 Outlook

The testbench can be used for demonstrating purposes or to evaluate new sensing and control techniques. For further development, parameter sets for different motors should be supplied (e.g. another parameter set for the Ohio Electric Motor). For an additional dynamic performance increase the PI controllers should be tuned and furthermore an online tuning of the PI controllers could be implemented.
For better characterization, a torque sensor between the two motors could be implemented. In this case the torque ripple could be measured directly. The comparison of the different current sensing techniques can be measured and evaluated with the released and bug-fixed pre-driver. One topic of interest would be the performance gain if using in-phase current measurement (TLI4970) compared to the low-side link current measurement (shunt-resistor sensing method).
Another point would be the comparison of other current-sensing techniques in a drive application. This could include the comparison of the TLI4970 with a flux concentrator current measurement.
The implementation of an out-of-shaft angle sensing technique could be done as a next step of angular position measurements. Furthermore a performance analysis compared to the optical encoder or end of shaft method could be done. A more advanced hall angle estimation algorithm could help to improve the dynamic performance, when using hall switches as angle sensors.
In addition to that, the speed calculations at lower speeds of the optical encoder and TLE5012 could be improved. At lower speeds, the number of pulses in a given time frame should be used to calculate the velocity of the rotor. This technique could be done besides the current implementation (see chapter 5.6.3.2) which is suitable for higher speeds.
Furthermore the testbench offers a complete setup to gain knowledge in the field of motor control algorithms as well as sensing requirements.

References

[1] Infineon Technologies AG. **Driving the Future of Automotive Electronics**. *Automotive Application Guide*, 2012. viii, 2

[2] Microchip Technology Inc. **Brushless DC (BLDC) Motor Fundamentals**. 2003. viii, 8, 11, 13

[3] E. Kiel and E. Kiel. *Drive Solutions: Mechatronics for Production and Logistics*. Springer, 2008. viii, 20, 21

[4] Infineon Technologies AG. **TLE5012B Datasheet v1.1**, 2012. viii, 20

[5] Dunkermotoren GmbH. **BG75 Datasheet**. viii, 36

[6] Ohio Electric Motors. **Brushless Motors Datasheet**. viii, 36

[7] The International Council on Clean Transportation (ICCT). **Global Comparison of Passenger Car and Light-commercial Vehicle Fuel Economy/GHG Emissions Standards**. 2014. 2

[8] Infineon Technologies AG. **Drive Application Basics**. *E2 Training*, 2013. 1, 3, 4

[9] A.F.M.S. Qadir. *ELECTRO-MECHANICAL MODELING OF SEDM(SEPARATELY EXCITED DC MOTOR) & PERFORMANCE IMPROVEMENT USING DIFFERENT INDUSTRIAL CONTROLLERS:*. A.F.M. Sajidul Qadir, 2013. 4, 5

[10] Microchip Technology Inc. **Brushed DC Motor Fundamentals**. 2004. 4

[11] Prof. Dr. M. Zahurul Haq. **ME 475: Mechatronics - DC Motors**, 2010. 5

[12] J.F. Gieras. *Permanent Magnet Motor Technology: Design and Applications, Third Edition*. Electrical and Computer Engineering. Taylor & Francis, 2011. 5

[13] Maxon Motor AG. **maxon EC motor - Technology**. 2011. 6

[14] Texas Instruments. **Switched Reluctance Motor Control - Basic Operation**. 2000. 7

[15] B. Fahimi, A. Emadi, and R.B. Sepe. **A switched reluctance machine-based starter/alternator for more electric cars**. *Energy Conversion, IEEE Transactions on*, **19**(1):116–124, March 2004. 7

[16] Infolytica Corporation. **Design and Analysis of a Switched Reluctance Motor**. 7

[17] Infineon Technologies AG. **Sensor Solutions for Automotive and Industrial Applications**. 2012. 8, 9

[18] R.C. ; Iu H.H.-C. ; Borle L.J. Ziegler, S.; Woodward. **Current Sensing Techniques: A Reviews**. *Sensors Journal, IEEE*, **9**(4):354–376, April 2009. 10

[19] University Paderborn Prof. Dr.-Ing. Joachim Böcker. **Geregelte Drehstromantriebe - Skript zur Vorlesung**, 2012. 12

[20] Manish Bhardwaj Texas Instruments, Bilal Akin. **Sensorless Field Oriented Control of Multiple Permanent Magnet Motors**. 2000. 16

[21] Microchip Technology Inc. **Sensorless Field Oriented Control of a PMSM**. *Application note AN1078*, 2010. 16, 17

[22] Infineon Technologies AG. **Field Oriented Control (FOC) of PMSM Motor with Encoder**. 2012. 17, 18, 19

[23] I.J. Rudas, J. Fodor, and J. Kacprzyk. *Computational Intelligence and Informatics: Principles and Practice*. Studies in Computational Intelligence. Springer, 2010. 22, 23

[24] K. Kalantar-zadeh and B. Fry. *Nanotechnology-Enabled Sensors*. Springer ebook collection / Chemistry and Materials Science 2005-2008. Springer, 2008. 23, 24

[25] R.B. Gmbh. *Bosch Automotive Electrics and Automotive Electronics: Systems and Components, Networking and Hybrid Drive*. Bosch Professional Automotive Information. Westdeutscher Verlag GmbH, 2013. 24

[26] H. Czichos, T. Saito, and L.E. Smith. *Springer Handbook of Metrology and Testing*. Springer handbook. Springer, 2011. 25, 26

[27] Infineon Technologies AG Konrad Kapser. **Infineon xMR Sensors Presentation**. 2013. 25, 26, 29

[28] C. Reig, S. Cardoso, and S.C. Mukhopadhyay. *Giant Magnetoresistance (GMR) Sensors: From Basis to State-Of-the-Art Applications*. Smart Sensors, Measurement and Instrumentation. Springer London, Limited, 2013. 26, 27, 29

[29] K. Reif. *Sensoren Im Kraftfahrzeug*. Bosch Fachinformation Automobil. Vieweg+Teubner Verlag, 2012. 26, 27, 28

[30] STMicroelectronics. **Two or three shunt resistor based current sensing circuit design in 3-phase inverters - Application note AN4076**, 2012. 32

[31] LEM. **Automotive current transducer HABT 100-V Datasheet**, 2012. 32, 33

[32] Infineon Technologies AG. **Current Sensor**, 2014. 33, 48

[33] Infineon Technologies AG. **XMC4500 Microcontroller Reference Manual v1.3**, 2013. 44

[34] Infineon Technologies AG. **TLE9180-31QK 3-Phase Bridge Driver IC Target Datasheet v1.11**, 2013. 45

[35] Infineon Technologies AG. **TLE8366 1.8A DC/DC Step-Down Voltage Regulator Datasheet v1.0**, 2009. 45

[36] Infineon Technologies AG. **IPLU300N04S4-R7 - OptiMOS-T2 Power-Transistor Datasheet**, 2013. 47

Appendix

In the following appendix the schematics of all boards is included:

- Drive Demonstrator Mainboard
- Power inverter board with TLI4970
- Power inverter board with Shunt current measurement
- Speed Sense Angle Board for reference measurements
- Angle Sense Board for interfacing the TLE5012 and TLE5009
- Angle Sensor Board 50xx - PCB which is used for end of shaft sensing

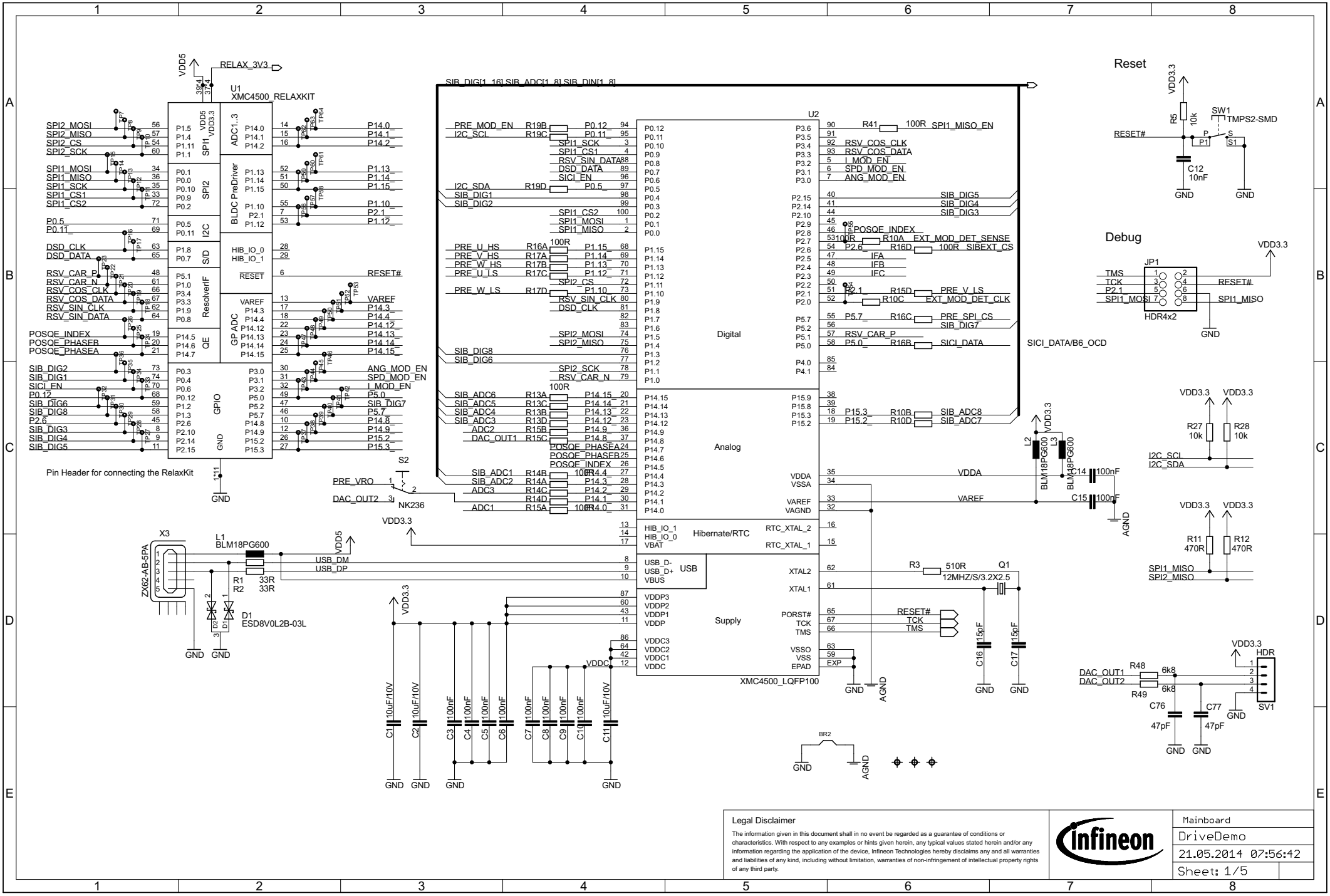
U1
XMC4500_RELAXKIT
U2
XMC4500_LQFP100
Digital
Analog
Supply
Hibernate/RTC
USB
Pin Header for connecting the RelaxKit
NK236
ESD8V0L2B-03L
BLM18PG600
ZX62-AB-5PA
Reset
Debug
HDR4x2
Legal Disclaimer
The information given in this document shall in no event be regarded as a guarantee of conditions or characteristics. With respect to any examples or hints given herein, any typical values stated herein and/or any information regarding the application of the device, Infineon Technologies hereby disclaims any and all warranties and liabilities of any kind, including without limitation, warranties of non-infringement of intellectual property rights of any third party.
Mainboard
DriveDemo
21.05.2014 07:56:42
Sheet: 1/5

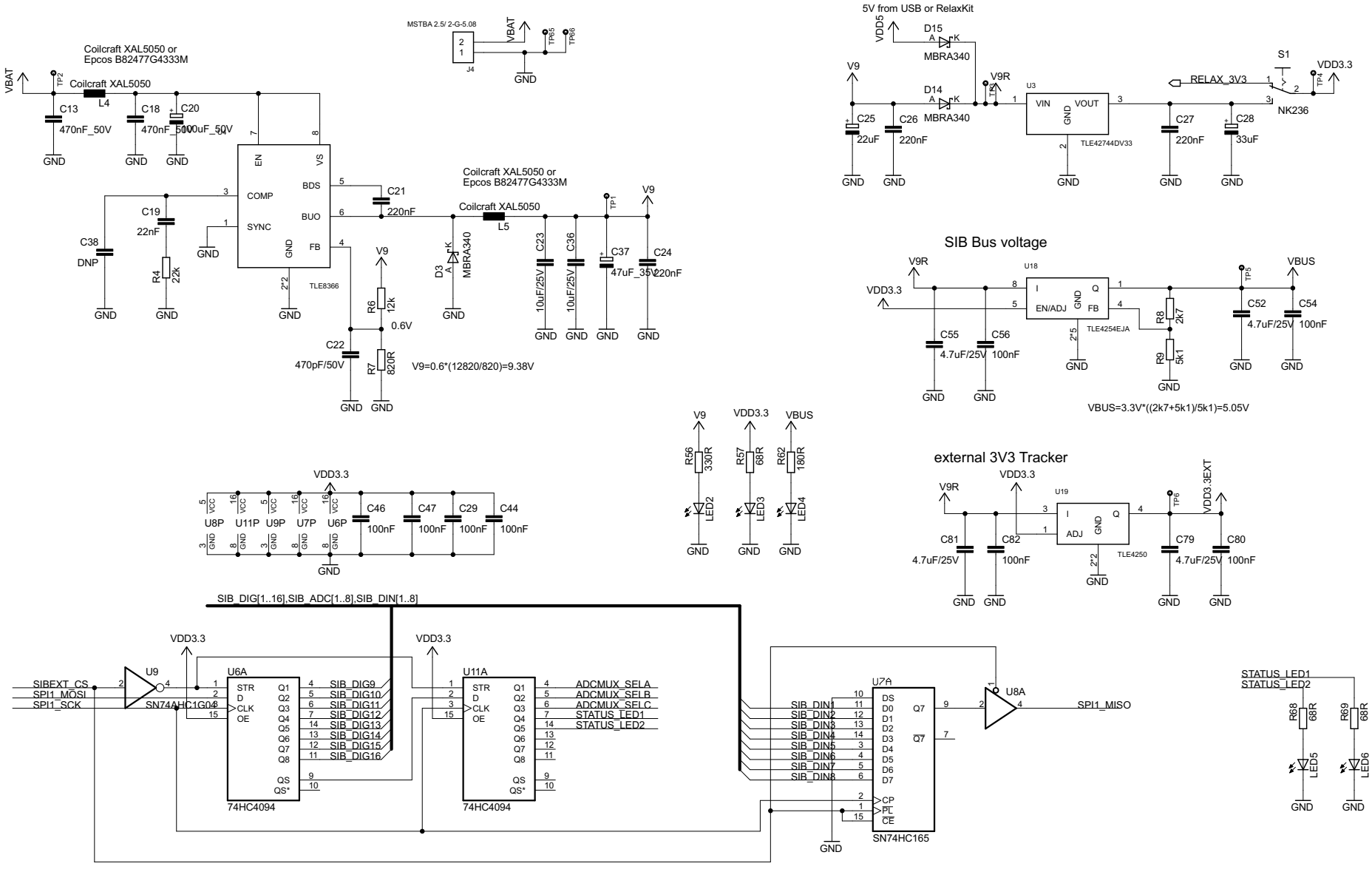

Legal Disclaimer

The information given in this document shall in no event be regarded as a guarantee of conditions or characteristics. With respect to any examples or hints given herein, any typical values stated herein and/or any information regarding the application of the device, Infineon Technologies hereby disclaims any and all warranties and liabilities of any kind, including without limitation, warranties of non-infringement of intellectual property rights of any third party.

Mainboard	
DriveDemo	
21.05.2014 07:56:42	
Sheet: 2/5	

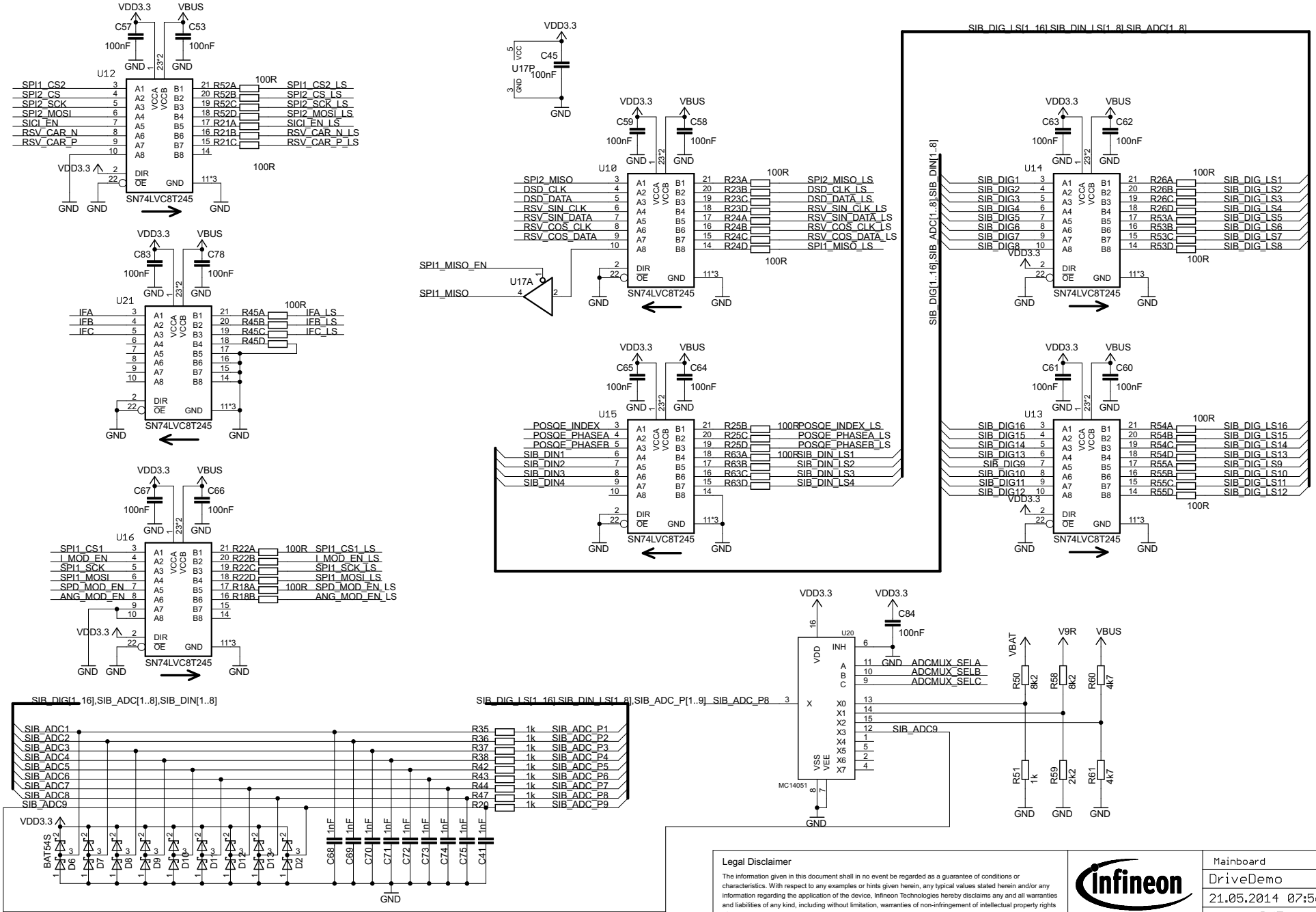
SIB_DIG_LS[1..16],SIB_DIN_LS[1..8],SIB_ADC[1..8]
SIB_DIG[1..16],SIB_ADC[1..8],SIB_DIN[1..8]
SIB_ADC_P[1..9]
SIB_ADC_P8
SIB_ADC9
U12
U10
U14
U21
U15
U13
U16
U17A
U17P
U20
SN74LVC8T245
MC14051
SPI1_CS2
SPI2_CS
SPI2_SCK
SPI2_MOSI
SICI_EN
RSV_CAR_N
RSV_CAR_P
SPI2_MISO
DSD_CLK
DSD_DATA
RSV_SIN_CLK
RSV_SIN_DATA
RSV_COS_CLK
RSV_COS_DATA
SPI1_MISO_EN
SPI1_MISO
IFA
IFB
IFC
POSQE_INDEX
POSQE_PHASEA
POSQE_PHASEB
SIB_DIN1
SIB_DIN2
SIB_DIN3
SIB_DIN4
SPI1_CS1
I_MOD_EN
SPI1_SCK
SPI1_MOSI
SPD_MOD_EN
ANG_MOD_EN
ADCMUX_SELA
ADCMUX_SELB
ADCMUX_SELC
VDD3.3
VBUS
V9R
VBAT
GND
BAT54S
Legal Disclaimer
The information given in this document shall in no event be regarded as a guarantee of conditions or characteristics. With respect to any examples or hints given herein, any typical values stated herein and/or any information regarding the application of the device, Infineon Technologies hereby disclaims any and all warranties and liabilities of any kind, including without limitation, warranties of non-infringement of intellectual property rights of any third party.
Mainboard
DriveDemo
21.05.2014 07:56:42
Sheet: 3/5

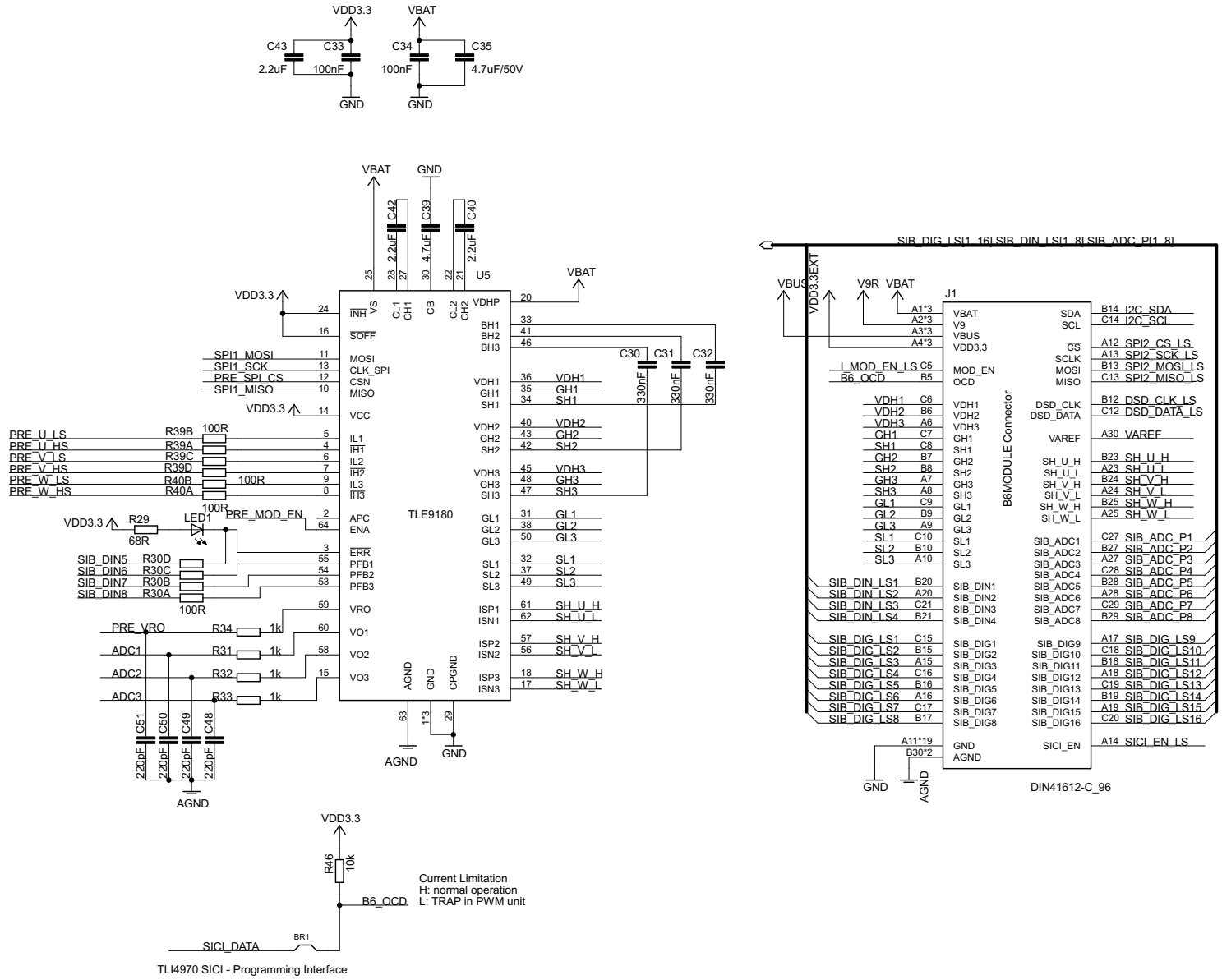

Legal Disclaimer

The information given in this document shall in no event be regarded as a guarantee of conditions or characteristics. With respect to any examples or hints given herein, any typical values stated herein and/or any information regarding the application of the device, Infineon Technologies hereby disclaims any and all warranties and liabilities of any kind, including without limitation, warranties of non-infringement of intellectual property rights of any third party.

Mainboard	
DriveDemo	
21.05.2014 07:56:42	
Sheet: 4/5	

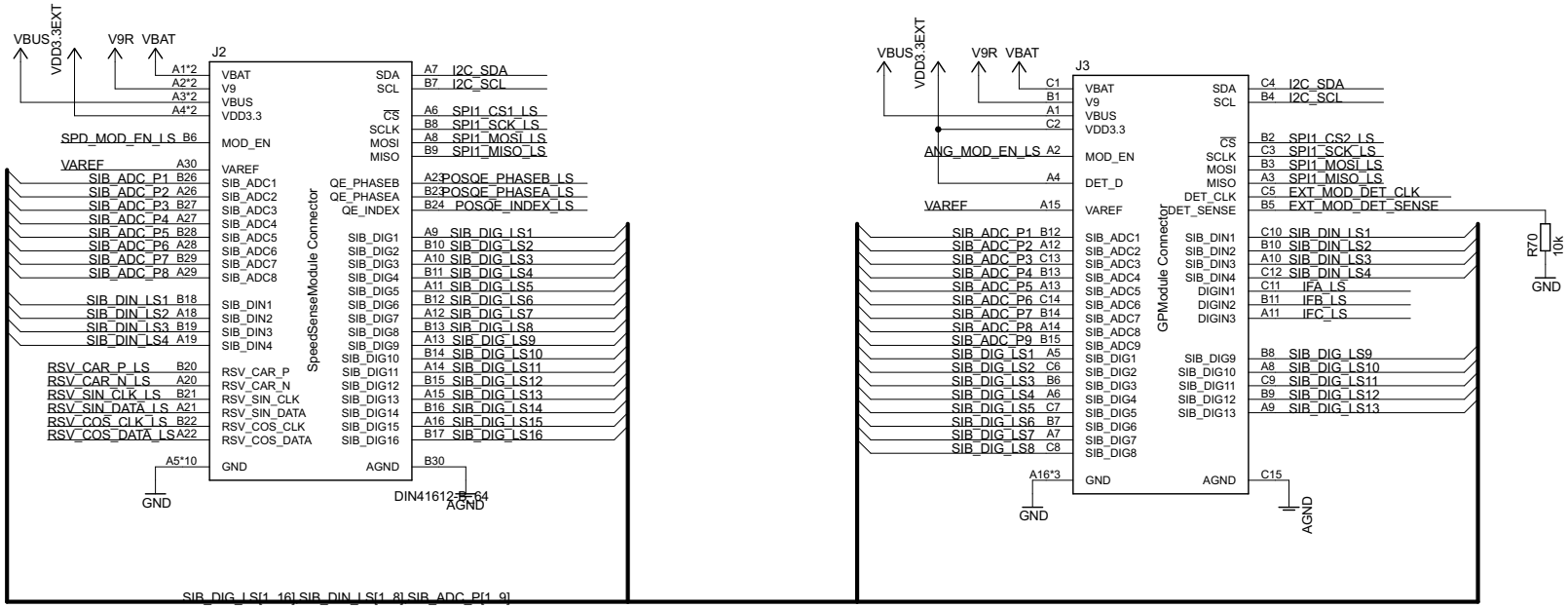

Legal Disclaimer

The information given in this document shall in no event be regarded as a guarantee of conditions or characteristics. With respect to any examples or hints given herein, any typical values stated herein and/or any information regarding the application of the device, Infineon Technologies hereby disclaims any and all warranties and liabilities of any kind, including without limitation, warranties of non-infringement of intellectual property rights of any third party.

Mainboard	
DriveDemo	
21.05.2014 07:56:42	
Sheet: 5/5	

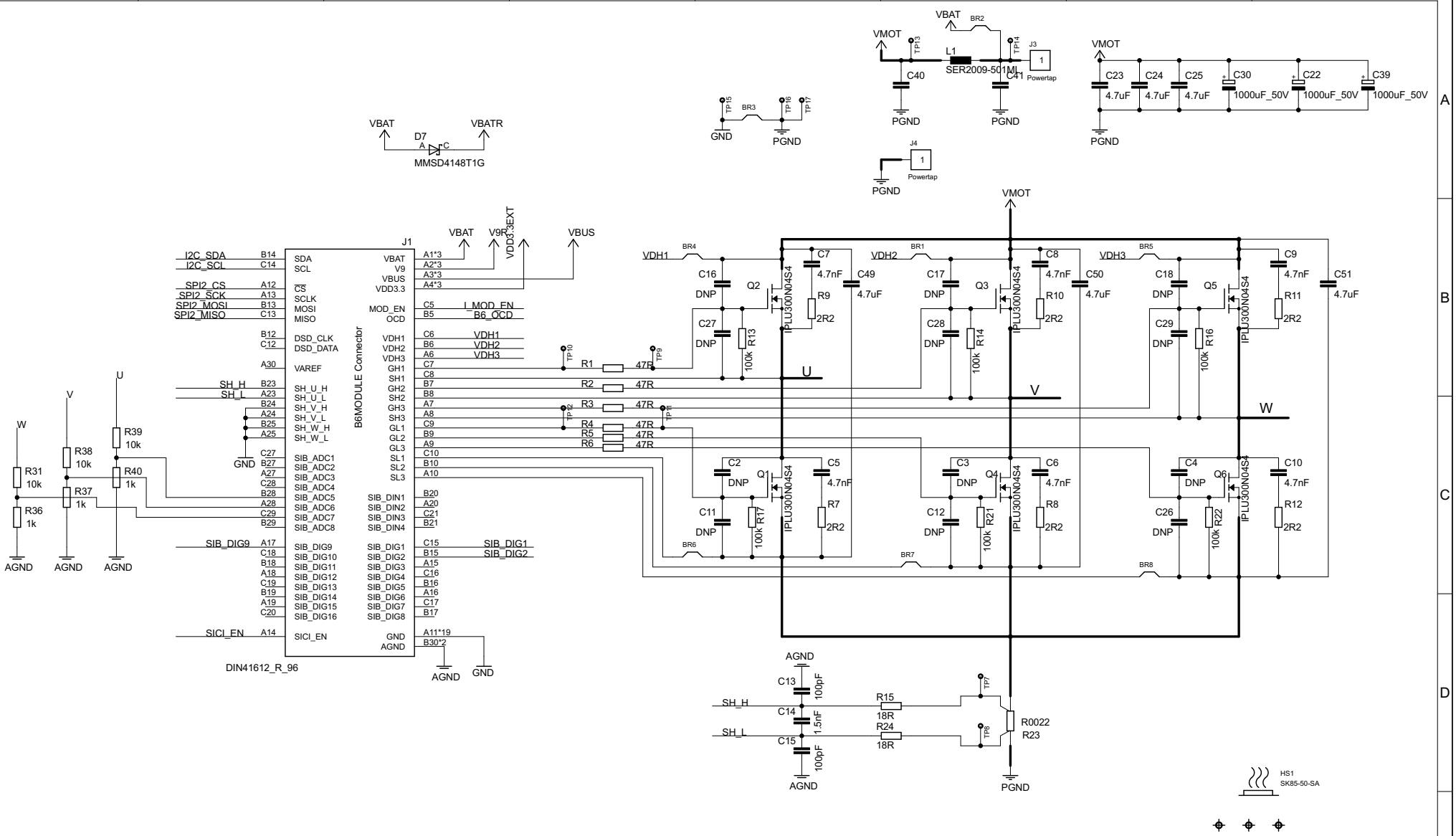

Legal Disclaimer

The information given in this document shall in no event be regarded as a guarantee of conditions or characteristics. With respect to any examples or hints given herein, any typical values stated herein and/or any information regarding the application of the device, Infineon Technologies hereby disclaims any and all warranties and liabilities of any kind, including without limitation, warranties of non-infringement of intellectual property rights of any third party.

B6Board_TLI4970

15.04.2014 08:44:45

Sheet: 1/3

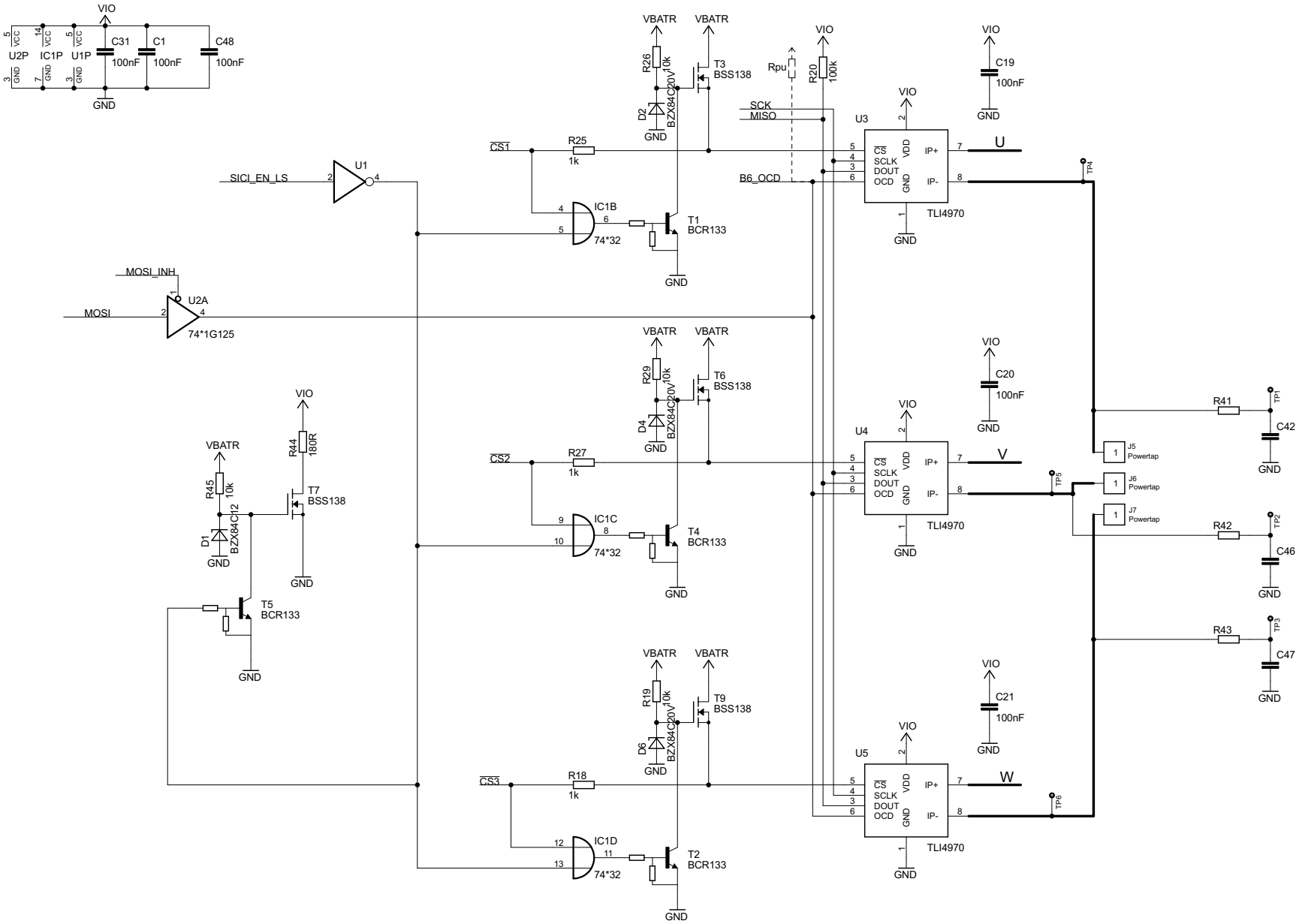

Legal Disclaimer

The information given in this document shall in no event be regarded as a guarantee of conditions or characteristics. With respect to any examples or hints given herein, any typical values stated herein and/or any information regarding the application of the device, Infineon Technologies hereby disclaims any and all warranties and liabilities of any kind, including without limitation, warranties of non-infringement of intellectual property rights of any third party.

B6Board_TLI4970

15.04.2014 08:44:45

Sheet: 2/3

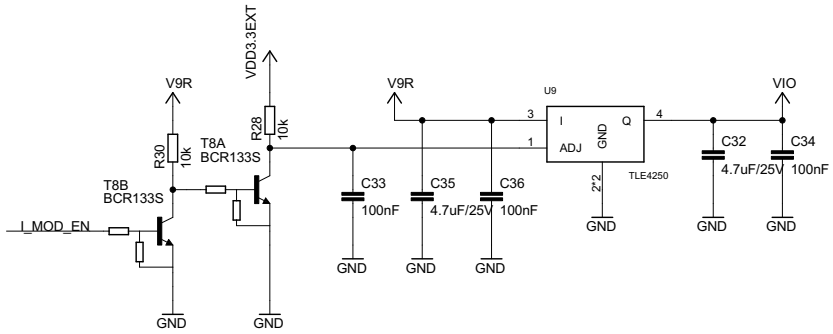

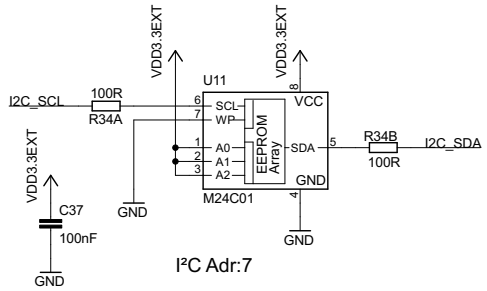

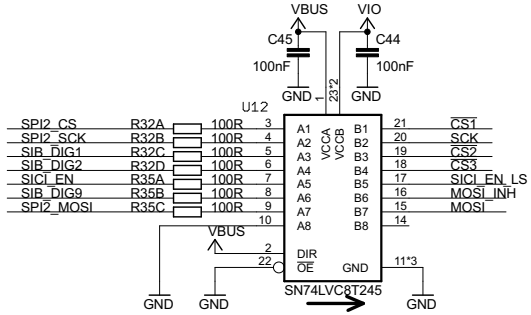

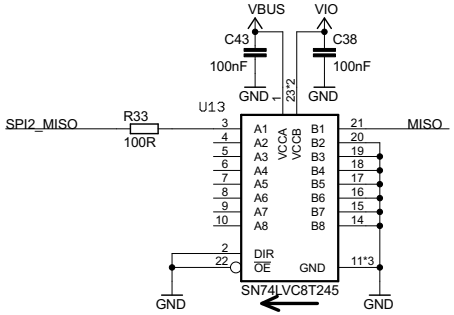

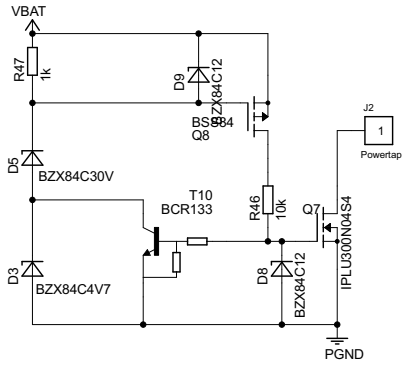

Legal Disclaimer

The information given in this document shall in no event be regarded as a guarantee of conditions or characteristics. With respect to any examples or hints given herein, any typical values stated herein and/or any information regarding the application of the device, Infineon Technologies hereby disclaims any and all warranties and liabilities of any kind, including without limitation, warranties of non-infringement of intellectual property rights of any third party.

B6Board_TLI4970

15.04.2014 08:44:45

Sheet: 3/3

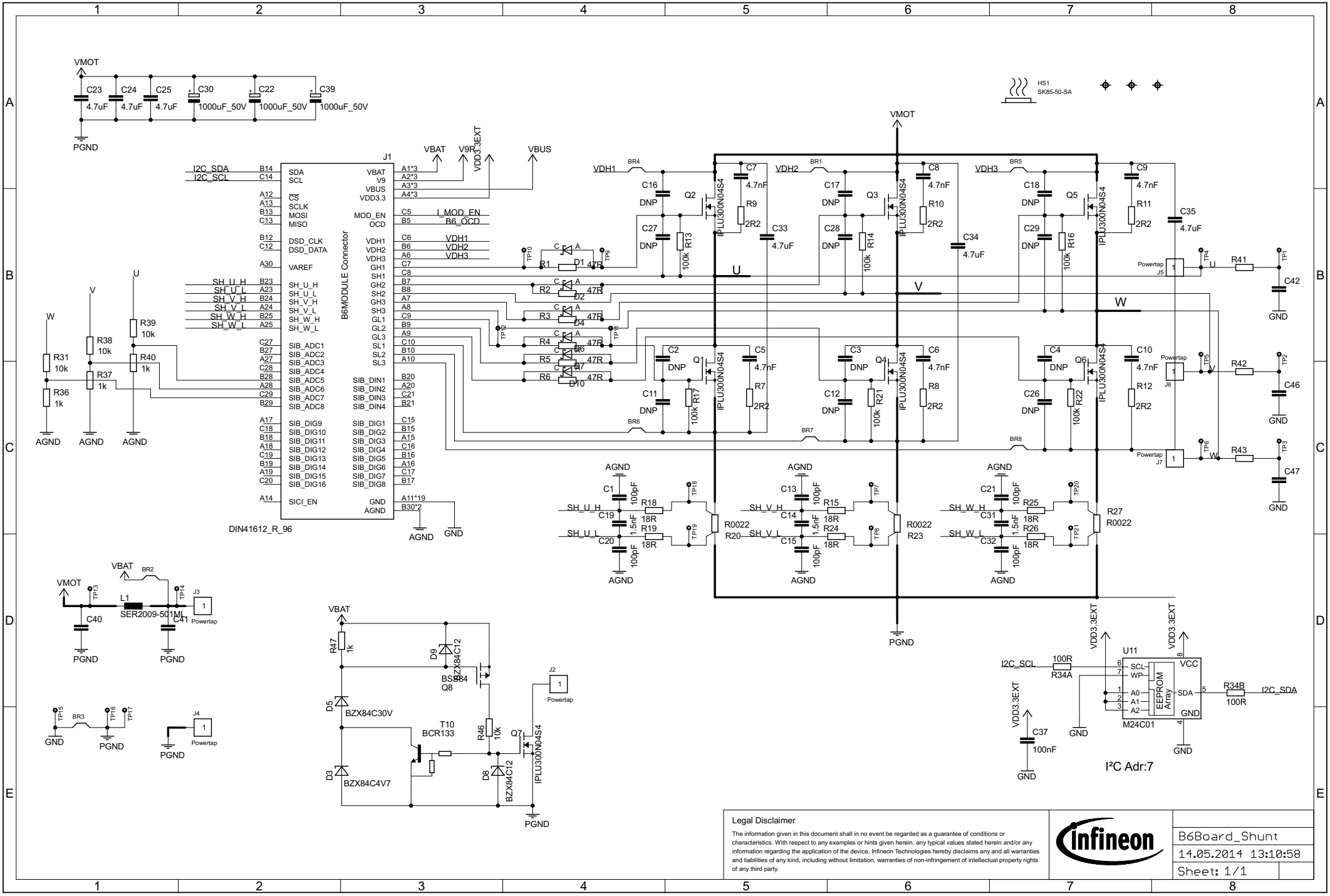

Legal Disclaimer

The information given in this document shall in no event be regarded as a guarantee of conditions or characteristics. With respect to any examples or hints given herein, any typical values stated herein and/or any information regarding the application of the device, Infineon Technologies hereby disclaims any and all warranties and liabilities of any kind, including without limitation, warranties of non-infringement of intellectual property rights of any third party.

B6Board_Shunt

14.05.2014 13:10:58

Sheet: 1/1

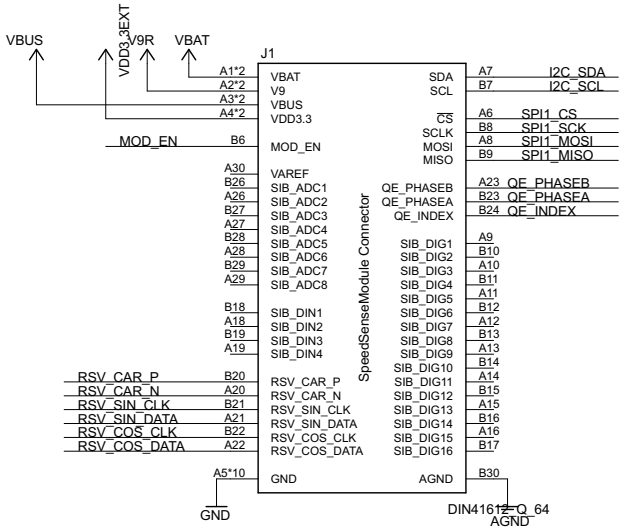

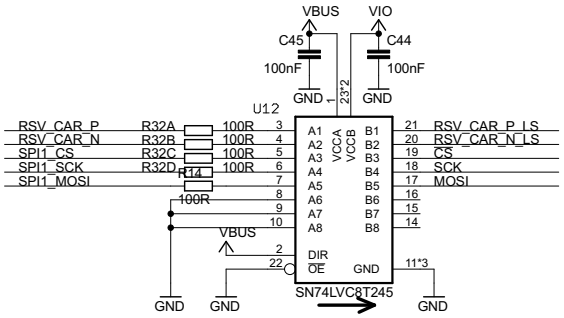

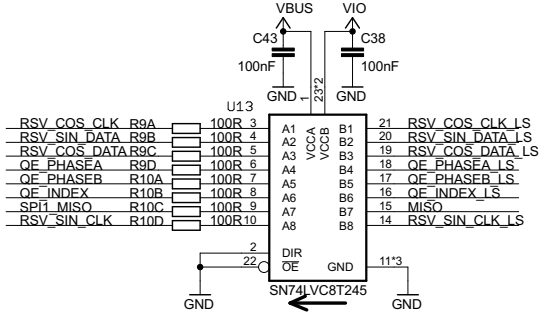

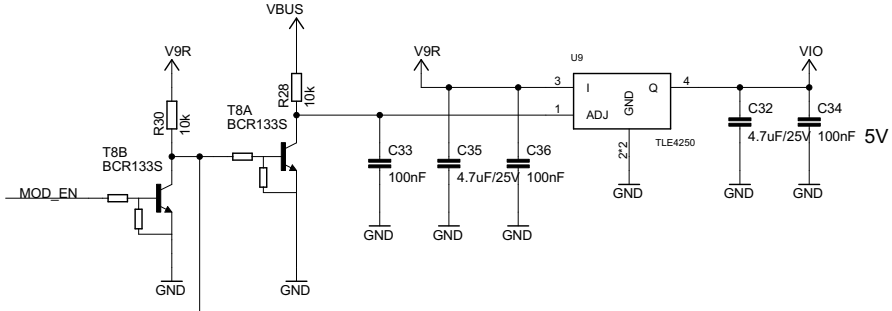

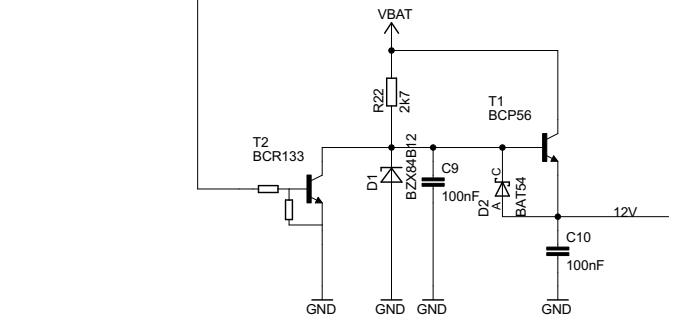

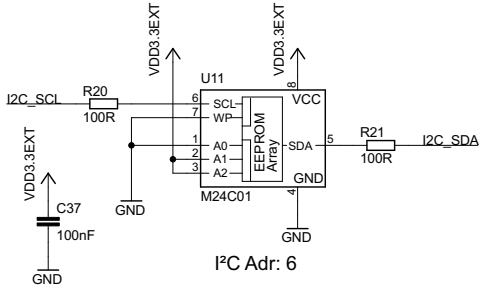

I²C Adr: 6

Legal Disclaimer

The information given in this document shall in no event be regarded as a guarantee of conditions or characteristics. With respect to any examples or hints given herein, any typical values stated herein and/or any information regarding the application of the device, Infineon Technologies hereby disclaims any and all warranties and liabilities of any kind, including without limitation, warranties of non-infringement of intellectual property rights of any third party.

SpeedSenseBoard

08.04.2014 14:07:33

Sheet: 1/2

Do Not Populate!

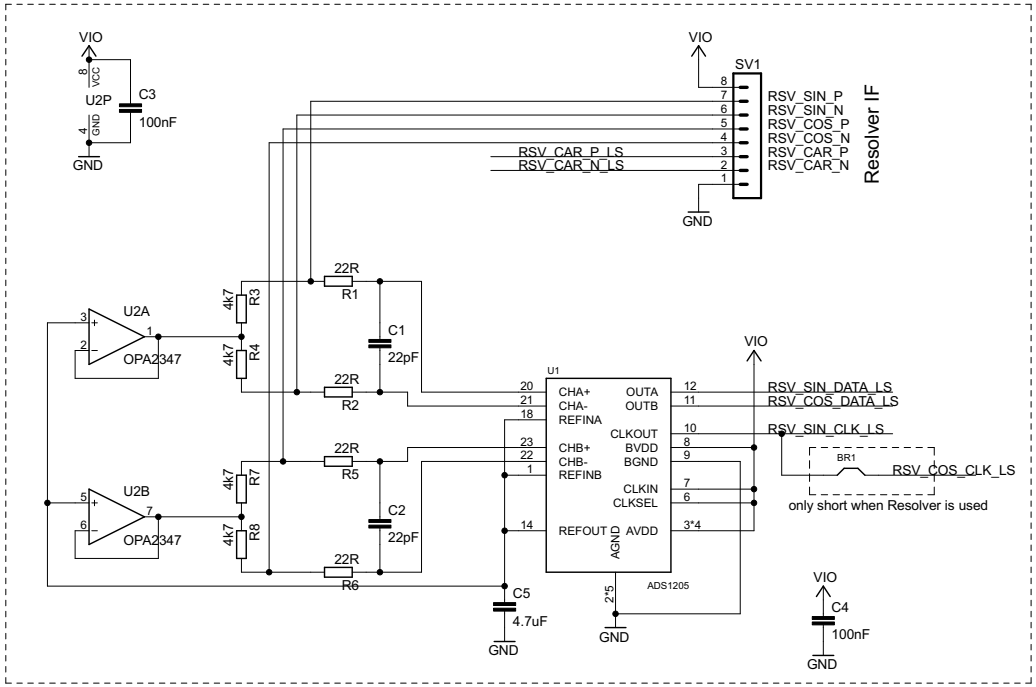

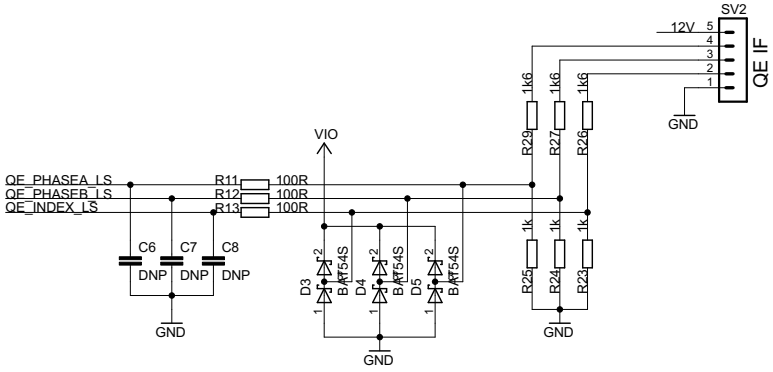

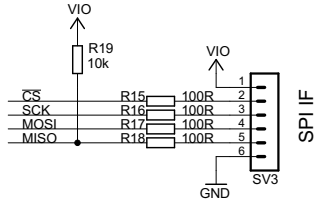

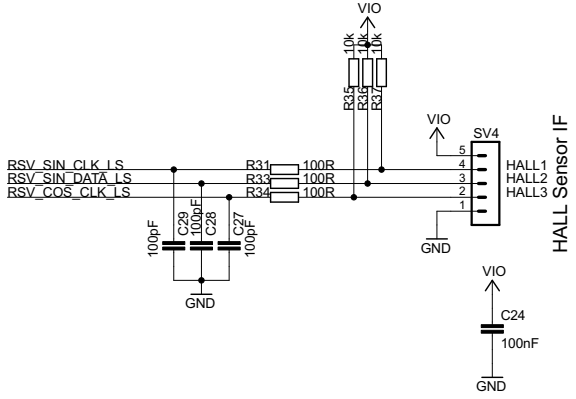

Legal Disclaimer

The information given in this document shall in no event be regarded as a guarantee of conditions or characteristics. With respect to any examples or hints given herein, any typical values stated herein and/or any information regarding the application of the device, Infineon Technologies hereby disclaims any and all warranties and liabilities of any kind, including without limitation, warranties of non-infringement of intellectual property rights of any third party.

SpeedSenseBoard

08.04.2014 14:07:33

Sheet: 2/2

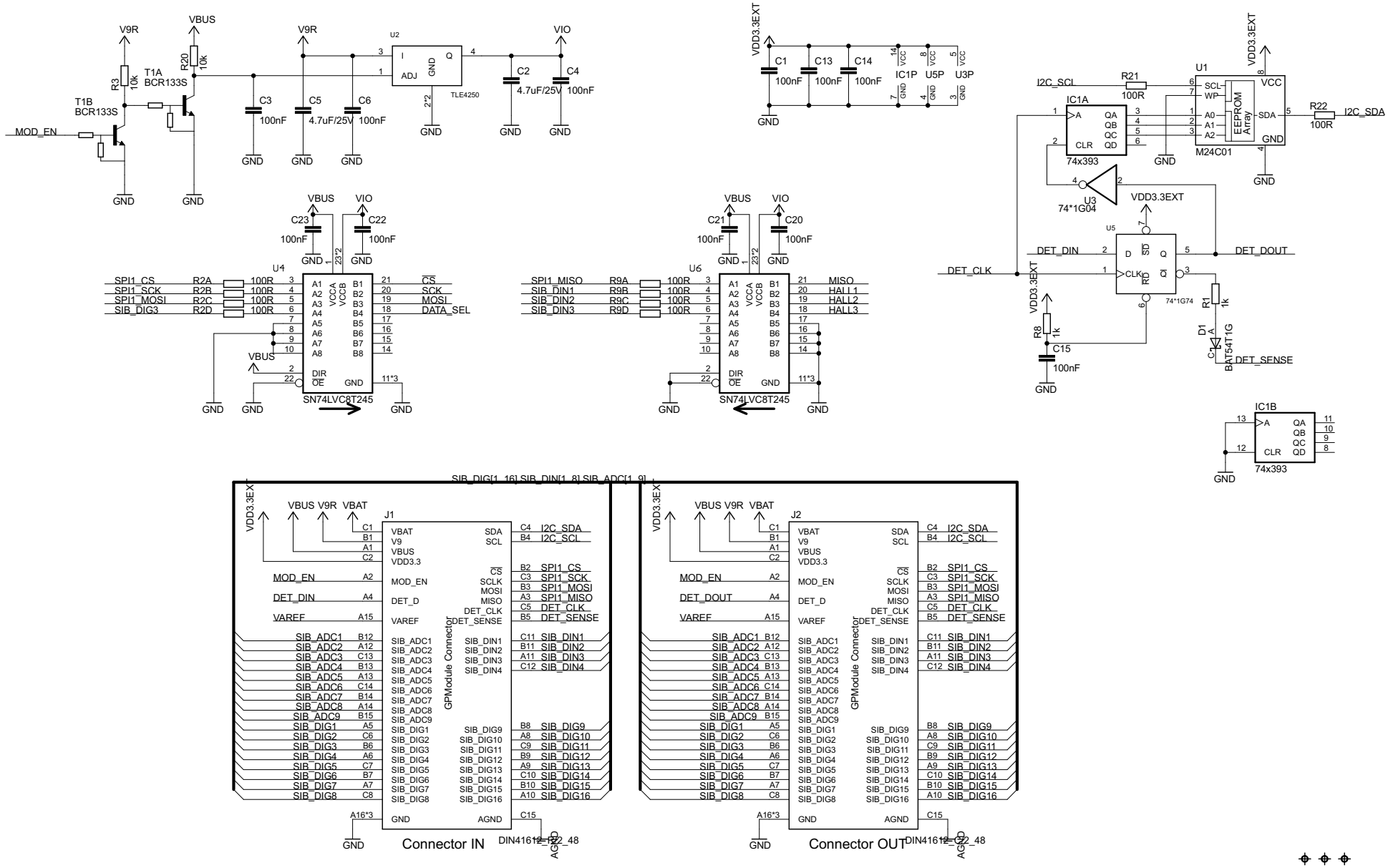

Legal Disclaimer

The information given in this document shall in no event be regarded as a guarantee of conditions or characteristics. With respect to any examples or hints given herein, any typical values stated herein and/or any information regarding the application of the device, Infineon Technologies hereby disclaims any and all warranties and liabilities of any kind, including without limitation, warranties of non-infringement of intellectual property rights of any third party.

AngleSenseBoard

11.02.2014 08:55:27

Sheet: 1/2

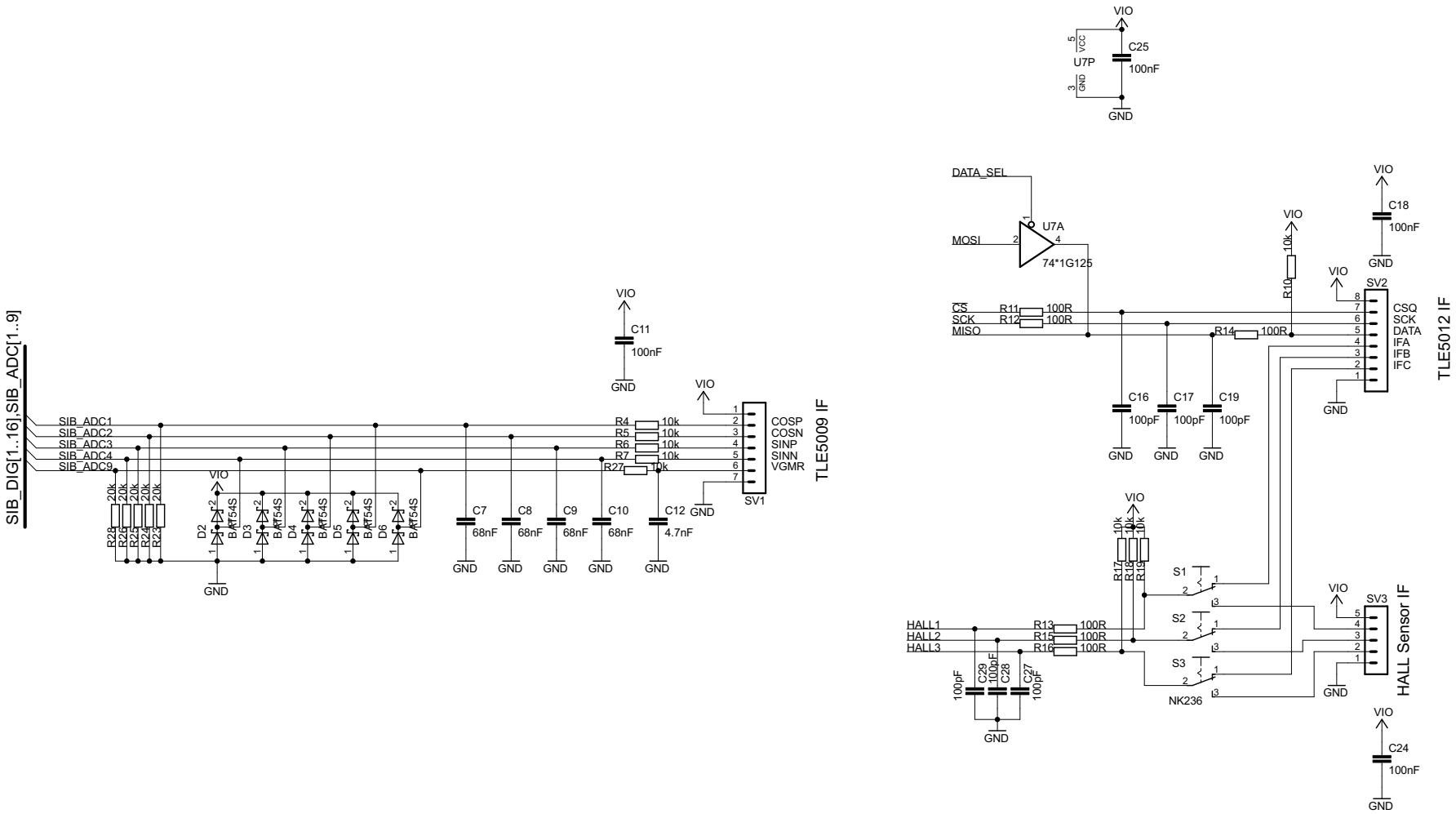

Legal Disclaimer

The information given in this document shall in no event be regarded as a guarantee of conditions or characteristics. With respect to any examples or hints given herein, any typical values stated herein and/or any information regarding the application of the device, Infineon Technologies hereby disclaims any and all warranties and liabilities of any kind, including without limitation, warranties of non-infringement of intellectual property rights of any third party.

AngleSenseBoard

11.02.2014 08:55:27

Sheet: 2/2

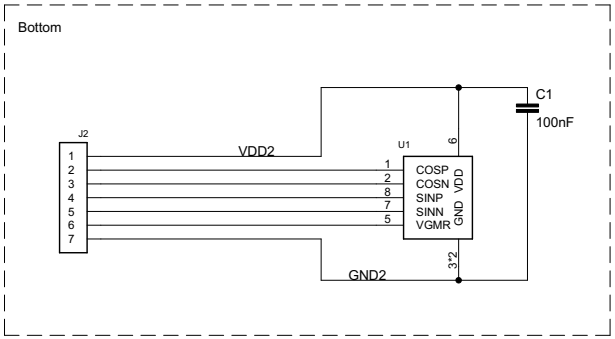

two different version:
populate one with TLE5009
and one with TLE5012

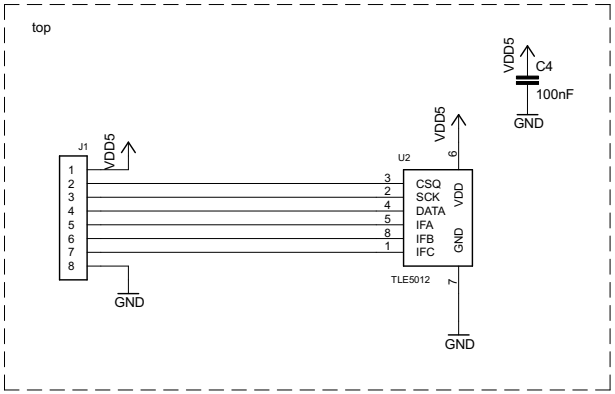

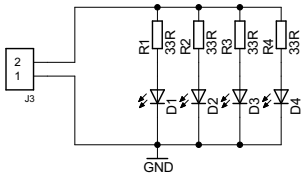

Legal Disclaimer

The information given in this document shall in no event be regarded as a guarantee of conditions or characteristics. With respect to any examples or hints given herein, any typical values stated herein and/or any information regarding the application of the device, Infineon Technologies hereby disclaims any and all warranties and liabilities of any kind, including without limitation, warranties of non-infringement of intellectual property rights of any third party.

AngleSensorBoard50xx
10.04.2014 15:03:12
Sheet: 1/1